Polarization in Infinite Chains

Dissertation

zur Erlangung des Grades
des Doktors der Naturwissenschaften
der Naturwissenschaftlich-Technischen Fakultät III
Chemie, Pharmazie, Bio- und Werkstoffwissenschaften
der Universität des Saarlandes

von

Violina Spurk geb. Tevekeliyska

Saarbrücken

2011

Tag des Kolloquiums:	28.02.2012
Dekan:	Prof. Dr. Wilhelm F. Maier
Berichterstatter:	Prof. Dr. Michael Springborg
	Prof. Dr.-Ing. Stefan Diebels
Vorsitz:	Prof. Dr. Guido Kickelbick
Akad. Mitarbeiter:	Dr. Harald Natter

Acknowledgment

This work has been completed under the supervision of Prof. Dr. Michael Springborg at the University of Saarland. I would like to express my appreciation to

Prof. Dr. Michael Springborg for his expert guidance, patience, continuous encouragement, for the erudite discussions and for his willingness to help me solving numerous problems during my work.

Prof. Dr. Benoît Champagne for his hospitality, for the fruitful discussions and the pleasant atmosphere during my stay in Namur, Belgium.

Dr. Valeri G. Grigoryan, Dr. Yi Dong and Dr. Michael Bauer for their support and many scientific and non-scientific conversations.

Assistant Prof. Anife Ahmedova for the proof-reading of this thesis and for the friendship.

M. Sc. Mohammad Molayem for all his help and just for everything.

Mrs. Ingelore Weidenfeld and Mrs. Silvia Nagel for their administrative help and for the many non-scientific conversations.

Our current and former group members Jorge Vargas, Sahar Abdalla, Dr. Max Ramirez, Nicolas Louis, Yong Pang, Dr. Denitsa Alamanova, Dr. Elisaveta Hristova, Dr. Habib ur-Rehman and Dr. Hanno Kamp for the pleasant working atmosphere and their readiness to help me.

Last but not least my husband Edgar for his faith in me, for his endless support and encouragement, for being always by my side and for his love.

Abstract

The present thesis focuses on large (macroscopic) systems that consist of a sequence of identical building blocks (units) in one dimension and are exposed to an external perturbation.

In the first part of the study is shown the implementation of a Vector Potential Approach (VPA) in an *ab initio* PLH (Polymer Linear Helical) code, which computes band structures of regular and helical polymers. This part of the work is a first step towards a full *ab initio* treatment of periodic systems in external electrostatic fields.

The second part deals with surface effects in electric field polarization of periodic systems. It is shown that by modifying the surface of large regular system, the polarization can be modified in units of a lattice vector times the elemental charge. Calculations on quasi-one-dimensional (quasi-1D) model system, exposed to an electrostatic field, show first that different terminations of identical chains lead to different responses, and second that the structural responses of a finite chain can be exactly reproduced by an infinite periodic treatment of the same system.

Hartree-Fock, *Ab Initio*, Electrostatic Field, Periodic Systems, Dipole Moment, Polarization, Polarizability

Zusammenfassung

Die vorliegende Arbeit konzentriert sich auf große (makroskopische) Systeme, die aus eindimensionalen identischen Bildungseinheiten bestehen und einer externen Störung (externem Feld) ausgesetzt sind.

Im ersten Teil dieser Forschung ist die Implementierung von der Vektor Potential Methode (VPA) in einem *ab initio* Polymer Linear Helical (PLH) Code dargestellt. Diese Arbeit ist ein erster Schritt in Richtung eines neuen *ab initio* Verfahrens zur Untersuchung von periodischen Systemen in externen elektrostatischen Feldern.

Der zweite Teil dieser Arbeit bezieht sich auf die Auswirkung der Oberfläche auf die Polarisation von endlichen und periodischen Systemen wenn ein externes elektrisches Feld eingeschaltet ist. Es wird gezeigt, dass die Modifizierung der Oberfläche eines großen regulären Systems zur Polarisationsänderung des selben Systems führt. Diese Änderung entspricht genau dem Gittervektor multipliziert mit der Elementarladung. Untersuchungen zeigen, dass unterschiedliche Endreste zu verschiedenen Ergebnissen führen und dass die strukturelle Änderung von einer endlichen Kette genau durch die Änderung der selben Kette, wenn sie als unendlich and periodisch betrachtet wird, reproduziert werden kann.

Hartree-Fock, *Ab Initio*, Elektrostatisches Feld, Periodische Systeme, Dipolmoment, Polarisation, Polarisierbarkeit

Abstract

The present work deals with large (macroscopic) systems that consist of a sequence of identical building blocks (units) in one dimension and are exposed to an external perturbation.

In the first part of the study is shown the implementation of a Vector Potential Approach (VPA), that allows for determining the combined electronic and structural response of an extended system to a finite electrostatic field, in an *ab initio* PLH (Polymer Linear Helical) code. It is known that the presence of a field (of an external perturbation) leads to an extra term $(\vec{E} \cdot \vec{\mu})$ to the Hamiltonian, where $\vec{E}$ is the field vector and $\vec{\mu}$ is the dipole moment of the system of interest. In the case of infinite periodic system the various properties are studied per repeated unit and the dipole moment $(\vec{\mu})$ translates into the polarization $(\vec{P})$. The main goal of this part of our project was to find out how a real polymer chain responds to the electric field, i.e., to calculate the dipole moment per repeated unit (i.e., the polarization). For this purpose, the mentioned extra term, which contains a charge and a current term for the polarization is added to an *ab initio* LCAO-SCF algorithm, which computes band structures of regular and helical polymers taking into account the one-dimensional translational symmetry. The current term of the polarization expression involves the derivatives of the orbital coefficient with respect to the wave vector k and the numerical differentiation is possible using an efficient so-called smoothing procedure. Linear and nonlinear responses of infinite hydrogen and lithium hydride chains to an external electric field are shown for different field strength and compared with previous results. The agreements show the successful implementation of the VPA in the PLH code, which is the first step towards a full *ab initio* treatment of periodic systems in external electrostatic fields.

The second part of the present study deals with surface effects in electric field polarization of periodic systems. It is shown that by modifying the surface of large regular system, e.g., by changing the end substituent and transferring the electrons from the donor (D) to acceptor (A) ends, the polarization of the macroscopic system can be modified in units of a lattice vector times the elemental charge. For the infinite periodic case, where the surfaces are neglected by construction, the effect of the terminations is indirectly included in the definition of the dipole moment per unit through an undefined integer $\tilde{n}$ associated with the phase of the crystal orbitals. Calculations on quasi-one-dimensional (quasi-1D) model system, exposed to an electrostatic field, show first that different terminations of identical chains lead to different responses, and second that the structural responses of

a finite chain can be exactly reproduced by an infinite periodic treatment of the same system.

Hartree-Fock, *Ab Initio*, Electrostatic Field, Periodic Systems, Dipole Moment, Polarization, Polarizability

Zusammenfassung

Die vorliegende Arbeit beschäftigt sich mit großen (makroskopischen) Systemen, die aus eindimensionalen identischen Bildungseinheiten bestehen und einer externen Störung (externem Feld) ausgesetzt sind.

Im ersten Teil unserer Forschung ist die Implementierung von der Vektor Potential Methode (VPA) in einem *ab initio* Polymer Linear Helical (PLH) Code dargestellt. Die VP Methode ermöglicht die Bestimmung von dem elektronischen und strukturellen Verhalten von erweiterten Systemen in einem endlichen elektrostatischen Feld. Es ist bekannt, dass die Anwesenheit von einem Feld (von einer äußeren Störung) zu einem zusätzlichen Ausdruck $(\vec{E} \cdot \vec{\mu})$ zu dem Hamilton-Operator führt. In diesem Fall ist $\vec{E}$ der Feldvektor und $\vec{\mu}$ das Dipolmoment von dem betrachteten System. Das Hauptziel von diesem Projektteil war es herauszufinden wie eine echte Polymerkette auf ein elektrisches Feld reagiert, d.h. das Dipolmoment pro Einheit (die Polarisation P) zu berechnen. Zur Erreichung dieses Ziels wurde der schon erwähnten zusätzlichen Ausdruck $(\vec{E} \cdot \vec{P})$, der einen Ladungs- und einen Strombeitrag zu der Polarisation enthält, einem *ab initio* LCAO-SCF Algorithmus hinzugefügt. Mit Hilfe von dem LCAO-SCF Algorithmus kann man die Bandstrukturen von regulären und spiralförmigen Polymeren ausrechnen, indem die eindimensionale Translationssymmetrie in Betracht gezogen wird. Da der Strombeitrag zu der Polarisation die Ableitungen der Orbitalkoeffizienten beinhaltet, ist die numerische Differentation nur mit Hilfe von einem effizienten sogenannten Glättungsverfahren möglich, bei dem die Koeffizienten als glatte Funktionen des Wellenvektors gemacht werden. In unseren Ergebnissen zeigen wir für verschiedene Feldstärken wie eine Wasserstoff- und eine Lithiumhydridkette auf das äußere elektrische Feld reagiert. Die Übereinstimmung von unseren Ergebnissen mit früheren Studien zeigt die erfolgreiche Implementierung von der VPA Methode in dem PLH Code. Deshalb ist unsere Arbeit ein erster Schritt in Richtung eines neuen *ab initio* Verfahrens zur Untersuchung von periodischen Systemen in externen elektrostatischen Feldern.

Der zweite Teil dieser Arbeit bezieht sich auf die Auswirkung der Oberfläche auf die Polarisation von endlichen und periodischen Systemen wenn ein externes elektrisches Feld eingeschaltet ist. Es wird gezeigt, dass die Modifizierung der Oberfläche eines großen regulären Systems, zum Beispiel indem die Reste auf den beiden Enden der Kette geändert werden, zur Polarisationsänderung des selben Systems führt. Diese Änderung entspricht genau dem Gittervektor multipliziert mit der Elementarladung. Für ein unendliches und periodisches System wird die Oberfläche grundsätzlich vernachlässigt, deshalb sind die Effekte von den Endresten indirekt in die Definition von dem Dipolmoment pro Einheit

einbezogen. Das geschieht durch eine undefinierte ganze Zahl $\tilde{n}$, die mit der Phase der Kristallorbitale zusammenhängt. Untersuchungen von einem quasi eindimensionalen Modelsystem, das sich in einem elektrostatischen Feld befindet, zeigen, dass unterschiedliche Endreste zu verschiedenen Ergebnissen führen und dass die strukturelle Änderung von einer endlichen Kette genau durch die Änderung der selben Kette, wenn sie als unendlich and periodisch betrachtet wird, reproduziert werden kann.

Hartree-Fock, *Ab Initio*, Elektrostatisches Feld, Periodische Systeme, Dipolmoment, Polarisation, Polarisierbarkeit

Contents

List of Figures

List of Tables

Chapter 1

Introduction

The present study deals with systems that are extended and regular in one dimension, but finite in the other two dimensions and are exposed to external perturbation. Since the systems are composed of three-dimensional atoms and materials, they are called quasi-one-dimensional (quasi-1D). As extended systems we will consider those that contain a central region, far from any surface, which presence is not felt by the electrons, and as regular those that, except for near the surface, consist of a large number of identical units. In theoretical studies extended and regular systems are most conveniently modelled as being infinite and periodic, since the number of units in the surface region relative to the total number is very small. Such large molecules have very large molecular mass and are known for instance as polymers (derived from the Greek words *poly* meaning "many" and *meros* meaning "part"). Fig. 1.1 shows three models of polymeric chains, from which the first one, the hydrogen chain, will be used as a test system in our study. Chain compounds, surfaces, films and crystals are examples for other infinite and periodic systems.

Since the variety of synthetic methods enables the production of polymeric materials with specific mechanical, optical, thermal and electronic properties, they have replaced nowadays the conventional materials in many areas, e.g., in informatics, medicine, clothing, packaging, cooking. Biopolymers, like nucleic acids (DNA and RNA), proteins, polysaccharides, lipids, play vital roles for human beings.

At the same time the properties of many new materials are unknown and characterizing them is crucial for their applications. To use the variety of spectroscopic methods for the characterization, the behaviour of the materials in external electromagnetic fields should be investigated and understood. Thus, to know how matter responds to external perturbation is of great fundamental and practical interest. Different procedures [5, 6, 7, 8] have been proposed, however, they tend to make serious assumptions regarding structure

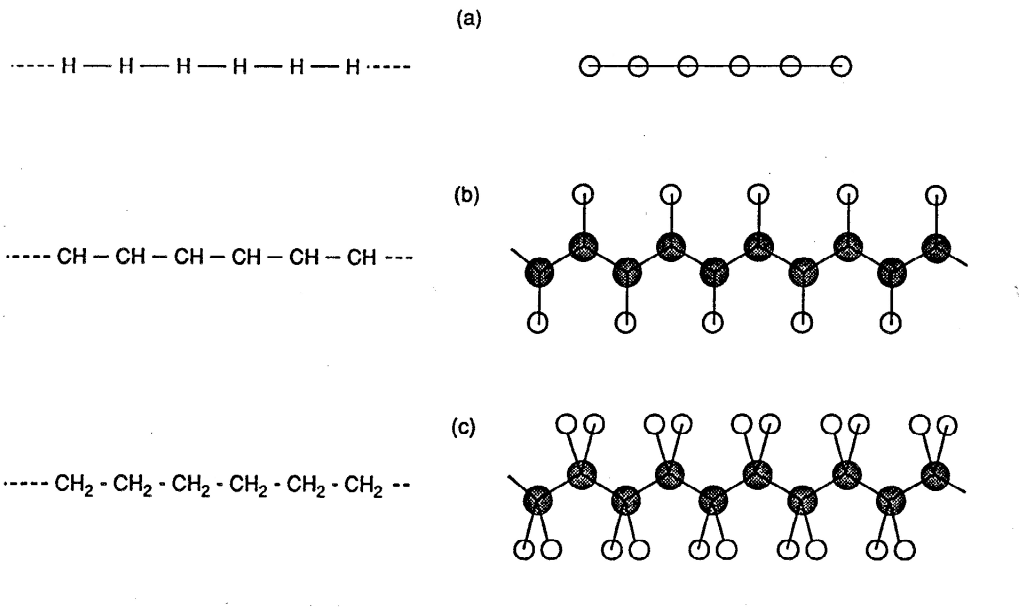

Figure 1.1: Model of a hydrogen (a), polyacetylene (b) and polyethylene (c) chain [1].

and are numerically tedious.

Whether the response is entirely electronic, or electrons and nuclei will both respond to the field, depends on the field frequency. If it is sufficiently high the first case is valid and at lower frequencies additionally nuclear degrees of freedom need to be considered. The interaction between the system and the field can be described through scalar or vector potential. The former one, normally used in atomic and molecular calculations, is proportional to the quantum-mechanical operator $\overrightarrow{r}$ (i.e., the electronic position), which is non-periodic and unbound. Thus, when an infinite and periodic systems are considered, the translational symmetry is destroyed using the scalar interaction potential. In [9] Springborg and Kirtman introduced two different approaches that result in the same single-particle Schrödinger-type equation for the crystal orbitals. The more general one employs the vector potential for the interaction between the system and the field [10, 11], retains the translational symmetry and is a numerically stable and efficient method that allows for the combined (non)linear electronic and structural response of infinite periodic systems to finite (static) electric fields [12, 9].

For a long, but finite, regular chain the presence of the field leads to an additional term $(\overrightarrow{E}_{\mathrm{DC}} \cdot \overrightarrow{\mu})$ to the Hamiltonian

$$\hat{H} \rightarrow \hat{H} - \overrightarrow{E}_{\mathrm{DC}} \cdot \overrightarrow{\mu}_{\mathrm{tot}}, \tag{1.1}$$

and to the total energy.

$$E_{\rm tot} = \langle \Psi | \hat{H}_{\rm tot} | \Psi \rangle = \langle \Psi | \hat{H}_{\rm tot,0} | \Psi \rangle - \overrightarrow{E}_{\rm DC} \cdot \overrightarrow{\mu}_{\rm tot}, \tag{1.2}$$

where $\hat{H}_{\rm tot}$ and $\hat{H}_{\rm tot,0}$ are the total Hamiltonian with and without the external field, respectively, $\overrightarrow{E}_{\rm DC}$ is the field strength and $\overrightarrow{\mu}_{\rm tot}$ the dipole moment of the system

$$\overrightarrow{\mu}_{\rm tot} = \int \overrightarrow{r} \rho_{\rm tot}(\overrightarrow{r}) d\overrightarrow{r} = \overrightarrow{\mu}_n - \overrightarrow{\mu}_e \tag{1.3}$$

that is split into a nuclear and an electronic part. In Fig. 1.2 are shown two finite, regular chains from which the lower one contains one extra unit, i.e., the size of the central part of the second chain has increased and automatically also the distance between the ends. Then, the total dipole moment

$$\overrightarrow{\mu}_{\rm tot} = \overrightarrow{\mu}_{\rm center} - \overrightarrow{\mu}_{\rm ends} \tag{1.4}$$

will change due to the two increases. The first term on the right site of the last equation is equivalent to the static charge distribution for the central part of a large finite chain, and the second one corresponds to the flow of charge from one to the other end of the chain. For this reason the dipole moment contains a contribution from the terminations (ends) that is not negligible in the thermodynamic limit, since it grows with the size of the system.

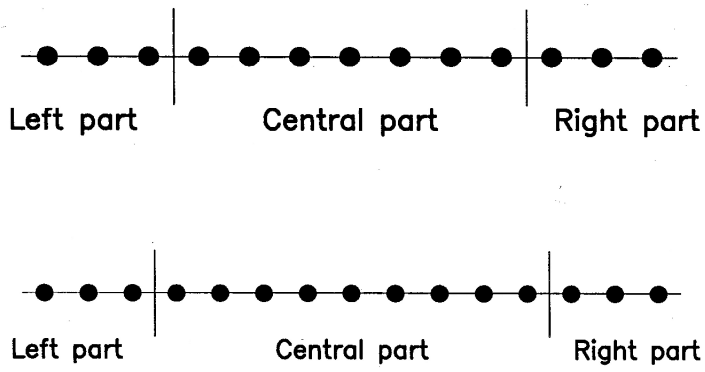

Figure 1.2: Two finite, regular chains split into three parts: left, central and right. Each filled circle, placed along the z axis, represents a building block containing one or more atoms. The lower chain consists one additional unit more.

In the case of infinite periodic system that consists of identical building blocks, the various properties are studied per repeated unit and the dipole moment, $\overrightarrow{\mu}$, translates into the polarization, $\overrightarrow{P}$. Then, the polarization, which does not depend on the size of the system (intensive property), can be determined through the extensive quantity dipole moment in the following way

$$\overrightarrow{P} = \lim_{N\to\infty} \frac{\overrightarrow{\mu}(N)}{N} = \lim_{N\to\infty} \left[\overrightarrow{\mu}(N+1) - \overrightarrow{\mu}(N)\right], \tag{1.5}$$

with the total number of units N. Since the effect of the surfaces is by construction neglected, we assume that the polarization depends only on the central region of the system, i.e., that the dipole moment per unit is a bulk property independent of the surfaces. Then, the question arises: what happens with the charge contribution from the terminations?

During the last two decades a mathematically correct description of the polarization has been obtained through the so-called Modern Theory of Polarization (MTP) [13, 14, 15, 16], which has its roots in earlier works of Blount [17]. In [18, 19] Springborg and co-workers show in details how one can arrive at different polarization expressions, including those related to the MTP, when one begins from the same starting point, i.e., from Blount formulation. Here, we will mention only one of the forms for the electronic part of the polarization that was suggested from King-Smith and Vanderbilt [13]

$$P_{\mathrm{KSV}} = \frac{2i}{N} \sum_{k=1}^{N} \sum_{n=1}^{B} \langle u_n(k) | \frac{\partial}{\partial k} u_n(k) \rangle, \tag{1.6}$$

where B is the number of doubly occupied bands, $u_n(k)$ a function that has the lattice periodicity and there is a gap between occupied and empty orbitals. Using symmetry-adapted basis functions, called Bloch waves and constructed through linear combination of atom-centred ones of different unit cells [20] (see also Chapter 2), we may write P_{KSV} as

$$\begin{aligned} P_{\mathrm{KSV}} &= \frac{2}{N} \sum_{k=1}^{N} \sum_{n=1}^{B} \sum_{l} e^{ikal} \sum_{pq} |C_{pn}(k)|^2 \langle \chi_p^0 | z - la | \chi_q^l \rangle \\ &+ \frac{2i}{N} \sum_{k=1}^{N} \sum_{n=1}^{B} \sum_{l} e^{ikal} \sum_{pq} C_{pn}^*(k) \langle \chi_p^0 | \chi_q^l \rangle \frac{d}{dk} C_{qn}(k) \\ &\equiv P_\rho + P_I. \end{aligned} \tag{1.7}$$

The total polarization is split into two terms - a charge (P_ρ) and a current term (P_I). The first one is related to the charge distribution along the central part of a large, finite chain, and the second is the answer of the question what happens with the part of the dipole moment from the charges at the terminations. Thus, the current contribution to the polarization is a consequence of approximating the system as being infinite and periodic. The evaluation of the charge term is normally not problematic and can be done through standard matrix multiplications involving known quantities, whereas to calculate the current term is not a trivial task, since it involves the $[(d)/(dk)]$ operator. An efficient smoothing procedure was developed within the vector potential approach [12, 9], that makes the occupied orbitals a smooth function of the wave vector k and is a numerically stable solution of the derivative problem. The parametrized model Hamiltonian, that was constructed to prove the method, contains all essential elements of an *ab initio* Hartree-Fock (or Kohn-Sham) Hamiltonian and therefore we could implement it in the *ab initio* LCAO-SCF algorithm that has been developed in Namur, Belgium [1, 2].

Electronic structure calculations for polyatomic molecules using a linear combination of atomic orbital (LCAO) scheme were already being carried out in the 1950s, whereas the first applications of quantum chemistry to polymers appeared in the second part of the 1960s [21, 22, 23, 24]. *Ab initio* programs for polymers are available and are currently applied in several groups, for example Erlangen [25], Vienna [26], Budapest [27], Torino [28], Kingston [29, 30], and Namur [31, 32]. The PLH (Polymer Linear Helical) code is an efficient program, designed for polymers through implementing fast techniques for evaluating integrals over Gaussian-type functions, and taking into account long-range electrostatic effects and the helical symmetry of the system. Some of the limitations, imposed in the algorithm, are that the chain is isolated, infinite, perfectly stereoregular and chain end effects are not considered. The stereoregularity allows to take into account the translational symmetry and enables the applications of concepts encountered in condensed matter physics in order to get a complete description of the electronic structure of polymers.

The starting theory in the *ab initio* LCAO-SCF algorithm is the Hartree-Fock method [33, 34, 35] where every electron moves in the field of the fixed nuclei and in the mean Coulombic and exchange fields of all the other electrons. The one-electron wavefunctions are the so-called Bloch's functions and together with the orbital energies are functions of the quasi-momentum, k, of the particle. The k-dispersion curves of the latter (one-electron energies) form the band structure of the regular polymer. There are different band structure calculations at the Hückel level of approximation, which enable the in-

terplay between the opening of a gap between the occupied and unoccupied levels and the bond length or electron density alternation [36, 37], whereas to treat polyethylene and polyacetylene extended Hückel was used [38, 39]. Also semiempirical techniques [40, 41, 42] and valence effective Hamiltonian (VEH) approach [43] are used to calculate the band structure of polymers, and electron correlations are taken into account using the semiempirical π-electron Pariser-Parr-Pople (PPP) method [23, 24, 44].

Band structure calculations can also be carried out using the Density Functional Theory (DFT) [45, 46] and a broad range of exchange-correlation functionals. At the beginning of the 1980s Mintmire and White [47, 48, 49] used the Local Density Approximation (LDA) for the exchange-correlation potential ($V_{\rm xc}$) and expressed the charge density as a linear combinations of auxiliary Gaussian basis sets [50]. At the end of the 1980s Springborg and co-workers developed a parameter-free, density functional, full-potential Linear Muffin-Tin Orbital (LMTO) method for calculating structural and electronic properties of infinite periodic systems [51, 52, 53, 54, 55, 56].

One of the limitations, considered in both methods that we used, is the absence of a surface, i.e., the influence of the surface (or of the terminations) on the dipole moment per unit is not taken into account and the polarization is a bulk quantity when infinite and periodic systems are studied. This statement has its origin in the work of Vanderbilt and King-Smith [14], whereas the discussions about the surface effects have already started in the 70's [57, 58, 59, 60, 61]. In our work we will show that for a long but finite system in the presence of field different chain ends can change the polarization, i.e., the electronic response will depend on the surface and neglecting it is not a very good approximation. On the other hand the dipole moment per unit depends upon the lattice constant, i.e., the latter will be affected from the surface and will change, and since it is coupled mechanically with internal structural parameters of the unit cell, they will change also. Model one-dimensional calculations will demonstrate that the measurable structural responses of the finite chain to an electrostatic field can be exactly reproduced by an infinite periodic treatment of the same system [62].

In the present study we consider that the quasi-1D chain and the field are parallel to the z axis, and in addition neglect spin polarization. Therefore, only the z component of the polarization is discussed and the vector symbol is omitted. However, the basic ideas of the method are transferable to 2D and 3D systems and to spin-polarized case.

This work is organized as follows: in Chapter 2, the most important concepts of the polymer quantum chemistry (e.g., Born-von Kármán periodic boundary conditions, Brillouin zone, Bloch functions) are shortly introduced. Chapter 3, involves the first part of

our study, i.e., the implementation of a Vector Potential Method in an *ab initio* Hartree-Fock program. The two different approaches and first *ab initio* results are presented. Comparison with previous results for the linear and nonlinear responses is made. The second part of the present work is introduced in Chapter 4. Results for model Hamiltonian calculations are listed and the role of the surface in electric field polarization of periodic systems is discussed. In Chapter 5, we summarise and conclude our work.

Chapter 2

Theoretical background

It is known that the polymer quantum chemistry is the bridge between condensed matter physics and molecular quantum chemistry. Although it deals with one-dimensional periodic systems, it is not a reduction of the solid-state physics to a single dimensional space, since the orbitals are truly three-dimensional. The following Chapter introduces briefly some of the main features of the polymer quantum chemistry only for the 1D case, but they are readily transferable to the 2D and 3D cases. Detailed information can be found in [20].

2.1 Born-von Kármán periodic boundary conditions

To illustrate some of the fundamentals of polymer quantum chemistry, a periodic and an infinite chain, as shown in Fig. 2.1, is considered. The larger the molecule (the chain) is (the larger the value of N), the more difficult becomes solving the matrix eigenvalue equation

$$\underline{\underline{H}} \cdot \underline{C}_i = \epsilon_i \cdot \underline{\underline{O}} \cdot \underline{C}_i \tag{2.1}$$

since the dimension of the matrix equation increases with the number of the basis functions K, e.g., if $K = 20$ a 20×20 equation has to be solved. Such equation could be simplified considerably by constructing a new symmetry-adapted basis functions using symmetry operations

$$\chi^{\tilde{k}} = \frac{1}{\sqrt{N}} \sum_{j=1}^{K} e^{i\tilde{k}j} \chi_j, \tag{2.2}$$

where the indices $\tilde{k}$ specify different irreducible representations.

When a rotation operation of $n \cdot (2\pi/N)$ about the C_N axis passing through the centre of the ring molecule from Fig. 2.1 (a) and perpendicular to the plane of the molecule is applied, the molecule and the symmetry-adapted orbitals are mapped into themselves

$$\hat{R}_n \chi^{\tilde{k}} = e^{i\tilde{k}n} \chi^{\tilde{k}}. \tag{2.3}$$

The same will happen when a translation operation is applied to the infinite chain from Fig. 2.1 (b) and the symmetry-adapted basis function $\chi^{\tilde{k}}$ obeys

$$\hat{T}_n \chi^{\tilde{k}} = e^{i\tilde{k}n} \chi^{\tilde{k}}. \tag{2.4}$$

Consequently, the values of the wavefunctions at the $(N+1)$st site in both cases are identical to those at the first site. These are the so-called Periodic Boundary Conditions (PBC). In addition, the ring molecule may be considered a finite approximation to an infinite linear chain. The size of the ring molecule defines a fragment of the infinite linear chain, which is known as the Born-von Kármán zone.

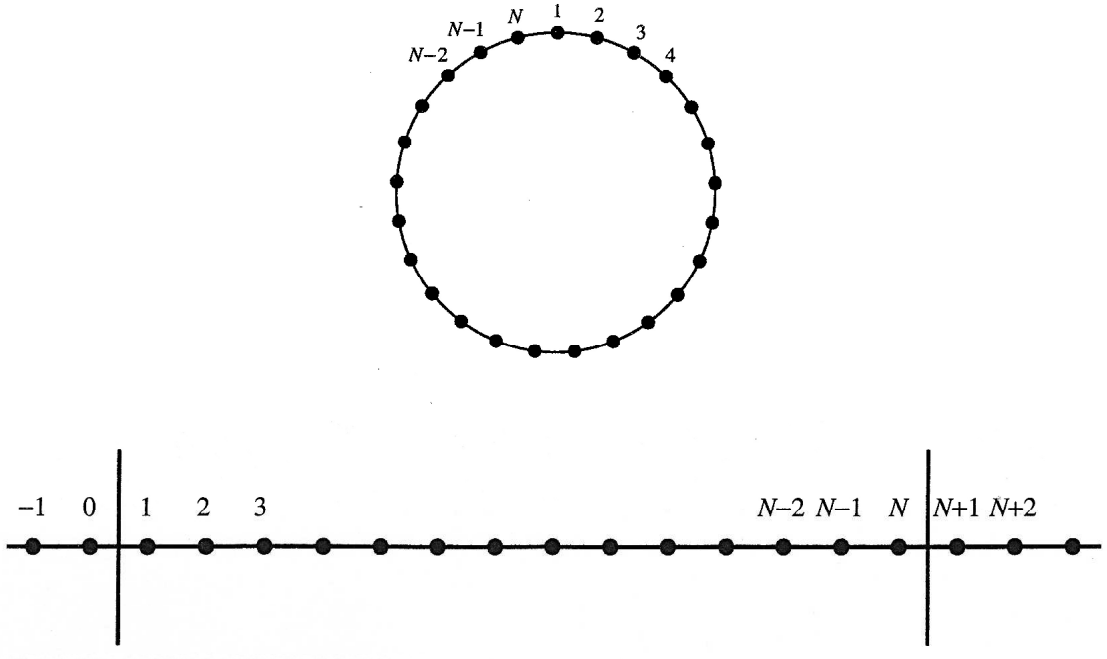

Figure 2.1: A periodic (ring) molecule consisting of N identical atoms (a) and an infinite linear chain containing a infinite set of equivalent atoms (b).

Dealing with extended and regular systems allows us to take into account the translational symmetry and to introduce the so called Born-von Kármán periodic boundary conditions.

2.2 Brillouin zones

The translation operation mentioned in the last section can be measured instead of number of units in a length unit. Then, the operator $\hat{T}_n$ can be described as translating the system by $n \cdot a$, with a being the lattice constant, and

$$\hat{T}_n \chi^{\tilde{k}} = e^{ina\tilde{k}/a} \chi^{\tilde{k}} \tag{2.5}$$

or

$$\hat{T}_n \chi^{k} = e^{inak} \chi^{k}, \tag{2.6}$$

where

$$k = \frac{\tilde{k}}{a} \tag{2.7}$$

is the wavevector and has the dimension of length^{-1}. If $\tilde{k}$ is restricted to

$$-\pi < \tilde{k} \leq \pi, \tag{2.8}$$

since the replacement $\tilde{k} \rightarrow \tilde{k} + 2\pi$ leads to no changes, then the so-called first Brillouin zone is defined through

$$-\frac{\pi}{a} < k \leq \frac{\pi}{a}. \tag{2.9}$$

To restrict the wavevector k to lie inside the first Brillouin zone is enough, since all information needed is contained within this interval.

The same can be applied to the 2D and 3D case. For instance, crystalline materials are supposed to be periodic in all three dimensions and the symmetry-adapted basis functions obey

$$\hat{T}_{n_a,n_b,n_c} \chi^{k} = e^{i\vec{R}_{n_a,n_b,n_c} k} \chi^{k}, \tag{2.10}$$

where

$$\vec{R}_{n_a,n_b,n_c} \equiv n_a\vec{a} + n_b\vec{b} + n_c\vec{c} \tag{2.11}$$

and the basis vectors $\vec{a}, \vec{b}$ and $\vec{c}$ have to be linearly independent.

2.3 Bloch functions

The symmetry-adapted basis functions, already mentioned in the previous two sections, were constructed from equivalent atom-centred ones of different unit cells using the symmetry of the system. They are called Bloch functions or Bloch waves and can be written in the form

$$\chi_p(k,\vec{r}) = \frac{1}{\sqrt{N}} \sum_{l=1}^{N} e^{ikal} \chi_p^l(\vec{r}). \tag{2.12}$$

Then, it applies

$$\begin{aligned} \psi_n(k,\vec{r}) &= \sum_{p=1}^{N_b} C_{pn}(k)\chi_p(k,\vec{r}) \\ &= \frac{1}{\sqrt{N}} \sum_{p=1}^{N_b} C_{pn}(k) \sum_{l=1}^{N} e^{ikal} \chi_p^l(\vec{r}). \end{aligned} \tag{2.13}$$

Here N_b denotes the number of basis functions per unit, p = 1, 2, 3, ..., N_b, l is the unit cell index, n is the so-called band index, a is the lattice constant and al corresponds to translation from the reference cell (origin cell, cell 0) along the z axis. The l sum is over the number of unit cells N in the Born-von Kármán zone and k is one of the equidistant k points in the first Brillouin zone, $[-\pi/a; \pi/a]$, with the spacing

$$\triangle k = \frac{2\pi}{Na}. \tag{2.14}$$

By means of another Bloch formulation, any electronic eigenfunction can be expressed through a function $u_n(k,\vec{r})$ that has the lattice periodicity

$$\psi_n(k,\vec{r}) = u_n(k,\vec{r})e^{ikz} = \frac{1}{\sqrt{N}} \sum_{p=1}^{N_b} \sum_{l=1}^{N} C_{pn}(k)\chi_p^l(\vec{r})e^{ikal}. \tag{2.15}$$

2.4 Band structures

For an infinite periodic quasi-one-dimensional system the electronic structure calculation proceeds almost as for a molecule. The important difference is that symmetry-adapted basis functions, characterized by the wavevector k, should be constructed in the polymer case. Thereby, the problem of solving the $\infty \times \infty$ secular equation

$$\underline{\underline{H}} \cdot \underline{C_n} = \epsilon_n \cdot \underline{\underline{O}} \cdot \underline{C_n} \tag{2.16}$$

is transformed into finite ones

$$\underline{\underline{H}}(k) \cdot \underline{C_n}(k) = \epsilon_n(k) \cdot \underline{\underline{O}}(k) \cdot \underline{C_n}(k) \tag{2.17}$$

with the $N_b \times N_b$ dimension.

When the number of k points in the first Brillouin zone, $[-\pi/a; \pi/a]$, tends to infinity, a whole continuum of k values exists, and the single-particle eigenvalue ϵ_n becomes a function of the wavevector

$$\epsilon_n = \epsilon_n(k). \tag{2.18}$$

Since $\epsilon_n(-k) = \epsilon_n(k)$ (it is shown in [20]), only the k values in the half first Brillouin zone $[0; \pi/a]$ can be considered. If all energy values are plotted as a function of k, the band structure of the correspondent system is obtained. The difference between the highest and the lowest energy level gives the band dispersion (band width). The smaller the distance between the atoms is, i.e., the stronger the interaction between the atoms, the bigger is the band dispersion. The highest occupied energy level is called HOMO (Highest Occupied Molecular Orbital) and the lowest unoccupied one - LUMO (Lowest Unoccupied Molecular Orbital). Then,

$$E_{\mathrm{F}} = \frac{\epsilon_{\mathrm{HOMO}} + \epsilon_{\mathrm{LUMO}}}{2} \tag{2.19}$$

is the so called *Fermi* boundary or *Fermi* level. If the *Fermi* level lies within the band, the system is metallic.

2.5 Polymer Quantum Chemistry in comparison with Molecular Quantum Chemistry

In the following we will introduce the basic formulae used in polymer quantum chemistry and compare them with those used in molecular quantum chemistry. In general, when using the LCAO Hartree-Fock methodology the molecular orbital is expanded in terms of basis functions, the eigenvalues, ϵ, of the secular systems of equations and determinants are the orbital energies, and from the LCAO coefficients, charges and bond orders are calculated. The convention adopted in the following formulae and maintained throughout the text is that lower indices (p, q, r, s) refer to the labelling of a given orbital (χ_p, χ_q, χ_r, or χ_s), while the superscript indices $(0, l, h, j)$ refer to the position of a given unit cell, corresponding to translations la, ha and ja from the reference cell 0 (or origin cell). The first formulae are used in molecular- and the second in polymer quantum chemistry.

Orbital

$$\psi_n(\vec{r}) = \sum_{p=1}^{N_b} C_{pn}\chi_p(\vec{r})$$

$$\psi_n(k,\vec{r}) = \frac{1}{\sqrt{N}} \sum_{p=1}^{N_b} C_{pn}(k) \sum_{l=1}^{N} e^{ikal}\chi_p^l(\vec{r}) \tag{2.20}$$

Secular system

$$\sum_{p=1}^{N_b} C_{pn}\left(h_{pq} - \epsilon_n S_{pq}\right) = 0$$

$$\begin{aligned} &\sum_{p=1}^{N_b} C_{pn}(k) \left\{ \sum_{l=1}^{N} e^{ikal} \left[h_{pq} - \epsilon_n(k) S_{pq}\right] \right\} \\ &\equiv \sum_{p=1}^{N_b} C_{pn}(k) \left[h_{pq}(k) - \epsilon_n(k) S_{pq}(k)\right] = 0 \end{aligned} \tag{2.21}$$

Overlap matrix

$$S_{pq} = \langle \chi_p | \chi_q \rangle$$

$$S_{pq}(k) = \sum_{l=1}^{N} e^{ikal} S_{pq}^{0l} = \sum_{l=1}^{N} e^{ikal} \left\langle \chi_p^0 | \chi_q^l \right\rangle \tag{2.22}$$

Fock matrix

$$F_{pq} = \left\langle \chi_p \right| \hat{F} \left| \chi_q \right\rangle = H_{pq} + G_{pq}$$

$$F_{pq} = \sum_{l=1}^{N} e^{ikal} F_{pq}^{0l} = \sum_{l=1}^{N} e^{ikal} \left\langle \chi_p^0 \right| \hat{F} \left| \chi_q^l \right\rangle = H_{pq}^{0l} + G_{pq}^{0l} \tag{2.23}$$

One electron part of the Fock matrix

$$H_{pq} = T_{pq} + V_{pq}$$

$$H_{pq}^{0l} = T_{pq}^{0l} + V_{pq}^{0l} \tag{2.24}$$

Two electron part of the Fock matrix

$$G_{pqrs} = \sum_{r} \sum_{s} D_{rs} \left[2 \left(pq|rs \right) - \left(pr|qs \right) \right]$$

$$G_{pqrs}^{0lhj} = \sum_{h} \sum_{j} \sum_{r} \sum_{s} D_{rs}^{hj} \left[2 \left(pq^{0l}|rs^{hj} \right) - \left(pr^{0h}|qs^{lj} \right) \right] \tag{2.25}$$

Electron repulsion integrals

$$\left(pq|rs \right) = \left\langle \chi_p \chi_q \right| \frac{1}{|r - r'|} \left| \chi_r \chi_s \right\rangle$$

$$\left(pq^{0l}|rs^{hj} \right) = \left\langle \chi_p^0 \chi_q^l \right| \frac{1}{|r - r'|} \left| \chi_r^h \chi_s^j \right\rangle \tag{2.26}$$

Density matrix

$$D_{rs} = \sum_{n} C_{rn}^{*} C_{sn}$$

$$D_{rs}^{0j} = \frac{a}{\pi} \int_{-\frac{\pi}{a}}^{\frac{\pi}{a}} dk \left[\sum_{n} C_{rn}^{*}(k) C_{sn}(k) \right] e^{ikja} \tag{2.27}$$

Kinetic energy term

$$T_{pq} = -\frac{1}{2}\left\langle \chi_p | \nabla^2 | \chi_q \right\rangle$$

$$T_{pq}^{0l} = -\frac{1}{2}\left\langle \chi_p^0 | \nabla^2 | \chi_q^l \right\rangle \tag{2.28}$$

Electron nuclear attraction

$$V_{pq} = \left\langle \chi_p \left| \frac{1}{|r - R_A|} \right| \chi_q \right\rangle$$

$$V_{pq}^{0l} = \left\langle \chi_p^0 \left| \frac{1}{|r - R_A|} \right| \chi_q^l \right\rangle \tag{2.29}$$

Results

$$\longrightarrow \epsilon_1, \epsilon_2, \epsilon_3, ...$$

$$\longrightarrow \epsilon_1(k), \epsilon_2(k), \epsilon_3(k), ... \tag{2.30}$$

Since in our study the translational symmetry of the polymer is taken into account, the lattice periodicity can be exploited and lattice summations can be introduced. It is obvious that in polymer quantum chemistry the orbitals, the systems of equation and the determinants have imaginary components. The results from the LCAO-SCF procedure are the eigenvalues, $\epsilon_n(k)$, of the Hartree-Fock equation as a function of the wavevector k, which plot gives the band structure of the corresponding system.

Chapter 3

Ab initio treatment of periodic systems in external electrostatic fields

3.1 Introduction

In this Chapter, we will show how a numerically stable and efficient Vector Potential Approach (VPA) is implemented in an *ab initio* Linear Combination of Atomic Orbitals Self-Consistent Field (LCAO-SCF) algorithm.

Based on the work of Genkin and Mednis [63], Kirtman and co-workers [10, 11] developed the VPA, which enables to obtain the electronic response of the system to a finite field and has been used to determine the linear and nonlinear polarizabilities [64, 65, 66, 67] of quasi-one-dimensional (quasi-1D) systems.

Springborg and Kirtman extended the VPA to one [12, 9] that allows, additionally to the electronic response, the structural response of infinite periodic systems to finite (static) electric field. In [9], the method and a model calculation results are presented in detail. Since the constructed model Hamiltonian contains all essential elements of an *ab initio* Hartree-Fock one, it was possible to implement the VPA in the *ab initio* LCAO-SCF method, which computes band structures of regular and helical polymers taking into account the one-dimensional translational symmetry.

As already mentioned, for extended and periodic systems exposed to an external electrostatic field the presence of the field leads to an extra term $(\vec{E} \cdot \vec{P})$ to the Hamiltonian

$$\hat{H} \rightarrow \hat{H} - \overrightarrow{E} \cdot \overrightarrow{P}, \tag{3.1}$$

and to the total energy

$$E_{\mathrm{tot}} = \langle\Psi|\hat{H}_{\mathrm{tot}}|\Psi\rangle = \langle\Psi|\hat{H}_{\mathrm{tot},0}|\Psi\rangle - \overrightarrow{E}\cdot\overrightarrow{P}, \tag{3.2}$$

where $\hat{H}_{\mathrm{tot}}$ and $\hat{H}_{\mathrm{tot},0}$ are the total Hamiltonian with and without external field, respectively, $\vec{E}$ is the field vector and $\vec{P}$ the polarization of the system of interest. In order to find out how a polymer chain responds to an external electric perturbation, the polarization expression

$$\begin{aligned} P_{\mathrm{KSV}} &= \frac{2}{N}\sum_{k=1}^{N}\sum_{n=1}^{B}\sum_{l} e^{ikal}\sum_{pq}|C_{pn}(k)|^2\langle\chi_p^0|z-la|\chi_q^l\rangle \\ &+ \frac{2i}{N}\sum_{k=1}^{N}\sum_{n=1}^{B}\sum_{l} e^{ikal}\sum_{pq}C_{pn}^*(k)\langle\chi_p^0|\chi_q^l\rangle\frac{d}{dk}C_{qn}(k) \\ &\equiv P_\rho + P_I, \end{aligned} \tag{3.3}$$

with the charge (P_ρ) and the current (P_I) term, is taken from the VPA and added to the *ab initio* Hartree-Fock Hamiltonian. Since the charge flow contribution to the polarization involves the derivatives of the orbital coefficients with respect to the wavevector k, to calculate it self-consistently, a smoothing procedure for the numerical differentiation was developed.

The Chapter is organized as follows: in Subchapters 3.2 and 3.3, the VPA and the *ab initio* LCAO-SCF algorithm are briefly introduced. Some difficulties and characteristics of the implementation are mentioned in Subchapter 3.4. Our first results for electronic responses of hydrogen (H_2) and lithium hydride (LiH) chains in a presence of an external electrostatic field are introduced, discussed and compared with available previous theoretical and experimental results in Subchapter 3.5. All results are in atomic units (a.u.). Detailed information about the methods can be found in [12, 9, 10, 19, 1].

3.2 Vector Potential Approach (VPA)

3.2.1 The Hartree-Fock equation

Here we will shortly introduce the VPA single-particle Schrödinger-type equation for the electrons of an infinite periodic system in an external electrostatic field and discuss its self-consistent field (SCF) solution.

Using the polarization expression suggested by King-Smith and Vanderbilt [13]

$$P_{\mathrm{KSV}} = \frac{2i}{N}\sum_{k=1}^{N}\sum_{n=1}^{B}\langle u_n(k)|\frac{\partial}{\partial k}u_n(k)\rangle, \tag{3.4}$$

the molecular orbital expression

$$\psi_n(k,\vec{r}) = \sum_{p=1}^{N_b} C_{pn}(k)\chi_p(k,\vec{r}), \tag{3.5}$$

where

$$\chi_p(k,\vec{r}) = \frac{1}{\sqrt{N}}\sum_{l=1}^{N} e^{ikal}\chi_p^l(\vec{r}) \tag{3.6}$$

are symmetry-adapted Bloch waves, constructed through linear combination of atom-centered basis functions of different unit cells, and a Hartree-Fock approximation, the orbital coefficients may be obtained by solving

$$\sum_p \left\{ F_{pq}(k) - E_{\mathrm{DC}}\cdot\left[M_{pq}(k) + iS_{pq}(k)\frac{\partial}{\partial k}\right]\right\} C_{pn}(k) = \epsilon_n(k)\sum_p S_{pq}(k)C_{pn}(k). \tag{3.7}$$

Here,

$$S_{pq}(k) = \sum_l e^{ikla}S_{pq}^{0l} = \sum_l e^{ikla}\langle\chi_p^0|\chi_q^l\rangle \tag{3.8}$$

$$M_{pq}(k) = \sum_l e^{ikla}M_{pq}^{0l} = \sum_l e^{ikla}\langle\chi_p^0|z-la|\chi_q^l\rangle = \sum_l e^{-ikla}\langle\chi_p^l|z|\chi_q^0\rangle \tag{3.9}$$

$$F_{pq}(k) = \sum_l e^{ikla} F_{pq}^{0l} = \sum_l e^{ikla} \langle \chi_p^0 | \hat{F} | \chi_q^l \rangle. \tag{3.10}$$

are the overlap, the unit cell dipole and the Fock matrix elements, respectively. S_{pq}^{0l}, M_{pq}^{0l} and F_{pq}^{0l} are the corresponding direct space matrices between the atomic orbitals χ_p of the reference cell (0) and χ_q of the lth cell. Due to the $\partial/\partial k$ term, Eq. (3.7) is not a standard matrix-eigenvalue problem. Using the normalization condition

$$\underline{\underline{1}} = \underline{\underline{C}}^\dagger(k) \cdot \underline{\underline{S}}(k) \cdot \underline{\underline{C}}(k), \tag{3.11}$$

the $\partial C_{pn}(k)/\partial k$ term can be converted to a desired multiplicative form

$$\underline{\underline{S}}(k) \frac{\partial}{\partial k} \underline{\underline{C}}(k) = \left[\underline{\underline{S}}(k) \left(\frac{\partial}{\partial k} \underline{\underline{C}}(k) \right) \underline{\underline{C}}^\dagger(k) \underline{\underline{S}}(k) \right] \underline{\underline{C}}(k). \tag{3.12}$$

Then, the quantity in the square brackets can be treated self-consistently in the same manner as the Fock matrix and Eq. (3.7) takes the form

$$\begin{aligned} &\left\{ \underline{\underline{F}}(k) - E_{\mathrm{DC}} \cdot \left[\underline{\underline{M}}(k) + i \underline{\underline{S}}(k) \cdot \left(\frac{\partial}{\partial k} \underline{\underline{C}}(k) \right) \cdot \underline{\underline{C}}^\dagger(k) \cdot \underline{\underline{S}}(k) \right] \right\} \cdot \underline{C}_n(k) \\ &= \epsilon_n(k) \cdot \underline{\underline{S}}(k) \cdot \underline{C}_n(k). \end{aligned} \tag{3.13}$$

If we compare the two terms in the square brackets of the last equation with the polarization expression of Eq. (3.3), we see that the first one corresponds to the charge distribution along the central part of a large finite chain

$$\frac{2}{N} \sum_{k=1}^{N} \sum_{n=1}^{B} \sum_l e^{ikal} \sum_{pq} |C_{pn}(k)|^2 \langle \chi_p^0 | z - la | \chi_q^l \rangle \equiv P_\rho \tag{3.14}$$

and the second one is related to the current contribution to the polarization

$$\frac{2i}{N} \sum_{k=1}^{N} \sum_{n=1}^{B} \sum_l e^{ikal} \sum_{pq} C_{pn}^*(k) \langle \chi_p^0 | \chi_q^l \rangle \frac{d}{dk} C_{qn}(k) \equiv P_{\mathrm{I}}. \tag{3.15}$$

Then, the electronic polarization, P_e, can be written as:

$$
\begin{aligned}
P_e &= 2i \sum_k \sum_n \langle \psi_n(k) | e^{ikz} \frac{\partial}{\partial k} e^{-ikz} | \psi_n(k) \rangle \\
&= 2 \sum_k \sum_n \sum_{pq} \left[C^*_{pn}(k) C_{qn}(k) M_{pq}(k) + i C^*_{pn}(k) \frac{\partial C_{qn}}{\partial k} S_{pq}(k) \right] \\
&\equiv P_\rho + P_I .
\end{aligned}
\tag{3.16}
$$

The total polarization, P_{tot}, is written as a sum of the self-consistent electronic polarization (P_e) and of the classical polarization contribution from the nuclei (P_n)

$$P_{\text{tot}} = P_e + P_n. \tag{3.17}$$

To calculate the charge term (P_ρ) from Eq. (3.16) is an easy task, since it involves known quantities, whereas the current term (P_I) requires the numerical differentiation of the coefficients, that is problematic since $\underline{\underline{C}}(k)$ contains an arbitrary (random) k-dependent phase factor. To compensate the randomness, a numerically stable approach, which makes the coefficients a smooth function of k was developed [12, 9].

3.2.2 The smoothing procedure

The smoothing procedure, as described in [9], is based on adding an extra phase factor

$$C_{qn}(k) \rightarrow C_{qn}(k) e^{i\varphi_n(k)}, \tag{3.18}$$

which is chosen so that the change in the coefficients from one k point to the next is minimized. Starting with the field-free expansion coefficients $\{C_{qn}(k)\}$ obtained by solving the single-particle equation, Springborg and Kirtman arrived at the following multistep procedure:

1) The first step is to identify band crossings. Assuming that orbitals for the same band have very similar expansion coefficients, band crossings are identified for each band n and k value using the relation

$$\sum_n C^*_{qn}(k) C_{qn}(k + \Delta k) \leq \delta_c, \tag{3.19}$$

where δ_c is a chosen threshold. If this inequality is fulfilled, the orbitals are taken as belonging to two different, crossing bands, n and $n+1$, and the coefficients $C_{qn}(k + \Delta k)$ and $C_{q,n+1}(k + \Delta k)$ are interchanged.

2) If two band orbitals are degenerate at given k point, a linear combination that makes the coefficients maximally similar to the two orbitals at $k + \Delta k$ is made.

3) All coefficients are made real at $k = 0$.

4) Considering positive k points and starting from $k = 0$ and $\varphi_n(0)$, the quantity is minimized

$$Q_n(k + \Delta k) = \sum_q |C_{qn}(k + \Delta k)e^{i\varphi_n(k+\Delta k)} - C_{qn}(k)e^{i\varphi_n(k)}|^2. \tag{3.20}$$

For negative k it is assumed that

$$C_{qn}(-k)e^{i\varphi_n(-k)} = C^*_{qn}(k)e^{-i\varphi_n(k)}. \tag{3.21}$$

This choice is always possible and it leads to coefficients that are smooth function of k for

$$-\frac{\pi}{a} < k < \frac{\pi}{a}, \tag{3.22}$$

but large jumps may occur at the zone boundaries $k = \pm\pi/a$.

5) In order to remove this discontinuities, the quantity

$$\begin{aligned} Q_n = &\sum_k \sum_q |C_{qn}(k + \Delta k)e^{i\varphi_n(k+\Delta k)} - C_{qn}(k)e^{i\varphi_n(k)}|^2 \\ &+ \lambda \sum_k \sum_q |C_{qn}(k + 2\Delta k)e^{i\varphi_n(k+2\Delta k)} - C_{qn}(k)e^{i\varphi_n(k)}|^2 \end{aligned} \tag{3.23}$$

is minimized for each band n under the constraint

$$\varphi_n\left(-\frac{\pi}{a}\right) = \varphi_n\left(\frac{\pi}{a}\right), \tag{3.24}$$

and with $\varphi_n(0)$ fixed.

By means of the five steps, one arrives at a set of smooth coefficients for the field-free case, that are used to calculate the polarization for $E_{\mathrm{DC}} = 0$ according to Eq. (3.16). The first four steps are necessary to provide good initial guess. The fifth step is the time-consuming one since it involves a nonlinear optimization carried out using conjugate gradients.

For the $E_{\mathrm{DC}} \neq 0$ case it is assumed that the field does not remove band crossings by lowering the symmetry and does not change the orbitals significantly. Therefore one starts with steps 2 and 3 and, then, skip to step 6 below.

6) The coefficients are made maximally similar to those of the field-free case, i.e., for each band and k value the quantity is minimized

$$\tilde{Q}_n(k) = \sum_q |C_{qn}(k)e^{i\varphi_n(k)} - \tilde{C}_{qn}(k)|^2. \tag{3.25}$$

7) Finally, only for aesthetic reason, all phases are modified by a k-independent but band-dependent constant so that the coefficients at $k = 0$ are all real.

Model calculations show [12, 9] that the smoothing procedure is numerically stable and enables the differentiation of the orbital coefficients.

3.2.3 Derivatives of the coefficients

After the coefficients are made a smooth function of the wave vector, is easy to obtain numerically stable derivatives. For this purpose the following equation is used

$$\frac{\partial C_{qn}(k)}{\partial k} \simeq \frac{1}{\Delta k} \sum_{j=1}^{N_k} \omega_{j,N_k} \left[C_{qn}\left(k + j \cdot \Delta k\right) - C_{qn}\left(k - j \cdot \Delta k\right)\right] \tag{3.26}$$

with

$$C_{qn}\left(k + \frac{2\pi}{a}\right) = C_{qn}(k). \tag{3.27}$$

Here, N_k is the number of points used in the numerical differentiation. In our calculations we used $N_k = 20$, which leads to more accurate results than when using $N_k = 1$. The coefficients $\{\omega_{j,N_k}\}$ are taken from Dvornikov [68].

3.2.4 Total energy expression

To get the total energy of the system of interest in the presence of external electrostatic field the polarization energy expression

$$
\begin{aligned}
E_{\mathrm{pol}} &= E_{\mathrm{DC}} \cdot P_{\mathrm{tot}} = E_{\mathrm{DC}} i \sum_k \sum_n \left\langle \psi_n^k \middle| e^{ikz} \frac{\partial}{\partial k} e^{-ikz} \middle| \psi_n^k \right\rangle \\
&= E_{\mathrm{DC}} \sum_k \sum_n \sum_{pq} \left[\underbrace{C_{pn}^*(k) C_{qn}(k) M_{pq}(k)}_{\text{charge term}} + \underbrace{i C_{pn}^*(k) \frac{\partial C_{qn}(k)}{\partial k} S_{pq}(k)}_{\text{current term}} \right] \\
&\equiv E_{\mathrm{DC}} \cdot \underbrace{(P_\rho + P_I)}_{P_{\mathrm{tot}}}
\end{aligned}
\tag{3.28}
$$

should be added to the Hartree-Fock contribution

$$
E_{\mathrm{tot}} = \langle \Psi | \hat{H}_{\mathrm{tot}} | \Psi \rangle = \langle \Psi | \hat{H}_{\mathrm{tot},0} | \Psi \rangle - E_{\mathrm{DC}} \cdot P_{\mathrm{tot}} - E_{\mathrm{DC}} \sum_{i=1}^{N_C} z_i, \tag{3.29}
$$

with z_i being the equilibrium position of the ith atom and N_C the number of atoms. The last term in the equation above gives the classical contributions from the external electrostatic field acting on the nuclear charges. E_{tot} is the quantity that is minimized during a geometry optimization procedure.

3.2.5 The Hückel-type model

The constructed modified Hückel-type model for the Hartree-Fock Hamiltonian in the VPA treatment [12, 9, 62] allows for the basis function flexibility and self-consistency and enables a realistic electronic-structure simulations, to perform many calculations on large, but finite and on infinite periodic systems and to present first *ab initio* results on realistic systems. The model calculations of Springborg and co-workers show that the approach for the infinite periodic systems is able to reproduce the results for the large finite systems.

A linear chain $-A=B-$ with alternating atoms and bond lengths is considered. The system has N unit cells, two atoms per cell, two orthonormal atom-centered functions per atom denoted by $\chi_{l\mathrm{X}p}$, with p being the basis function on atom X of the lth unit, i.e., $p = 1, 2$ and $X =$ A or B. Corresponding to each spatial orbital $\chi_{l\mathrm{X}p}$, there are two spin-orbitals $\chi_{l\mathrm{X}p}\alpha$ and $\chi_{l\mathrm{X}p}\beta$. The nuclear charges are $2|e|$. a is the lattice constant and u_0 describes the bond-length alternation, so that alternating atoms are displaced by $+u_0$ and $-u_0$ away from the equidistant positions. Thus, the two atoms of the nth unit cell are placed at

$$
z = \mp \frac{a}{4} + n \cdot a \pm u_0, \tag{3.30}
$$

where the upper (lower) sign is used for the A (B) atoms, and the two bond lengths have the values $\frac{a}{2} \pm 2u_0$.

Predetermined values for the field-free structural constants u_0 and a are obtained by adding an elastic contribution to the electronic energy. This contribution contains terms of 2nd and 4th order in the nearest and next-nearest bond lengths,

$$\begin{aligned} E_{\text{elastic}} = &\frac{f_1}{2}\sum_i (z_i - z_{i-1} - \frac{d_0}{2})^2 + \frac{f_3}{4}\sum_i (z_i - z_{i-1} - \frac{d_0}{2})^4 \\ &+ \frac{f_2}{2}\sum_i (z_i - z_{i-2} - d_0)^2 + \frac{f_4}{4}\sum_i (z_i - z_{i-2} - d_0)^4. \end{aligned} \tag{3.31}$$

Here z_i is the z coordinate of the A atom of the $\frac{i+1}{2}$th unit cell for odd i and of the B atom of the $\frac{i}{2}$th unit cell for even i. The parameters of this function (i.e., f_1, f_2, f_3, f_4, and d_0) are varied so that the field-free optimized geometry gives the desired values for a and u_0. In the finite chain calculations the structure of the central part of the chain containing N units is used for comparison with the infinite periodic chain as follows [the notation is the same as in Eq. (3.31)]

$$\begin{aligned} a &= \frac{1}{2}\left[(z_{N+1} - z_{N-1}) + (z_{N+2} - z_N)\right] \\ u_0 &= \frac{\pm 1}{8}\left[z_{N+2} - 3z_{N+1} + 3z_N - z_{N-1}\right], \end{aligned} \tag{3.32}$$

with the upper (lower) sign in the 2nd identity for odd (even) N. When the finite chain is sufficiently long the values of a and u_0, so obtained, agree with those of the infinite periodic chain. The origin of the coordinate system is chosen as the arithmetic average of all nuclear positions for the finite chains and as that of all nuclei in the Born von Kármán zone for the infinite periodic chains.

Two-center matrix elements of the field-free Hamiltonian are nonvanishing only between functions on neighboring atoms and vary linearly as a function of the interatomic distance. The one-electron contribution $\langle \chi_{l\mathrm{X}i}\sigma | \hat{h}_0 | \chi_{l\mathrm{X}j}\sigma \rangle$ to the one-center matrix elements, where $\hat{h}_0$ is the field-free one-electron operator, is non-zero only for $i = j$. From the two-electron matrix elements the only retained are $\langle \chi_{l\mathrm{X}i}\sigma_1\chi_{l\mathrm{X}i}\sigma_2 | v | \chi_{l\mathrm{X}i}\sigma_1\chi_{l\mathrm{X}i}\sigma_2 \rangle$, where $\hat{v}$ is the field-free two-electron operator.

For the finite chain the DC field is included in the electronic Hamiltonian through the term $-\sum_i E_{\mathrm{DC}} z_i$, where z_i is the z coordinate of the ith electron, E_{DC} is the amplitude of the DC field, and we have set the magnitude of the elementary charge $|e| = 1$. It turns

out to be important for this term that the matrix elements of the dipole moment operator are consistent with the overlap matrix elements. This is most conveniently achieved by fixing the spatial form of the basis functions, which for simplicity are chosen to be

$$\chi_{l\mathrm{X1}}(z) = \frac{1}{\sqrt{w_{\mathrm{X1}}}} \tag{3.33}$$

for

$$|z - z_0| \leq \frac{w_{\mathrm{X1}}}{2}, \tag{3.34}$$

and zero elsewhere;

$$\chi_{l\mathrm{X2}}(z) = \frac{1}{\sqrt{w_{\mathrm{X2}}}} \tag{3.35}$$

for

$$\frac{w_{\mathrm{X2}}}{4} \leq |z - z_0| \leq \frac{w_{\mathrm{X2}}}{2}, \tag{3.36}$$

and

$$\chi_{l\mathrm{X2}}(z) = \frac{-1}{\sqrt{w_{\mathrm{X2}}}} \tag{3.37}$$

for

$$|z - z_0| \leq \frac{w_{\mathrm{X2}}}{4}, \tag{3.38}$$

and zero elsewhere, where z_0 is the position of the atom X in the lth unit. The widths, w ($w_{\mathrm{X1}} > w_{\mathrm{X2}}$), are kept sufficiently small so that functions on non-neighboring atoms do not overlap.

The constructed parametrized model allows for extensive exploratory calculations and contains all essential elements of an *ab initio* Hartree-Fock (or Kohn-Sham) Hamiltonian including band orbitals with phases that may vary randomly from one k point to the next. Model calculations have demonstrated [12, 69, 62] that large finite chains and infinite periodic chains lead to the same results for polarization and structure as a function of field strength.

3.3 *Ab initio* LCAO-SCF algorithm

In this Subchapter we will give a short overview of the *ab initio* Linear Combination of Atomic Orbitals Self-Consistent Field (LCAO-SCF) method that is implemented in the so-called PLH (Polymer Linear Helical) code, one of the several existing *ab initio* programs for polymers, developed from the group in Namur, Belgium [1, 2, 31, 32].

3.3.1 LCAO basic principles

As already mentioned, the *ab initio* LCAO-SCF algorithm is based on the Hartree-Fock method and the one-electron wavefunctions are Bloch's functions. The Born-von Kármán periodic boundary conditions impose that the Bloch's functions are identical in the 0th and $2N+1$th unit cells (as implemented in the PLH code), with N tending to ∞. The crystalline orbitals are built as a linear combination of atom-centred basis functions

$$\psi_n(k,\vec{r}) = \sum_{p=1}^{N_b} C_{pn}(k) \frac{1}{\sqrt{2N+1}} \sum_{l=-N}^{N} e^{ikal} \chi_p^l(\vec{r}) = \sum_{p=1}^{N_b} C_{pn}(k) \chi_p(k,\vec{r}), \tag{3.39}$$

where the discrete k values have the spacing

$$\triangle k = \frac{2\pi}{(2N+1)a}. \tag{3.40}$$

N defines the short-range region consisting of $2N+1$ unit cells.

The orbital coefficients, $C_{pn}(k)$, and the orbital energies, $\epsilon_n(k)$, depend on the wavevector k and the k-dispersion curves of the latter form the band structure of the regular polymer. They are generally plotted in the half of the first Brillouin zone from $k=0$ to $k=\pi/a$, since

$$\epsilon_n(-k) = \epsilon_n(k) \tag{3.41}$$

and

$$\psi_n(-k) = \psi_n^*(k). \tag{3.42}$$

The first Brillouin zone, $[-\pi/a, \pi/a]$, is the equivalent of the Wigner-Seitz unit cell in the direct space. The $C_{pn}(k)$ are obtained from the iterative solution (SCF) of the Hartree-Fock equation

$$\underline{\underline{F}}(k) \cdot \underline{C_n}(k) = \epsilon_n(k) \cdot \underline{\underline{S}}(k) \cdot \underline{C_n}(k), \tag{3.43}$$

where n is the band index and the k-dependent matrices $\underline{\underline{S}}(k)$ and $\underline{\underline{F}}(k)$ are given by Eq. (3.8) and Eq. (3.10), respectively. Since long-range electrostatic effects are taken into account, we will show here only the direct space Fock matrix element between the atomic orbitals χ_p of the reference cell (0) and χ_q of the lth cell

$$\begin{aligned} F_{pq}^{0l} &= H_{pq}^{0l} + \sum_{l=-N}^{N} \sum_{r} \sum_{s} D_{rs}^{0j} \sum_{h=-\infty}^{\infty} G_{pqrs}^{0lhj} - \frac{1}{2} \sum_{l=-N}^{N} \sum_{h=-N}^{N} \sum_{r} \sum_{s} D_{rs}^{0j} G_{prqs}^{0hlj} \\ &= \underbrace{-\frac{1}{2} \left\langle \chi_p^0 \middle| \nabla^2 \middle| \chi_q^l \right\rangle}_{\text{kinetic energy term}} \underbrace{- \frac{1}{2} \sum_{h=-\infty}^{\infty} \sum_{A=1}^{N_C} \left\langle \chi_p^0 \middle| \frac{Q_A}{|r - R_A - hae_z|} \middle| \chi_q^l \right\rangle}_{\text{nuclear attraction}} \\ &+ \underbrace{\sum_{l=-N}^{N} \sum_{r} \sum_{s} D_{rs}^{0j} \sum_{h=-\infty}^{\infty} G_{pqrs}^{0lhj}}_{\text{electron repulsion}} \underbrace{- \frac{1}{2} \sum_{l=-N}^{N} \sum_{h=-N}^{N} \sum_{r} \sum_{s} D_{rs}^{0j} G_{prqs}^{0hlj}}_{\text{exchange term}}, \end{aligned} \tag{3.44}$$

with Q_A and R_A being the nuclear charge and the position in the reference unit cell of atom A. N_C is the number of atoms in the reference unit cell, D_{rs}^{0j} is the density matrix element obtained by integration over the first Brillouin zone according to Eq. (2.27), and the two electron integrals can be expressed as in Eq. (2.26). The sum over h in the nuclear attraction and electron repulsion terms (the Coulomb terms) runs from $-\infty$ to ∞ (long-range interaction), whereas it is restricted to N (short-range interaction) in the exchange term (see Fig. 3.1).

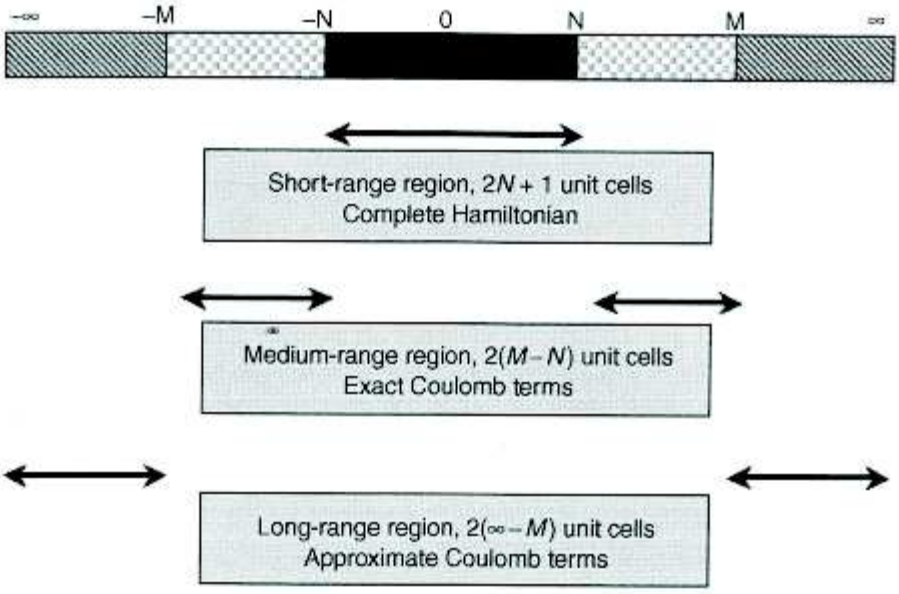

Figure 3.1: Sketch of the Namur threshold scheme for band structure calculations [2].

3.3.2 Specific aspects of the Hartree-Fock LCAO-SCF algorithm

Translational symmetry

One of the limitations, usually imposed in standard quantum chemical polymeric calculations, is the perfect stereoregularity of the infinite linear chain, which allows translational symmetry to be taken into account. This has the advantage that a lot of integral formulae are significantly simplified and the number of two-electron integrals to be stored decreases. For example, using the identities between translationally equivalent density matrix elements

$$D_{rs}^{hj} = D_{rs}^{0j-h}, \tag{3.45}$$

the electron density for polymers can be defined by

$$\begin{aligned} \rho(r) &= \sum_h \sum_j \sum_r \sum_s 2D_{rs}^{hj} \chi_r^h(r) \chi_s^j(r) \\ &= \sum_h \sum_j \sum_r \sum_s 2D_{rs}^{0j-h} \chi_r^h(r) \chi_s^j(r), \end{aligned} \tag{3.46}$$

where D_{rs}^{0j-h} is the density matrix element between atomic orbital χ_r in the origin cell 0 and atomic orbital χ_s in cell $j-h$. When using a new index $m = j-h$, the equation for the electron density becomes

$$\begin{aligned} \rho(r) &= \sum_h \sum_j \sum_r \sum_s 2D_{rs}^{0j-h} \chi_r^h(r) \chi_s^j(r) \\ &= \sum_m \sum_r \sum_s 2D_{rs}^{0m} \chi_r^h(r) \chi_s^{h+m}(r). \end{aligned} \tag{3.47}$$

The use of the translational symmetry is a considerable speed-up of the integral and SCF parts of the PLH program.

Integration of the density matrix

As it will be mentioned later, two procedures for integrating the density matrix from reciprocal to real space using Eq. (2.27) are implemented in the PLH code. The first one, called Gauss-Legendre (GL) [70], is a part of the so-called *nonoscillatory techniques*, which integrate the product of the density matrix elements by the exponential as a whole.

In the GL procedure the D_{rs}^{0j} are integrated at 12 non-equidistant k points in the half of the first Brillouin zone

$$\begin{aligned} D_{rs}^{0j} &= \frac{a}{\pi}\int_{-\frac{\pi}{a}}^{\frac{\pi}{a}} dk \left[\sum_n C_{rn}^*(k)C_{sn}(k)\right] e^{ikja} \\ &= \sum_{i=1}^{12} W_i \left[\sum_n C_{rn}^*(k)C_{sn}(k)\right] e^{ik_i ja}, \end{aligned} \tag{3.48}$$

with k_i and W_i being the abscissas and the weights [1] of the Gauss-Legendre procedure.

The second integration possibility, part of the *oscillatory techniques* and implemented in PLH, is the so-called Filon quadrature [71]. In

$$\begin{aligned} D_{rs}^{0j} &= \frac{a}{\pi}\int_{-\frac{\pi}{a}}^{\frac{\pi}{a}} dk \left[\sum_n C_{rn}^*(k)C_{sn}(k)\right] e^{ikja} \\ &= \frac{a}{\pi}\int_{-\frac{\pi}{a}}^{\frac{\pi}{a}} dk D_{rs}(k) e^{ikja} \\ &= \frac{2a}{\pi}\int_0^{\frac{\pi}{a}} dk \left\{\Re\left[D_{rs}(k)\right]\cos(kja) - \Im\left[D_{rs}(k)\right]\sin(kja)\right\} \end{aligned} \tag{3.49}$$

the numerical integration over half of the first Brillouin zone considers the trigonometric functions. This is a big adventure compared with the GL technique, which affords accurate results only for small number of unit cells. The Filon scheme is very efficient for slowly varying density matrix elements but requires the use of many integration points to reach high accuracies. In our calculation the density matrices are integrated using the Filon procedure.

There are other strategies [72] for dealing with the oscillation of D_{rs}^{0j} when a large number of unit cells is used. Their pros and cons as a function of the accuracy and the computational resources are compared from D. Jacquemin et al. in [73].

Quasi-linear dependencies

Quasi-linear dependencies, also called pseudolinear dependencies, may occur when the eigenvalues of the overlap matrix $S(k)$ are of the order of magnitude of 10^{-2} or smaller and, therefore, make the convergence of the SCF procedure difficult. For comparison, in molecular calculations linear dependence problems start when the eigenvalues are smaller than 10^{-6}. The reason of this different behaviour is the different truncation of the infinite

lattice sums. Beside the properly truncation of the latter, another way to remove the linear dependencies is through the canonical orthogonalization procedure of Löwdin [74]. The transformation matrix $T(k)$, which is used to transform the generalized eigenvalue problem (Eq. (3.43)) into the classical eigenvalue equation

$$\mathbf{F}^{'}(k)\mathbf{U}(k) = \mathbf{U}(k)\varepsilon(k), \tag{3.50}$$

where

$$\mathbf{F}^{'}(k) = \mathbf{T}^{\dagger}(k)\mathbf{F}(k)\mathbf{T}(k) \tag{3.51}$$

and

$$\mathbf{U}(k) = \mathbf{T}^{-1}(k)\mathbf{C}(k), \tag{3.52}$$

must obey

$$\mathbf{T}^{\dagger}(k)\mathbf{S}(k)\mathbf{T}(k) = \mathbf{1}. \tag{3.53}$$

In the Löwdin's canonical procedure $\mathbf{T}(k)$ is defined as

$$\mathbf{T}(k) = \mathbf{W}(k)\mathbf{s}^{-1/2}(k), \tag{3.54}$$

where $\mathbf{W}(k)$ and $\mathbf{s}(k)$ are the eigenvector and the eigenvalue matrices of the overlap matrix $\mathbf{S}(k)$, respectively,

$$\mathbf{S}(k)\mathbf{W}(k) = \mathbf{W}(k)\mathbf{s}(k). \tag{3.55}$$

If given eigenvalues $s_i(k)$ are very small, the matrix $\mathbf{T}(k)$ has columns with very large values, the inaccuracies in the Fock matrix elements increase cycle after cycle and the SCF procedure can oscillate that leads to a very slow convergence or nonconvergence. A possibility to circumvent this problem will be to eliminate the columns with the large values, i.e., those corresponding to small $s_i(k)$, in the matrix $\mathbf{W}(k)$ and to use a reduced transformed orthonormal Bloch basis set. These new functions will span the same region of space as the original one if the eliminated eigenvalues were exactly zero.

SCF convergence

There are several ways to stabilize and accelerate the convergence of the iterative SCF procedure, for instance through extrapolation, damping or level shifting. In the PLH code, this is done using a damping factor and can be expressed as

$$D_{rs}^{0j}(i^{\text{th}}\text{iteration}) = (1-d) \times D_{rs}^{0j}(i^{\text{th}}\text{iteration}) + d \times D_{rs}^{0j}(i-1^{\text{th}}\text{iteration}), \tag{3.56}$$

i.e., the new density matrix includes a percentage of the previous one. The damping factor is specified at the beginning and all iterations are "damped" until the end of the SCF procedure. To ensure the idempotency of the density matrix an iteration with $d = 0$ is needed [75].

3.3.3 Longitudinal polarizability and second hyperpolarizability

Theoretical descriptions of the linear (polarizability α) and nonlinear (first β and second γ hyperpolarizability) properties of materials provide important complementary information to the experimental studies, therefore, in the last years there is an intense research activity in this field. According to the quantities required to compute the polarizability, there are two classes of methods. In the first, one needs to know the field-perturbed wavefunctions and energies, whereas in the second the polarizabilities can be obtained directly without any knowledge of these field-perturbed wavefunctions.

In the presence of electric field, a dipole moment is induced in the system and the total dipole moment is given by

$$\mu(\mathbf{E}) = \mu_0 + \mu^{ind}(\mathbf{E}), \tag{3.57}$$

where $\mathbf{E}$ is the field strength E_{DC}, μ_0 is the permanent dipole moment per unit cell in the absence of electric field and

$$\mu^{ind}(\mathbf{E}) = \alpha\mathbf{E} + \frac{1}{2!}\beta\mathbf{E}^2 + \frac{1}{3!}\gamma\mathbf{E}^3 + \dots \tag{3.58}$$

The last expression is consistent with the definition of μ as the derivative of the energy, $\mathcal{E} \equiv E_{\text{tot}}$, with respect to the field

$$\mu(\mathbf{E}) = -\frac{\partial\mathcal{E}(\mathbf{E})}{\partial\mathbf{E}}. \tag{3.59}$$

In our case the field is applied in the z-direction along the polymer axis

$$\mathbf{E} = E_z \mathbf{e}_z, \tag{3.60}$$

and the total energy of the system can be expressed as

$$\begin{aligned}\mathcal{E}(E_z) = \mathcal{E}_0 + \left(\frac{d\mathcal{E}}{dE_z}\right)_{E_z=0} E_z + \frac{1}{2!}\left(\frac{d^2\mathcal{E}}{dE_z^2}\right)_{E_z=0} E_z^2 \\ + \frac{1}{3!}\left(\frac{d^3\mathcal{E}}{dE_z^3}\right)_{E_z=0} E_z^3 + \frac{1}{4!}\left(\frac{d^4\mathcal{E}}{dE_z^4}\right)_{E_z=0} E_z^4 + \dots\end{aligned} \tag{3.61}$$

Using the Hellmann-Feynman theorem [76] and procedures that are variational with respect to all parameters in the case of Hartree-Fock approximation, the following relations can be stated. For the dipole moment

$$\mu_z = -\left(\frac{d\mathcal{E}}{dE_z}\right)_{E_z=0} \tag{3.62}$$

and for the polarizability

$$\alpha_{zz} = -\left(\frac{d^2\mathcal{E}}{dE_z^2}\right)_{E_z=0} = \left(\frac{d\mu}{dE_z}\right)_{E_z=0}, \tag{3.63}$$

i.e., the polarizability can be considered as the second-order term in the perturbation expansion of the electronic energy with respect to the field or as the linear response of the dipole moment to an external electric field.

For the first and second hyperpolarizability one can respectively apply

$$\beta_{zzz} = -\left(\frac{d^3\mathcal{E}}{dE_z^3}\right)_{E_z=0} = \left(\frac{d^2\mu}{dE_z^2}\right)_{E_z=0} \tag{3.64}$$

$$\gamma_{zzzz} = -\left(\frac{d^4\mathcal{E}}{dE_z^4}\right)_{E_z=0} = \left(\frac{d^3\mu}{dE_z^3}\right)_{E_z=0}. \tag{3.65}$$

These double equalities lead to two ways to compute β_{zzz} and γ_{zzzz}; either as the negative of the third- and fourth-order perturbation term of the energy with respect to the applied field or as the second- and third-order response of the dipole moment to this field.

In our results and discussions we will concentrate on the polarizability and the second hyperpolarizability, therefore, here we will show how they can be calculated using the two

classes of methods mentioned above. In the case of centrosymmetric systems, like the hydrogen chain, the first hyperpolarizability, β_{zzz}, is zero.

In the first class, the most simple method to use is the numerical Self-Consistent Field Finite-Field method (SCF-FF) of Cohen and Roothaan [77], which is equivalent to a coupled Hartree-Fock (CHF) scheme and can always be used if there is no analytical procedure available. The FF technique consists of computing the energy of the system and the dipole moment per unit (corresponds to the polarization in the case of infinite periodic systems) for different field strengths and considering the finite-difference formulae. For the polarizability using the field-dependent energy one can apply

$$\alpha_{zz} = -\left(\frac{d^2\mathcal{E}(E_z)}{dE_z^2}\right)_{E_z=0} = \lim_{E_z\to 0} -\frac{\mathcal{E}(E_z)+\mathcal{E}(-E_z)-2\mathcal{E}(0)}{E_z^2} \tag{3.66}$$

and when centrosymmetric systems are considered

$$\alpha_{zz} = -\left(\frac{d^2\mathcal{E}(E_z)}{dE_z^2}\right)_{E_z=0} = \lim_{E_z\to 0} 2\frac{\mathcal{E}(0)-\mathcal{E}(E_z)}{E_z^2}. \tag{3.67}$$

Using the dipole moment per unit the following relation is valid

$$\alpha_{zz} = \left(\frac{d\mu_z}{dE_z}\right)_{E_z=0} = \lim_{E_z\to 0} \frac{\mu_z(E_z)-\mu_z(-E_z)}{2E_z} \tag{3.68}$$

and for centrosymmetric systems

$$\alpha_{zz} = \left(\frac{d\mu_z}{dE_z}\right)_{E_z=0} = \lim_{E_z\to 0} \frac{\mu_z(E_z)}{E_z}. \tag{3.69}$$

If the Hellmann-Feynman theorem is not satisfied the expressions Eq. (3.66) and Eq. (3.68) and for centrosymmetric compounds Eq. (3.67) and Eq. (3.69) will provide different solutions. When dealing with methods including electron correlation where the dipole moment is not directly available, Eq. (3.66) and Eq. (3.67) are often used. Electron correlation can be investigated in the framework of Møller-Plesset partitioning [78] at the second (MP2), third (MP3) or fourth (MP4) level of electron correction or dealing with the coupled-cluster (CC) ansatz [79] including all double (CCD), all single and double excitations (CCSD), and all single and double as well as a perturbational estimate of the connected triple excitations (CCSDT). Champagne and co-workers investigated the effects of electron correlations on the static longitudinal polarizability [3, 4] and on the static longitudinal second hyperpolarizability [80], using all the methods mentioned above, together with the uncoupled (UCHF) (equivalent to the SOS method described bellow)

and coupled Hartree-Fock (CHF) (equivalent to the FF technique) calculations. In our investigations electron correlations are not taken into account.

The second hyperpolarizability can also be calculated using the FF procedure

$$\gamma_{zzzz} = -\left(\frac{d^4\mathcal{E}(E_z)}{dE_z^4}\right)_{E=0} = \lim_{E_z\to 0} -\frac{8\mathcal{E}(E_z) - 2\mathcal{E}(2E_z) - 6\mathcal{E}(0)}{E_z^4}, \tag{3.70}$$

where the field amplitude has to be sufficiently small to satisfy the $E_z \to 0$ condition, since the contaminations from the higher-order hyperpolarizabilities increase as the even powers of the field amplitude.

In the absence of an external electric field, the linear and non-linear properties of the system can be calculated with a method based on the Sum Over States (SOS) perturbation expansion of the Roothaan-Hartree-Fock wavefunction. Then, the polarizability is expressed through wavefunctions and state energies as

$$\alpha_{\sigma\nu} = 2\sum_m \frac{\langle\Psi_0|\mu_\sigma|\Psi_m\rangle\,\langle\Psi_m|\mu_\nu|\Psi_0\rangle}{\mathcal{E}_m - \mathcal{E}_0}, \tag{3.71}$$

where the sum is over the excited states m, and Ψ_0 and Ψ_m are the ground and excited states Hartree-Fock wavefunctions associated with the energies $\mathcal{E}_0$ and $\mathcal{E}_m$, respectively. The relation can be transformed to

$$\alpha_{\sigma\nu} = 4\sum_i \sum_a \frac{\langle\psi_i|\mu_\sigma|\psi_a\rangle\,\langle\psi_a|\mu_\nu|\psi_i\rangle}{\mathcal{E}_a - \mathcal{E}_i}. \tag{3.72}$$

ψ_i and ψ_a represent the doubly-occupied and unoccupied molecular orbitals with the corresponding energies $\mathcal{E}_i$ and $\mathcal{E}_a$.

Then, the longitudinal polarizability per unit cell in the case of infinite periodic systems is written as

$$\alpha_{zz} = 4\sum_i \sum_a \sum_k \sum_{k'} \frac{|\,\langle\psi_i(k')|z|\psi_a(k)\rangle\,|^2}{\mathcal{E}_a(k') - \mathcal{E}_i(k)}, \tag{3.73}$$

where the summations i and a are over the occupied and unoccupied molecular orbitals and the other two summations over the quasimomenta k and k', respectively. In [1] is shown how the dipole integrals can be expressed through the so-called dipole transition strengths or oscillator strengths, $\Omega_{ia}(k)$, between the occupied and unoccupied crystal orbitals i and a. Here we will give only the end formula for the longitudinal polarizability

$$\alpha_{zz} = 4 \sum_{i} \sum_{a} \sum_{k} \frac{|\Omega_{ia}(k)|^2}{\mathcal{E}_a(k) - \mathcal{E}_i(k)}, \tag{3.74}$$

where

$$\Omega_{ia}(k) = \sum_{p} \sum_{q} C^*_{pi}(k) \left[\frac{\partial}{\partial k} S_{pq}(k) - i M_{pq}(k) + S_{pq}(k) \frac{\partial}{\partial k} \right] C_{qa}(k). \tag{3.75}$$

The k-dependent dipole matrix elements are defined as

$$M_{pq}(k) = \sum_{l=-N}^{N} e^{ikla} M^{0l}_{pq} = \sum_{l=-N}^{N} e^{ikla} \langle \chi^0_p | z | \chi^l_q \rangle \tag{3.76}$$

and the derivatives of the overlap matrices

$$S_{pq}(k) = \sum_{l=-N}^{N} e^{ikla} S^{0l}_{pq} \tag{3.77}$$

as

$$\frac{\partial}{\partial k} S_{pq}(k) = ia \sum_{l=-N}^{N} l e^{ikla} S^{0l}_{pq}. \tag{3.78}$$

The derivatives of the orbital coefficients with respect to the wavevector k are calculated analytically using procedure developed by Pople [81] and shortly introduced in [1]. It involves the differentiation of the generalized eigenvalue problem

$$\begin{aligned} \mathbf{F}(k)\mathbf{C}(k) &= \mathbf{S}(k)\mathbf{C}(k)\mathbf{E}(k) \\ \mathbf{F}'\mathbf{C}(k) + \mathbf{F}(k)\mathbf{C}'(k) &= \mathbf{S}'(k)\mathbf{C}(k)\mathbf{E}(k) + \mathbf{S}(k)\mathbf{C}'(k)\mathbf{E}(k) + \mathbf{S}(k)\mathbf{C}(k)\mathbf{E}'(k) \end{aligned} \tag{3.79}$$

and of the orthogonalization condition

$$\begin{aligned} \mathbf{C}^\dagger(k)\mathbf{S}(k)\mathbf{C}(k) &= 1 \\ \mathbf{C}^{\dagger\prime}(k)\mathbf{S}(k)\mathbf{C}(k) + \mathbf{C}^\dagger(k)\mathbf{S}'(k)\mathbf{C}(k) + \mathbf{C}^\dagger(k)\mathbf{S}(k)\mathbf{C}'(k) &= 0. \end{aligned} \tag{3.80}$$

The derivative of the Fock matrix $\mathbf{F}'(k)$ is obtained in the same way as $\mathbf{S}'(k)$. Assuming that

$$\mathbf{C}'(k) = \mathbf{C}(k)\mathbf{U}(k) \tag{3.81}$$

and multiplying the above equations on the left by $\mathbf{C}^{\dagger}(k)$, after some manipulations it follows that

$$\mathbf{G}(k) + \mathbf{E}(k)\mathbf{U}(k) = \mathbf{R}(k)\mathbf{E}(k) + \mathbf{U}(k)\mathbf{E}(k) + \mathbf{E}^{'}(k) \tag{3.82}$$

and

$$\mathbf{U}^{\dagger}(k) + \mathbf{R}(k) + \mathbf{U}(k) = 0, \tag{3.83}$$

where

$$\begin{aligned} \mathbf{G}(k) &= \mathbf{C}^{\dagger}(k)\mathbf{F}^{'}(k)\mathbf{C}(k) \\ \mathbf{R}(k) &= \mathbf{C}^{\dagger}(k)\mathbf{S}^{'}(k)\mathbf{C}(k). \end{aligned} \tag{3.84}$$

One arrives to the following equation for the elements of the dipole oscillator strength matrix

$$\Omega_{ia}(k) = U_{ia}(k) + \sum_{p}\sum_{q} C^{*}_{pi}(k)\left[\frac{\partial}{\partial k}S_{pq}(k) - iM_{pq}(k)\right]C_{qa}(k) \tag{3.85}$$

with

$$U_{ia}(k) = \frac{G_{ia}(k) - R_{ia}(k)\mathcal{E}_a(k)}{\mathcal{E}_a(k) - \mathcal{E}_i(k)} \tag{3.86}$$

when $i \neq a$ and

$$\begin{aligned} U_{ii}(k) &= -\frac{1}{2}R_{ii}(k) \\ \mathcal{E}^{'}_{i}(k) &= G_{ii}(k) - R_{ii}(k)\mathcal{E}_i(k). \end{aligned} \tag{3.87}$$

The equation for calculating the longitudinal second hyperpolarizabiliy using the SOS method is more complicated since γ_L is related to the fourth-order energy term. Starting from the standard time-independent perturbation theory, it can be written as [80]

$$\begin{aligned} \gamma_L = &-24\sum_{m}\sum_{p}\sum_{q}\frac{\langle\Psi_0|\mu_L|\Psi_m\rangle\overline{\langle\Psi_m|\mu_L|\Psi_p\rangle\langle\Psi_p|\mu_L|\Psi_q\rangle}\langle\Psi_q|\mu_L|\Psi_0\rangle}{(\mathcal{E}_0 - \mathcal{E}_m)(\mathcal{E}_0 - \mathcal{E}_p)(\mathcal{E}_0 - \mathcal{E}_q)} \\ &+24\sum_{p}\frac{\langle\Psi_0|\mu_L|\Psi_p\rangle\langle\Psi_p|\mu_L|\Psi_0\rangle}{(\mathcal{E}_0 - \mathcal{E}_p)}\sum_{m}\frac{\langle\Psi_0|\mu_L|\Psi_m\rangle\langle\Psi_m|\mu_L|\Psi_0\rangle}{(\mathcal{E}_0 - \mathcal{E}_m)^2}, \end{aligned} \tag{3.88}$$

where Ψ_0 and Ψ_m are the ground and the mth excited state wavefunctions, respectively, with the corresponding energies $\mathcal{E}_0$, and $\mathcal{E}_m$. μ_L is the longitudinal dipole moment and

$$\overline{\langle \Psi_m | \mu_L | \Psi_p \rangle} = \langle \Psi_m | \mu_L | \Psi_p \rangle - \langle \Psi_0 | \mu_L | \Psi_0 \rangle \delta_{mp}. \tag{3.89}$$

The SOS method for calculating directly the longitudinal polarizability per unit cell of infinite systems is implemented in the PLH package. Since field-induced electron reorganizational effects are not considered and the wave functions are constructed from Hartree-Fock occupied and unoccupied one-electron spin orbitals, the Sum Over States technique is equivalent to an uncoupled Hartree-Fock (UCHF) scheme.

3.3.4 The PLH (Polymer Linear Helical) package

The PLH program is a Fortran coding of different techniques, developed, mainly in the Namur group, for the calculation of the electron band structures of regular or helical polymers and their polarizabilities. It consists of five consecutive program modules:

1) PLH0: input geometry and basis set.

2) PLH1: computation of one-electron integrals.

3) PLLD: test of possible linear dependence effects.

4) PLH2: calculation of two-electron integrals.

5) PLH3: self-consistent field (SCF) iterations, printing of energy bands and a short population analysis.

A preliminary program is added in order to test the input geometry:

PLMDIS: generates input file used in molecular graphics programs.

and an additional module:

PLHSOS: calculates longitudinal polarizabilities per unit cell and per unit length using the Sum Over States (SOS) method.

The results obtained from running PLH can be represented graphically using:

BANDDOS: a highly interactive graphics package, which permits the ordering of the band structure and the display of the density of states and their convolution.

The present version of the package accepts s, p and d atomic orbitals and the total number of atoms and shells in the unit cell are limited to 50 and 80, respectively. A maximum of 6 primitive Gaussians are allowed to represent the atomic orbital and the number of basis functions per unit cell is limited to 255. Some notable features include:

- Extension of the multipole expansion to the helical case [82].

- The use of compact Coulomb integrals formalism, which drastically reduces the storage required for the two-electron integrals of the Coulomb contribution [83, 32, 84].

- The numerical integration of the density matrices using 12-point Gauss-Legendre quadrature, allowing a numerically precise integration over the first Brillouin zone [85].

- The possibility of using a Filon-like quadrature procedure to perform the integration of the density matrices [71].

- The Löwdin canonical orthogonalization procedure to treat the possible basis linear dependence problems [74].

- The direct calculation of the first derivative of the energy bands required for getting the correct indexing and labelling of bands in the density of states (DOS) calculations [86, 87].

- The calculation of the longitudinal SOS (Sum Over States) polarizability per unit cell [88].

For the computation of the two-electron integrals, two separate algorithms are implemented - the Pople and Hehre method [89] and the McMurchie-Davidson scheme [90]. For basis sets including just s and p orbitals, the two-electron integrals are calculated using the first method and when d orbitals are included in the basis set, the second one is used. The choice of the algorithm to use is decided internally by the program.

The input file of PLH consists of two "data groups", $GEOM and $BASIS, and optional "keyword cards", e.g., $AU, $NOLONG, $ONEINT, $TWOINT, $SCF and $SOS. An example for a polyacetylene input file is given in Fig. (3.2).

Each "data group" begins with a card, which has an & (Ampersand) or a $ (Dollar) sign as its first character and ends with a "blank" card or card with the keywords & END or $END. Each "data group" can be located anywhere in the input data file, however, the data must be introduced in the order indicated within each "data group". A "keyword

```
$GEOM

     Polyacetylene   STO-3G     GEOM SUHAI

21 2.47709   41 0 0
  C      0.33065        0.000000    0.59614
  C     -0.33065        0.000000   -0.59614
  H      1.41772        0.000000    0.57926
  H     -1.41772        0.000000   -0.57926

$BASIS
33033030309
  1 2
         1S   S 3 5.67
       2.227660    0.154329 0.0
       0.405771    0.535328 0.0
       0.109818    0.444635 0.0
        2SP  SP 3 1.72
       0.9942030  -0.0999672  0.155916
       0.2310310   0.3995130  0.607684
       0.0751386   0.7001150  0.391957
****
  3 4
         1S   S 3 1.24
       2.22766     0.154329 0.0
       0.405771    0.535328 0.0
       0.109818    0.444635 0.0
****
$END
$SCF  PRINT 3 DEPTHR 4 FILON
&END
```

Figure 3.2: Example for an input file for a polyacetylene chain when a $STO-3G$ basis set is used.

card" begins also with an & or $ sign in the first column, followed by the keyword card name and eventually some keywords. It can occur anywhere in the input data file, except inside a "data group", and can be absent. The "keyword cards" are optional and the order in which they appear is not important.

In our example (Fig. (3.2)) the following data are evident:

"Data group" $GEOM

CARD 0

$GEOM - in the program the geometry is default to be given in Angstöm. If there is the optional keyword <AU>, then the nuclear coordinates and the cell length are expressed in atomic units.

The following three cards are intended for title designation. Or like in Fig. (3.2):

CARD 1
Blank card.

CARD 2
Title format: "Polyacetylene STO-3G GEOM SUHAI"

CARD 3
Blank card.

CARD 4
NUMCEL, CEL, NCELH, <IALPHA, ITURN (or FALPHA)>

NUMCEL - the total number of cells used in the lattice summations. Maximum allowed value is 21 (like in our example).

CEL - the length of the unit cell (=2.47709).

NCELH - the number of cells defining the short and intermediate regions in the calculations of the long-range Coulomb interactions. The default and minimal value is $(4*N+1)$, where $N = (\text{NUMCEL} - 1)/2$. In these regions, the two-electron integrals are explicitly computed. Outside these regions, the third-order multipole expansion technique is used.

<IALPHA, ITURN (or FALPHA)> - are defined when helical symmetry is used. In our example this is not the case, therefore, they are zero.

CARD 5
LABEL, X, Y, Z - define the atomic symbols and the coordinates of the atoms in the unit cell.

CARD 6
Blank line or &END or $END keyword defining the end of the list of atoms.

"Data group" $BASIS - defines the atomic basis set and is read in the PLH0 program.

CARD 0
$BASIS

CARD 1

ISHELL(I) - number of Gaussian functions (degree of contraction) in each shell. The maximum permitted degree of contraction is 6. The order of the atomic centers must correspond to the order of the center definition in "data group" GEOM. The centers are delimited by a contraction of 0 and the list by a 9. In our example the sequence 33033030309 has the following meaning:

- The first center (the first carbon atom) has 3 Gaussians to describe the atomic orbital(s) in the first shell and 3 for the second shell

- The second center (the second carbon atom) has also 3 contracted Gaussians for each of the two shells.

- The third center (the first hydrogen atom) has a single shell formed by 3 Gaussians.

- The fourth center (the second hydrogen atom) has also a single shell with 3 Gaussians.

CARD 2

ICENT(I) - gives the center serial numbers (1 and 2 for the two carbon atoms or 3 and 4 for the two hydrogen atoms).

CARD 3

IORB, ITYPE, NGAUSS, SC define:

IORB - the orbital used in printing (1S, 2SP),

ITYPE - the type of shell (S, P, D),

NGAUSS - the number of Gaussians (3) (degree of contraction),

SC - a scale factor (5.76, 1.72 and 1.24) for the current shell.

CARD 4

$****$ in columns 1-4.

The cards 2, 3 and 4 are repeated for each different shell definition block corresponding to each type of atom.

CARD 5

Ends the input of the atomic basis set with a blank card or &END or $END keyword.

"Keyword cards" - their specification is optional and they are used to modify the default execution of the program.

In (Fig. (3.2)) the following "keyword cards" are used:

$SCF PRINT 3 DEPTHR 4 FILON - change the default value in the SCF program and are read in the PLH3.

PRINT 3 - prints eigenvalues and MO coefficients for each iteration in the SCF procedure.

DEPTHR 4 - threshold 10^{-4} used in the test of possible near linear dependence in the basis set.

FILON - the Filon quadrature procedure is used, instead of the Gauss-Legendre, to compute the density matrix elements.

Another optional modifications in this card could be:

THRESHOLD n - the SCF is assumed to converge when density matrix elements do not differ by a value greater than 10^{-n}.

NKP k - the number $(2^k + 1)$ defines the number of equidistant k-points in the first Brillouin zone used in the printing of the band structure.

EPS n - threshold for the convergence of the Filon quadrature. It is assumed to converge when the difference between the values obtained when using 2^i and $2^{(i-1)}$ points do not differ by a value greater than 10^{-n} at the ith iteration.

ISUBMX - fixes the number of iterations in the Filon procedure. Default value is ISUBMX = 6.

DAMPING na - an integer that corresponds to the percentage of the density matrix calculated at the $(n-1)$th iteration used in the calculation of the density matrix at the nth iteration. The default value is zero, corresponding to no damping. The use of a small damping factor can stabilize the iterative procedure in the case of convergence problems.

The input files for the investigated systems are similar to those in (Fig. (3.2)) and will be shown later.

3.4 From VPA to *ab initio* LCAO-SCF as implemented in the PLH code

The goal of this part of our study is twofold: (1) to calculate the dipole moment per unit, i.e., the polarization, of a real polymer in absence of electric field and (2) to find out how such infinite periodic chain responds to external perturbation, i.e., to determine the polarization but in the presence of electrostatic field. For these purposes, the required expressions are taken from the vector potential approach (VPA) and implemented in the self-consistent field (SCF) procedure of the *ab initio* PLH code, which is run two times - without and with external field. Fig. (3.3) shows a flowchart of a typical SCF algorithm together with the additional quantities and the places where they should be implemented.

At the first run the polarization of the system in absence of electric field is calculated at each SCF iteration {(1)}. After convergence the SCF procedure is run again and the polarization energy expression (E_{pol}) is added to the Fock matrix direct at the first iteration {(2)}. A new convergence provides the total polarization (P_{tot}) and the total energy (E_{tot}) of the system in the case of external perturbation.

In the following the main steps of the SCF algorithm are briefly discussed.

'R_A, Z_A, N, φ'

At the beginning the input geometry of the system is specified (R_A - nuclear coordinates, Z_A - atomic numbers, N - number of electrons) and the basis set φ is defined. All this is done in PLH0. For a very small set of functions per atom a Slater-type functions are used. In polyatomic calculations and for a large number of functions per atom Gaussian-type functions are utilized.

'Calculate S_{pq}, H_{pq}^{core}, $pq|rs$'

The one- (H_{pq}^{core}) and two-electron ($pq|rs$) integrals are evaluated in PLH1 and PLH2 by means of Eq. (2.24) and Eq. (2.26), respectively, and the overlap matrix (S_{pq}) is determined using Eq. (2.22). The three quantities are calculated only once, since they remain constant during the iterative calculation.

'Diagonalize S to get X'

The overlap matrix is diagonalized and the transformation matrix **X** is obtained.

'First guess for D'

The simplest possible guess for the density matrix is to use a **zero** matrix, which is equivalent to approximating **F** as **H** and neglecting all electron-electron interactions in

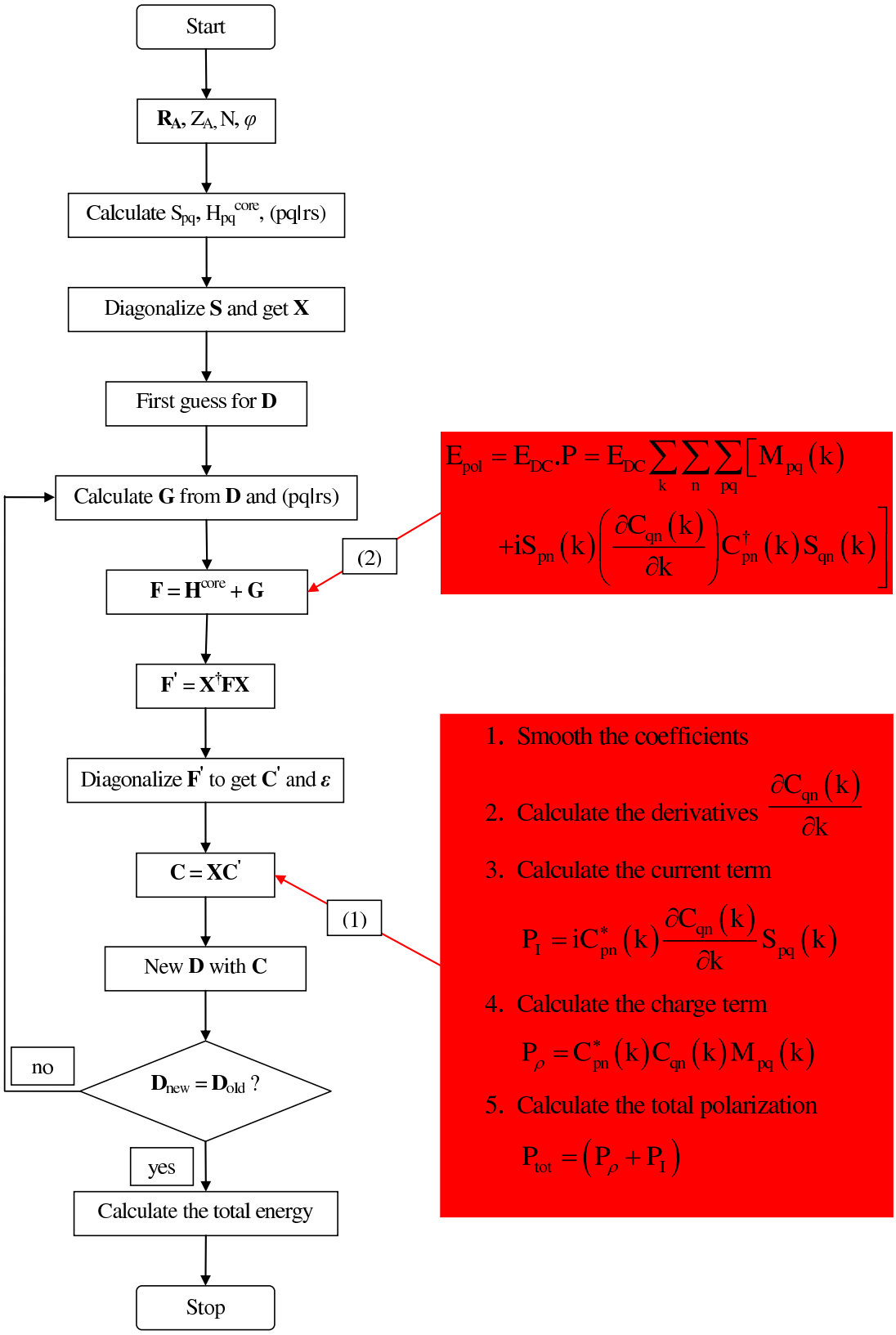

Figure 3.3: Flowchart of the self-consistent field (SCF) procedure. On the right in red are shown the additional quantities that should be implemented.

the first iteration, since $\mathbf{G}$=0 (see Eq. (2.25) and Eq. (2.23)).

'Calculate G from D and $pq|rs$'

The two-electron part of the Fock matrix is calculated using Eq. (2.25). At the first iteration $\mathbf{G}$ is zero since the first guess of the density matrix is the **zero** matrix.

'$\mathbf{F} = \mathrm{H}^{\mathrm{core}} + \mathbf{G}$'

$\mathbf{G}$ is added to the core-Hamiltonian to obtain the Fock matrix. At the first iteration $\mathbf{F} = \mathrm{H}^{\mathrm{core}}$.

'$\mathbf{F}' = \mathbf{X}^{\dagger}\mathbf{F}\mathbf{X}$'

The transformed Fock matrix ($\mathbf{F}'$) is calculated by means of the transformation one ($\mathbf{X}$).

'Diagonalize $\mathbf{F}'$ to get $\mathbf{C}'$ and ϵ'

$\mathbf{F}'$ is diagonalized to obtain the transformed orbital coefficients matrix ($\mathbf{C}'$) and the eigenvalues ϵ.

'$\mathbf{C} = \mathbf{X}\mathbf{C}'$'

The orbital coefficient matrix is evaluated using the transformation ($\mathbf{X}$) and the transformed orbital coefficients matrix ($\mathbf{C}'$).

Before calculating the new density matrix, the additional steps $\{(1)\}$, shown in the red box on the right of Fig. (3.3), are added to the SCF procedure. First, the orbital coefficients are made a smooth function of the wavevector k using the implemented smoothing procedure, then the derivatives of the coefficients ($\frac{\partial C_{qn}(k)}{\partial k}$), the current ($P_{\mathrm{l}}$) and the charge ($P_{\rho}$) contributions to the polarization, and at the end the total polarization (P_{tot}) of the system in the case when there is no field are calculated.

'New D with C'

The new density matrix is formed from the orbital coefficients using Eq. (2.27). The utilized smoothing procedure do not affect $\mathbf{D}$, i.e., the density matrix calculated with the smooth coefficients is equal to the one evaluated using the nonsmooth coefficients.

'$\mathbf{D}_{new} = \mathbf{D}_{old}$?'

The new formed density matrix is compared with the old one if it is the same within a specified criterion in order to check if the procedure has converged. If $D_{new} \neq D_{old}$ i.e., if there is no convergence, one returns to the step **'Calculate G from D and $pq|rs$'**,

where the two-electron part of the Fock matrix is calculated using D_{new} and the second iteration is starting. The next steps are repeated till convergence, i.e., till $D_{new} = D_{old}$ within a specified criterion.

'Calculate $E_{\rm tot}$'

The quantities $\mathbf{C}, \mathbf{D}, \mathbf{F}$ calculated at the last iteration are the final ones and are used to evaluate the total energy ($E_{\rm tot}$) of the system via Eq. (3.29) and other quantities of interest.

At the second run of the SCF procedure the polarization energy expression ($E_{\rm pol}$) is added to the Fock matrix $\{(2)\}$ directly at the first iteration. The field strength is different from zero and the two terms in the square brackets (see also Eq. (3.13)) correspond to the field free P_ρ and $P_{\rm I}$, respectively, calculated at the first SCF run. Again steps **'Calculate G from D and** $pq|rs$**'** to **'$\mathbf{D}_{new} = \mathbf{D}_{old}$?'** are repeated till the new density matrix is equal to the old one within a specified criterion. At each iteration the orbital coefficients are smoothed and the total polarization is calculated. After convergence the total energy of the system in the case of field is determined.

Our calculations show that for larger field strength ($E_{\rm DC} > 0.001$ a.u.) the second run of the SCF procedure converges more slowly than the first one, whereas when the field is weak the field free case requires more iterations till convergence.

3.5 Hydrogen chain

In order to highlight our first *ab initio* results, we use model hydrogen systems, which have already been used many times in atomic, molecular, polymeric and solid state forms to demonstrate new quantum chemical techniques and features. Fig. (3.4) shows different chain models for N from 1 to 4. Adding more and more unit cells, an infinite chain with $N \to \infty$ can be achieved.

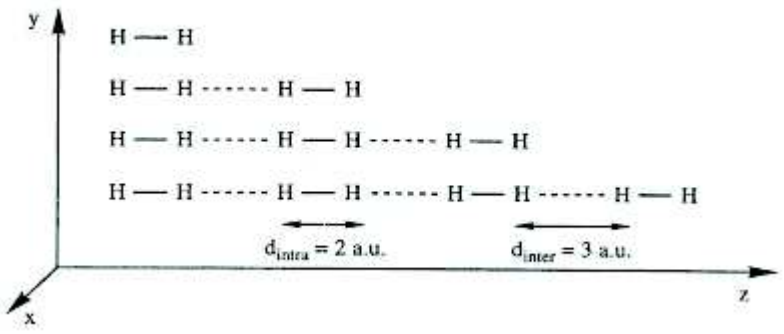

Figure 3.4: Space representation of the different hydrogen chain models [3].

In our calculations we use the minimal ($STO-3G$) and the double-zeta ($3-21G$) atomic basis sets and compare the results with experimental and previous theoretical investigations. Fig. (3.5) and Fig. (3.6) show the input files for the $STO-3G$ and the $3-21G$ basis sets, respectively. In both cases the intermolecular (intramolecular) distances are 3.0 a.u. (2.0 a.u.) that correspond to unit cell lengths of $a = 5.0$ a.u. and $H-H$ bond lengths of $d_{\mathrm{H-H}} = 2.0$ a.u. The single shell (s) ($STO-3G$) of the two hydrogen atoms is formed by 3 contracted Gaussians with the corresponding exponents, and the s and p shells ($3-21G$) by 2 and 1 Gaussians, respectively. For the minimal basis set we evaluated all the quantities in the field range of $0 \leq E_{\mathrm{DC}} \leq 0.01$ a.u. and for the larger one in the range $0 \leq E_{\mathrm{DC}} \leq 0.006$ a.u.

The results for the hydrogen chain model with the two basis sets are shown in parallel and organized as follows: first the successful implementation of the smoothing procedure is demonstrated (3.5.1) through the change of the phases φ_{pn} with the wavevector k. Then, we investigated the dependence of the total energy, E_{tot}, of the system and of the polarization, P, on the applied electric field, E_{DC}; calculated the polarizability, α, and compared our results with previous ones (3.5.2). How E_{tot}, P and α change with the $H-H$ distance, $d_{\mathrm{H-H}}$ (3.5.3), and with the unit cell length, a (3.5.4), is also explored. At

```
$GEOM AU
    HYDROGEN
H2 : bond length alternation 2/3 a.u.

21   5.0    41   0 0
 H      0.00000000  0.00000000  1.00000000
 H      0.00000000  0.00000000 -1.00000000

$BASIS
3039
 1 2
        1S   S 3  1.24
2.227660584,  0.1543289673, 0.0
0.4057711562, 0.5353281423, 0.0
0.1098175104, 0.4446345422, 0.0
****

$END
$SCF  PRINT 3 DEPTHR 4 FILON  NKPRT 5
```

Figure 3.5: Input file for a hydrogen chain in the case of $STO-3G$ basis set. The distance between the two hydrogen atoms in the unit cell is 2.0 a.u. and the unit cell length is 5.0 a.u.

```
$GEOM AU
    HYDROGEN
H2 : bond length alternation 2/3 a.u.

21    5.0    41   0 0
 H      0.00000000  0.00000000  1.00000000
 H      0.00000000  0.00000000 -1.00000000

$BASIS
210219
 1 2
        1S   S 2  1.10
4.50180,  0.156285, 0.0
0.681444, 0.904691, 0.0
        2S   S 1  1.10
0.151398, 1.000000, 0.0
****

$END
$SCF  PRINT 3 DEPTHR 4 FILON  NKPRT 5
```

Figure 3.6: The same like in Fig. (3.5) but in the case of $3-21G$ basis set.

the end the second hyperpolarizability is calculated and compared with previous results. Due to the symmetrical placed hydrogen atoms in the unit cell, the nuclear contribution to the polarization (P_n) is zero and $P_{\text{tot}} = P_e$. For the same reason, all quantities are calculated only for $E_{\text{DC}} > 0$.

3.5.1 The change of the phases φ_{pn} with the wavevector k

To check the implementation of the smoothing procedure in the PLH code, we calculated the change of the phases from one k point to the next one and plotted the distribution toward ka/π. If the orbital coefficients are successfully smoothed at each iteration in the SCF procedure, the φ_{pn} should change smoothly with the wavevector in the first Brillouin zone. Discontinuities may occur at the zone boundaries, $k = \pm\pi$. The following formula was used to evaluate the φ_{pn}

$$\varphi_{\text{pn}} = \arcsin \frac{c_{pn}}{A_{pn}} = \arccos \frac{a_{pn}}{A_{pn}}, \tag{3.90}$$

where the trigonometrical functions arcsin and arccos are multi-valued and non-unique. a_{pn} and c_{pn} are the real and the imaginary part of the orbital coefficients, respectively, and

$$A_{pn} = \left(a_{pn}^2 + c_{pn}^2\right)^{1/2} \tag{3.91}$$

the amplitude that should not change before and after smoothing. Fig. (3.7) and Fig. (3.8) show the results with the minimal basis set for $E_{\text{DC}} = 0$ and $E_{\text{DC}} = 0.001$ a.u., respectively.

In the case of $STO - 3G$ basis set, we have two basis functions per unit cell and two molecular orbitals (MO), each built as a linear combination of two atomic orbitals (AO). The two graphics on the left show respectively the first and the second MO without smoothing the coefficients, and the two on the right are the corresponding MO after smoothing. Comparing both figures, without and with field, it becomes evident that the effect of the external perturbation is negligible, but the effect of the smoothing is major, especially in the case of the first molecular orbital. However the 2π jump at $k = 0$ remains also after smoothing.

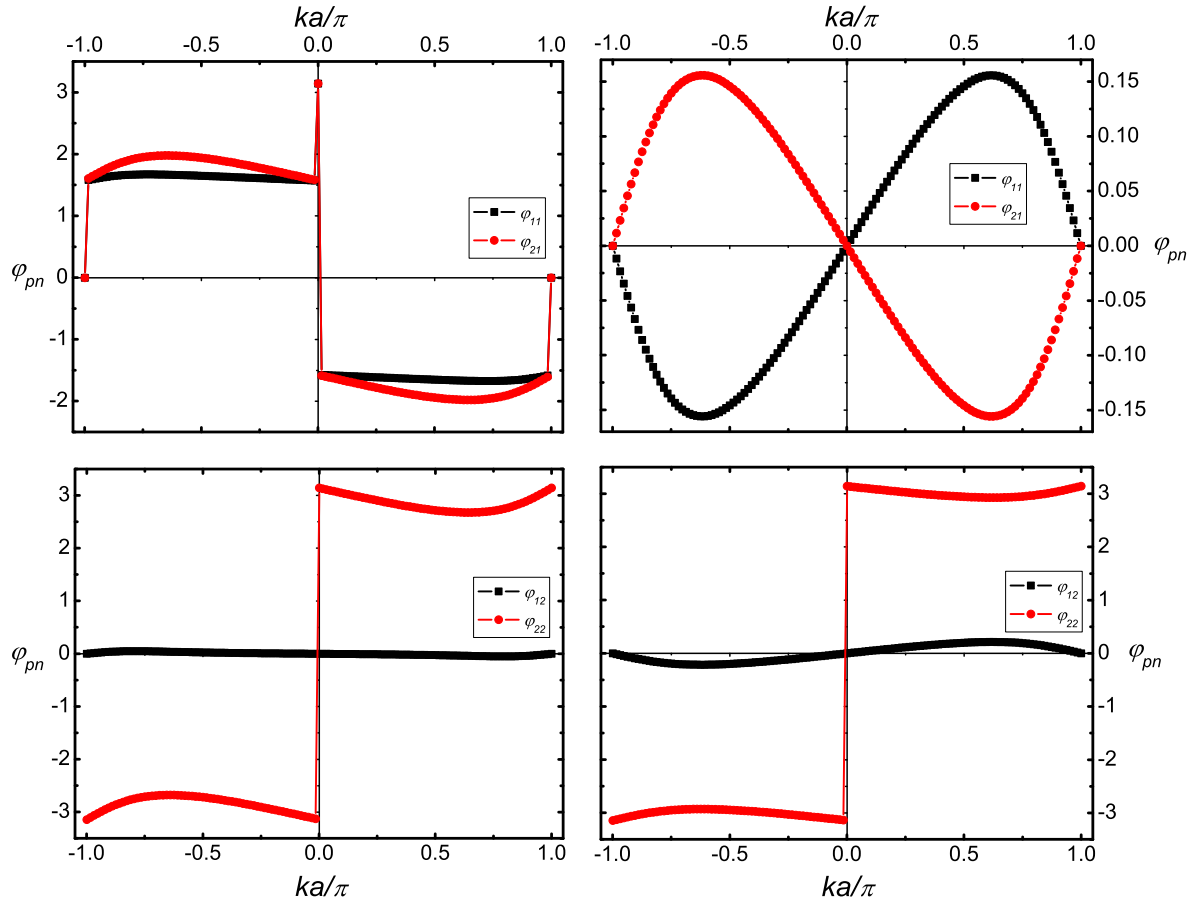

Figure 3.7: The change of the phases for the two orbitals of H_2 chain using $STO-3G$ basis set in the case of $E_{\mathrm{DC}}=0$. The two graphics on the left show the phases without using the smoothing procedure and the two on the right the phases with the smooth coefficients. $ka/\pi=-1$ and $ka/\pi=1$ define the first Brillouin zone.

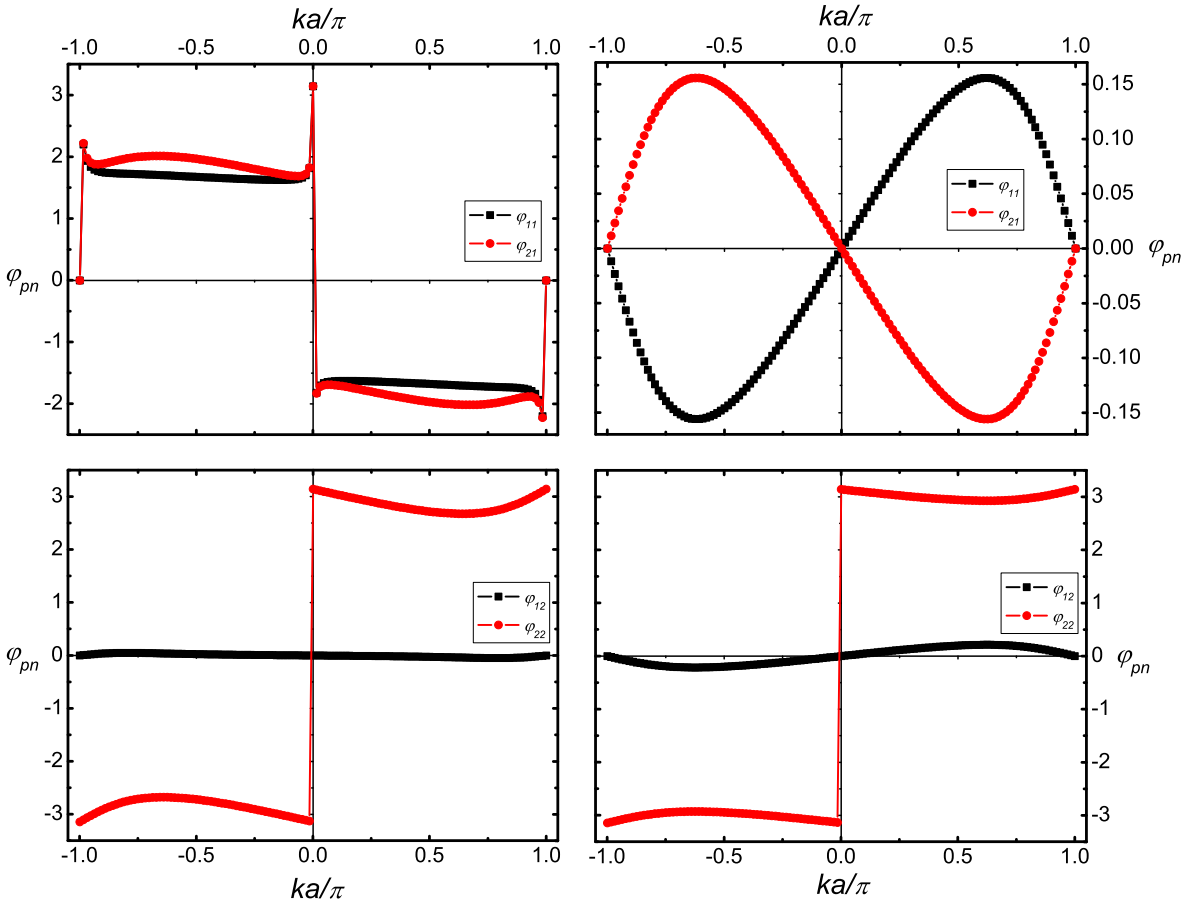

Figure 3.8: The same like in Fig. (3.7) but in the case of $E_{\mathrm{DC}} = 0.001$ a.u.

The next four pictures show the results when dealing with $3-21G$ basis set. In this case four basis functions per unit are available and accordingly four molecular orbitals. Fig. (3.9) and Fig. (3.10) illustrate the findings in the case of $E_{\mathrm{DC}}=0$ for the first and second, and for the third and fourth MO, respectively, and Fig. (3.11) and Fig. (3.12) the corresponding orbitals when $E_{\mathrm{DC}}=0.001$ a.u.

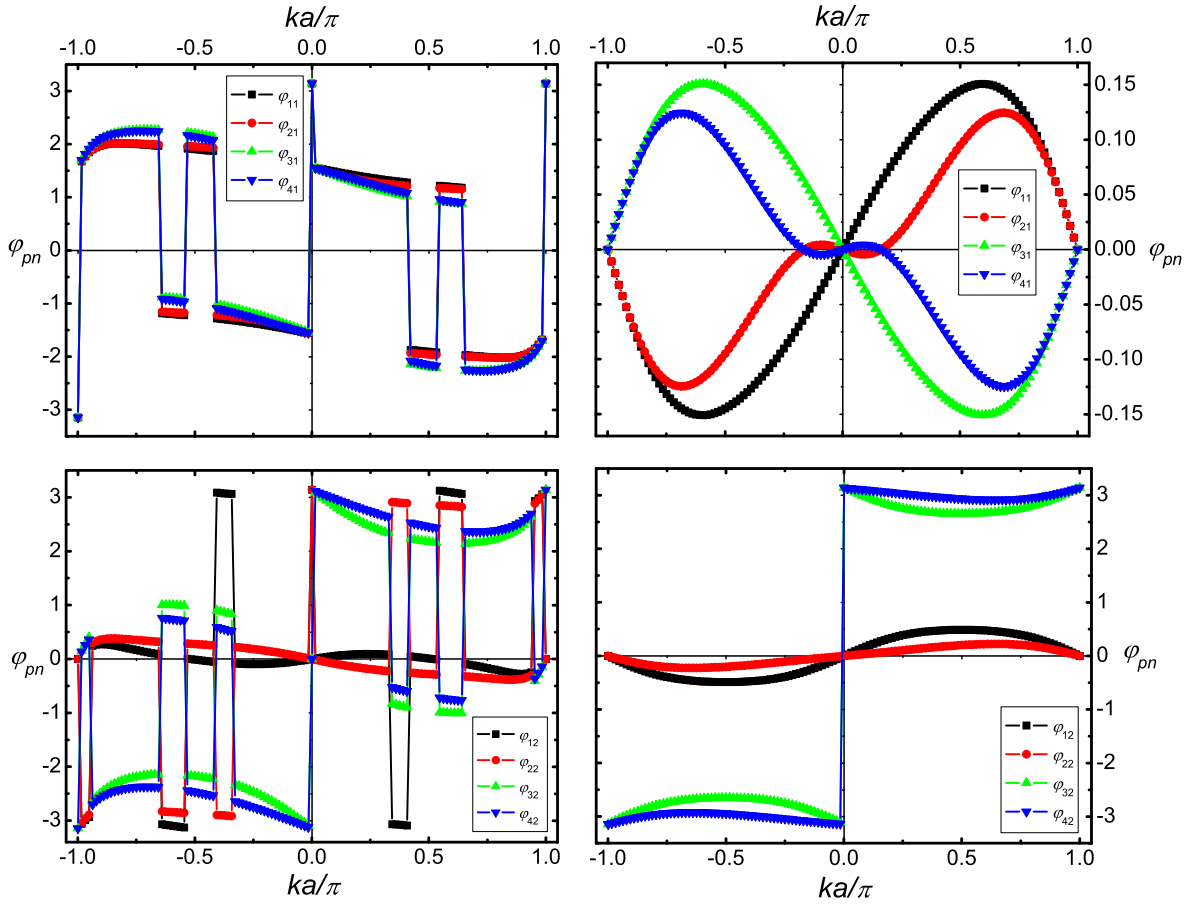

Figure 3.9: The change of the phases for the first and the second orbital of H_2 chain using $3-21G$ basis set without field. The two graphics on the left show the phases without using the smoothing procedure and the two on the right the phases with the smooth coefficients. $ka/\pi=-1$ and $ka/\pi=1$ define the first Brillouin zone.

The two graphics on the left in each figure show the first and the second, and the third and the fourth MO without smoothing the coefficients, and the two on the right are the corresponding MO after smoothing. Again, there are almost no changes in the phases when an electric field is applied, but the crucial effect of the smoothing procedure is evident. The large 2π jumps at $k=0,\pm\pi$ remain also after smoothing, however, they do not affect the derivatives of the coefficients.

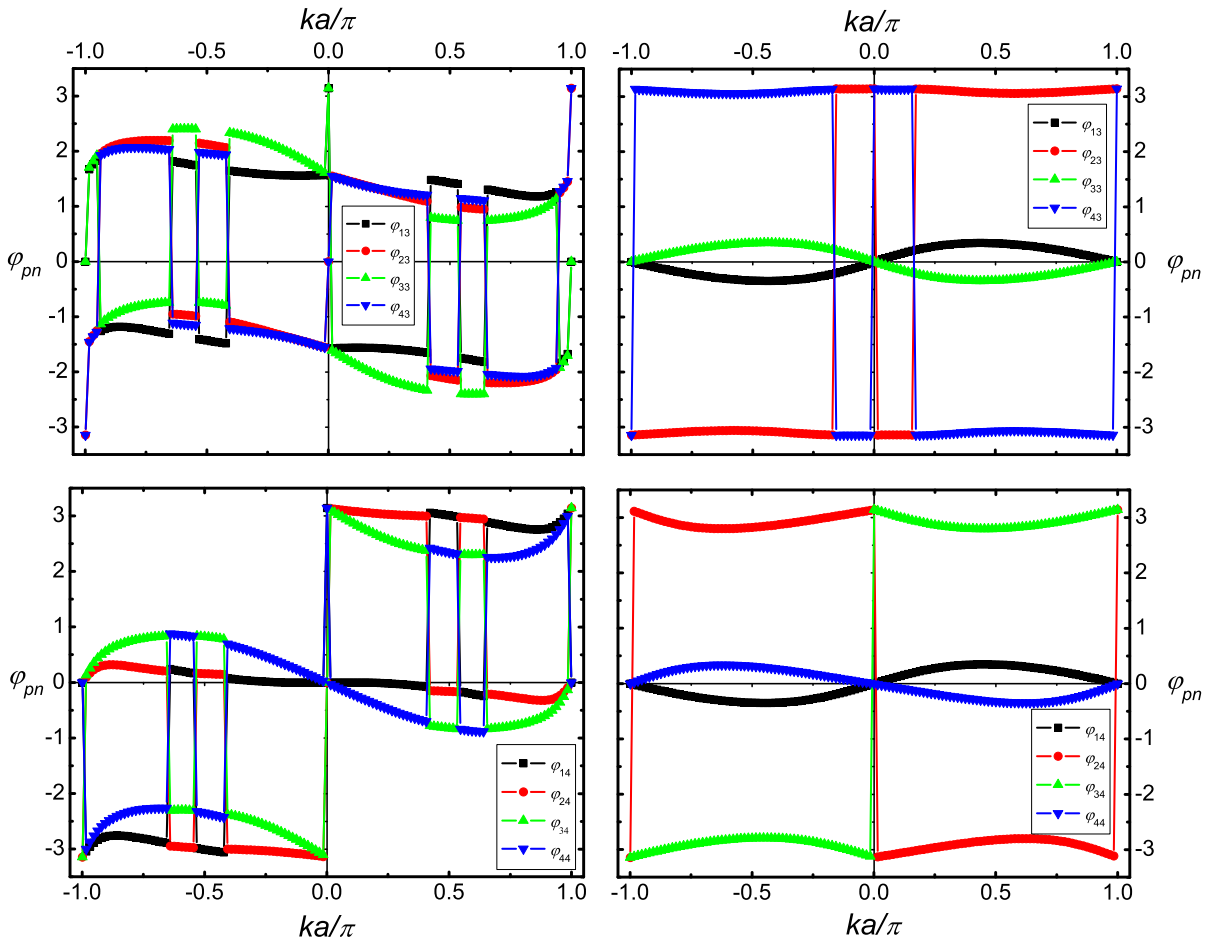

Figure 3.10: The change of the phases for the third and the fourth orbital of H_2 chain using $3-21G$ basis set without field. The two graphics on the left show the phases without using the smoothing procedure and the two on the right the phases with the smooth coefficients. $ka/\pi = -1$ and $ka/\pi = 1$ define the first Brillouin zone.

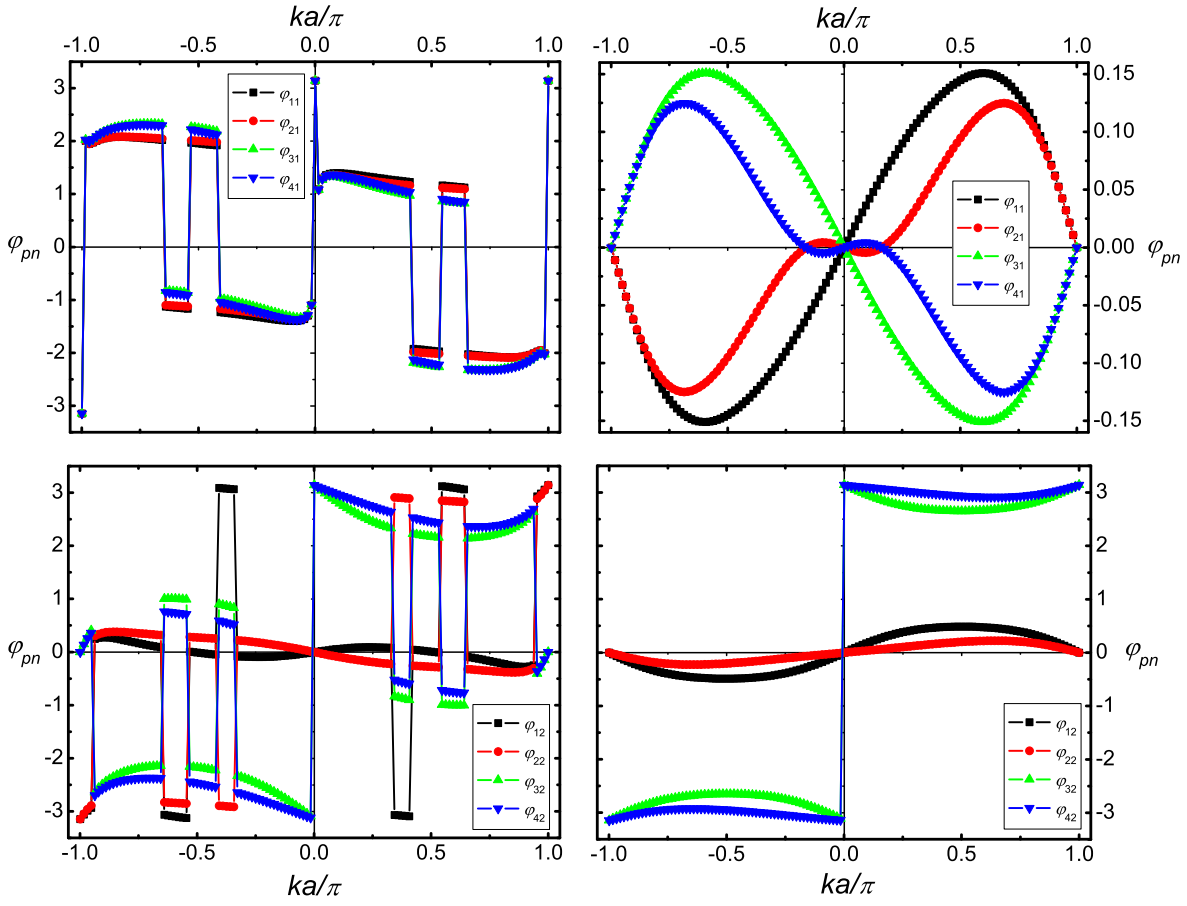

Figure 3.11: The same like in Fig. (3.9) but for $E_{\mathrm{DC}} = 0.001$ a.u.

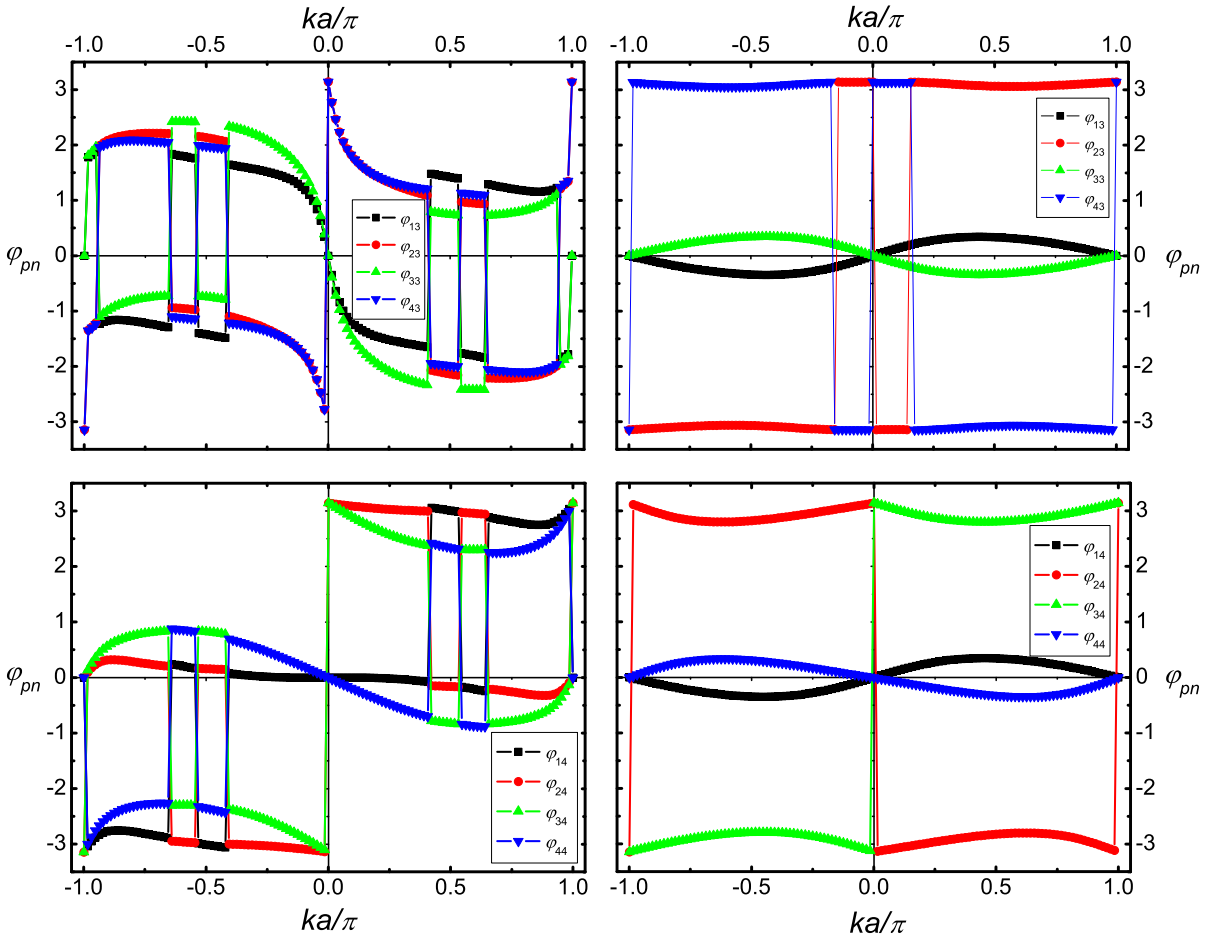

Figure 3.12: The same like in Fig. (3.10) but for $E_{\mathrm{DC}} = 0.001$ a.u.

It can be conclude that the smoothing procedure was successfully implemented in the PLH code. Results for a lithium hydride chain will confirm this statement.

3.5.2 The electric field (E_{DC}) dependency

After implementing the electric field expression in the SCF part of the PLH code, we were interested in the effect of the external perturbation on the total energy and on the polarization of the investigated system. Therefore, they were calculated as a function of E_{DC}. The polarizability of the hydrogen chain was also determined and compared with previous results.

Total energy (E_{tot})

In Table 3.1 are shown the total energies of our system in atomic units for the $STO-3G$ and the $3-21G$ basis sets when the field strength is zero. The $3-21G$ results afford more stable chain than the $STO-3G$ results, which will be confirmed later when the change of E_{tot} with the unit cell length is investigated.

E_{DC}	$E_{\mathrm{tot}}(STO-3G)$	$E_{\mathrm{tot}}(3-21G)$
0	-1.04513	-1.07604

Table 3.1: The total energy in atomic units without field using the two basis sets.

The total energy of the system in the case of $E_{\mathrm{DC}} \neq 0$ was calculated by means of Eq. (3.29). The findings for the two basis sets are plotted in Fig. (3.13), the top panel for the minimal and the bottom one for the larger basis set. The two curves have the same tendency, while the values for $3-21G$ are lying under those from $STO-3G$.

For the sake of simplicity the two curves are plotted in one graph, Fig. (3.14), where the $STO-3G$ curve has been shifted by a constant value. For weaker fields ($0 < E_{\mathrm{DC}} \leq 0.001$ a.u.) the total energy does not change significantly, whereas for $E_{\mathrm{DC}} > 0.001$ a.u. the decrease is rapidly.

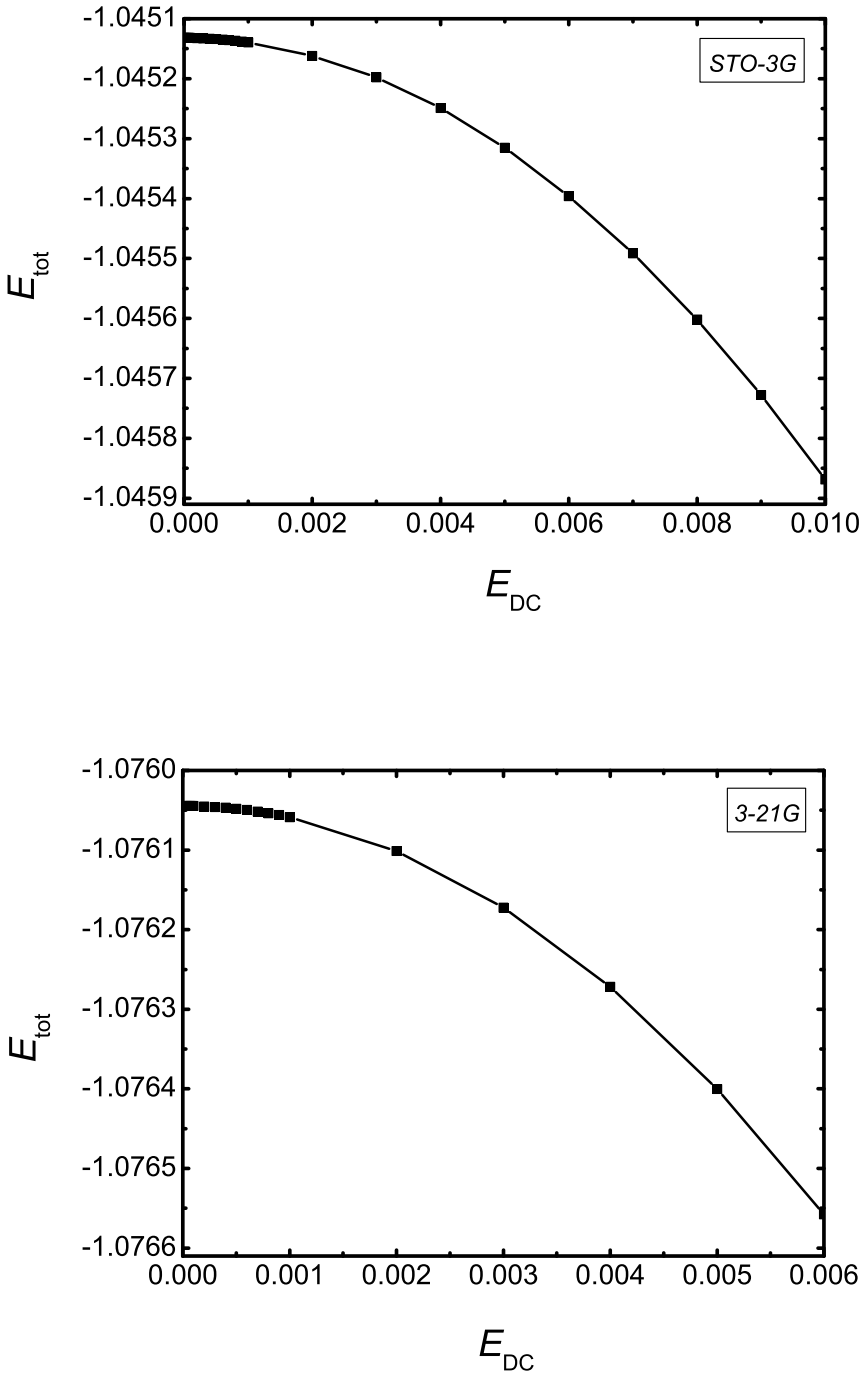

Figure 3.13: The total energy as a function of the field strength using the minimal $STO-3G$ (top graph) and the $3-21G$ basis set (bottom one). In the first case $E_{\rm DC} \leq 0.01$ a.u. and in the second $E_{\rm DC} \leq 0.006$ a.u.

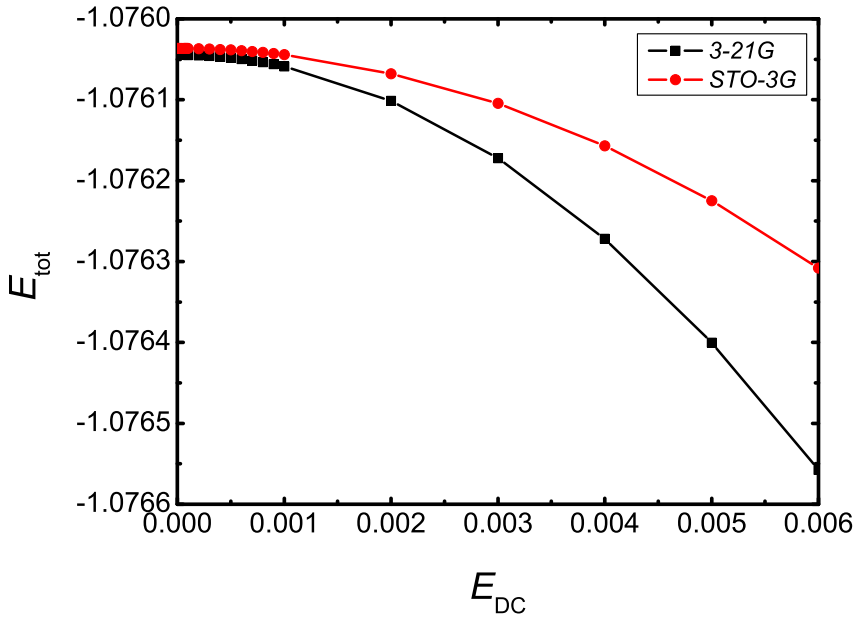

Figure 3.14: The total energy as a function of the field strength for the both cases, using the minimal $STO-3G$ basis set (red curve) and the $3-21G$ basis set (black curve), in comparison. The $STO-3G$ curve is shifted by a constant value.

Polarization (P)

The total polarization (P_{tot}) was determined via Eq. (3.17).

In Fig. (3.15), the results from the $STO-3G$ basis set calculations for the total polarization, together with its two contributions, are plotted against the electric field strength. In the top graph the distribution in the whole field range ($0.00002 \leq E_{\text{DC}} \leq 0.01$ a.u.) is shown, and in the bottom one only in the range $0.00002 \leq E_{\text{DC}} \leq 0.001$ a.u. The polarization values from the $3-21G$ calculations are presented in Fig. (3.16).

The linear dependency of P_{tot}, P_1 and P_2 on the field is evident. For small external perturbations the changes in the polarization are slight, whereas for $E_{\text{DC}} > 0.001$ a.u. P increase rapidly. Furthermore, the contribution from the current term, which is equivalent to the charge flow in the chain, is relatively large and neglecting it will be not a good approximation.

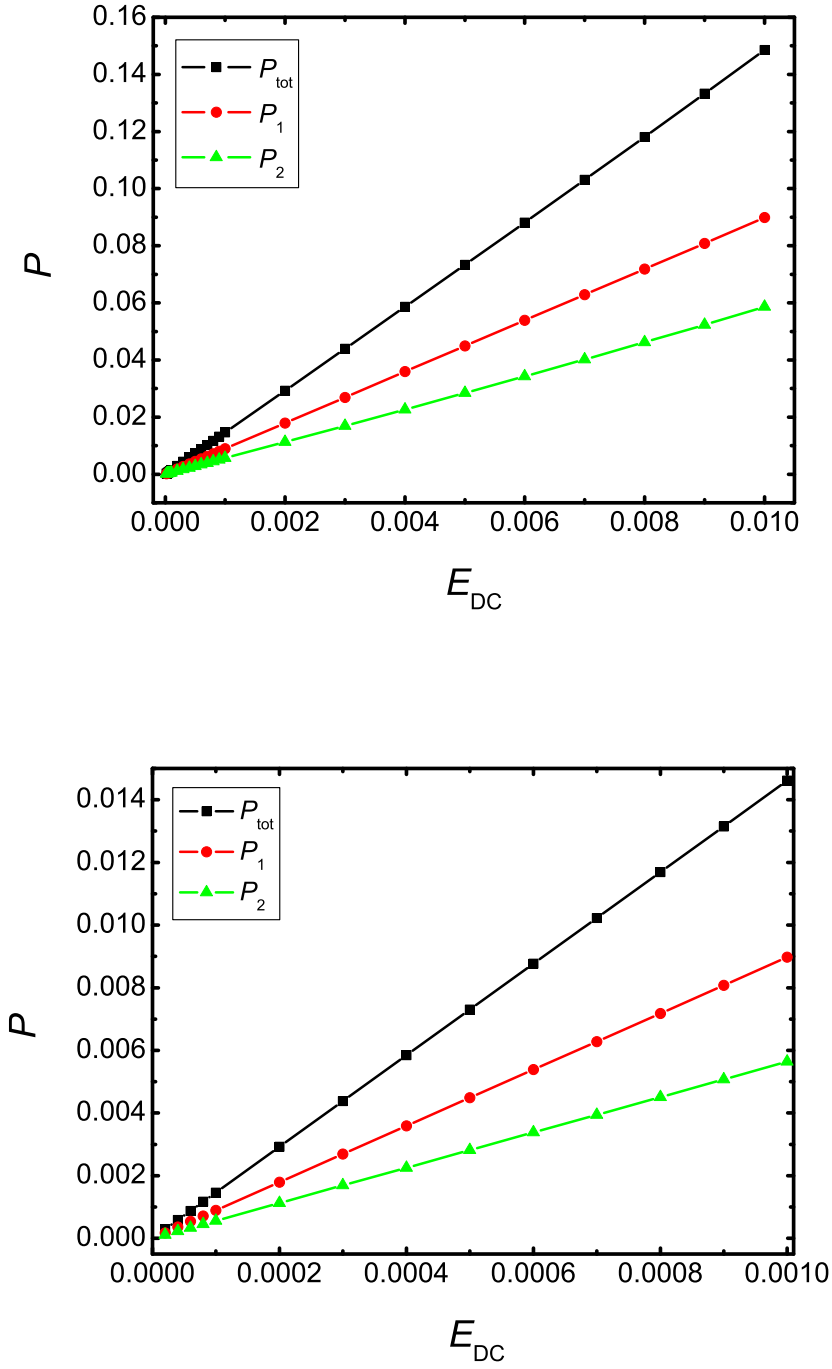

Figure 3.15: The change of the polarization with the field for the $STO-3G$ case. The black curve shows the total electronic polarization (P_{tot}), the red the charge (P_1) and the green one the current contribution (P_2) to P_{tot}. The bottom panel shows the results for $10^{-4} \leq E_{\text{DC}} \leq 10^{-3}$ a.u.

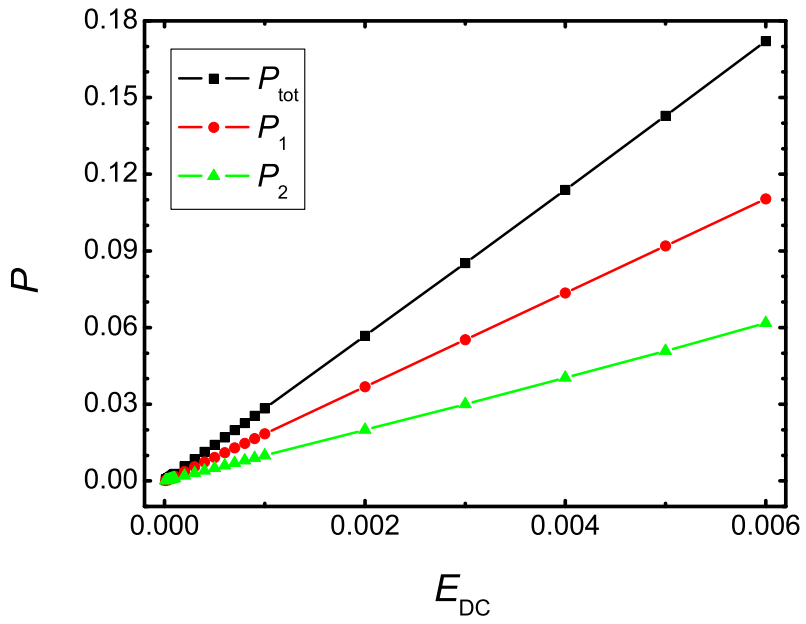

Figure 3.16: The change of the polarization with the field for the $3-21G$ case. The black curve shows the total electronic polarization (P_{tot}), the red the charge (P_1) and the green one the current contribution (P_2) to P_{tot}.

Polarizability (α)

To calculate the longitudinal polarizability per unit cell (i.e., the polarizability along the polymer chain axis, in our case along the z axis), we utilize the already mentioned Finite Field (FF) technique. For the two basis sets α was determined via the polarization values

$$\alpha_P = \lim_{E_{\rm DC}\to 0} \frac{P(E_{\rm DC})}{E_{\rm DC}}, \tag{3.92}$$

and via the field-dependent energy

$$\alpha_{E_{\rm tot}} = \lim_{E_{\rm DC}\to 0} 2\frac{E_{\rm tot}(0) - E_{\rm tot}(E_{\rm DC})}{E_{\rm DC}^2}. \tag{3.93}$$

For simplicity the zz symbols are omitted. Our results for α_P and $\alpha_{E_{\rm tot}}$ for the two basis sets are listed in Table 3.2. Three field amplitudes ($0.0004, 0.0006$ and 0.0008 a.u.) were employed.

$E_{\rm DC}$	α_P $(STO-3G)$	$\alpha_{E_{\rm tot}}$ $(STO-3G)$	α_P $(3-21G)$	$\alpha_{E_{\rm tot}}$ $(3-21G)$
0.0004	14.611	14.610	28.330	28.325
0.0006	14.612	14.610	28.332	28.333
0.0008	14.612	14.610	28.333	28.334

Table 3.2: The longitudinal polarizability as calculated using Eq. (3.92) (α_P) and Eq. (3.93) ($\alpha_{E_{\rm tot}}$). The values are in a.u.

Atomic basis set	here	CHF [3]
$STO-3G$	14.61	14.60
$3-21G$	28.33	28.31

Table 3.3: Longitudinal polarizabilities of infinite hydrogen chain computed at the CHF level of approximation by means of $STO-3G$ and $3-21G$ atomic basis set. The values are given in a.u.

To prove our results we compare them with those from [3], where electron correlation effects on the static longitudinal polarizability of polymeric chains were investigated, amongst others. Champagne and co-workers calculated the asymptotic α per unit cell of molecular hydrogen model chains at various levels of approximation (UCHF, CHF, MP2,

MP3, MP4, CCD, CCSD and CCSDT) by using different atomic basis sets ($STO-3G$, $3-21G$, $6-31G^{(*)*}$ and $6-311G^{(*)*}$) through extrapolation procedure. The comparison is made in Table 3.3. It is obvious that our findings are in excellent agreement with previous theoretical investigation on polymeric hydrogen chain.

3.5.3 The dependence on the $H-H$ distance ($d_{\mathrm{H-H}}$)

In order to pursue the changes in the quantities, characterizing our system, when the distance between the two hydrogen atoms in the H_2 molecule is varying and an electric field is applied, we defined a large unit cell, for instance $a \geq 20$ a.u. The latter is necessary if one wants to be sure that two intermolecular hydrogen atoms are enough far away from each other and the two H atoms in one unit cell can be considered as a single molecule. For our calculations a was chosen to be 20 a.u., the intramolecular distance was changed in the range from $d_{\mathrm{H-H}} = 0.50$ a.u. to $d_{\mathrm{H-H}} = 8.0$ a.u. and the field strength was set to $E_{\mathrm{DC}} = 0.0002$ a.u.

Of the total energy (E_{tot})

The dependence of the total energy of the system on the distance between the two atoms in the hydrogen molecule will give its equilibrium geometry with the equilibrium distance d_{eq} in the case of field. The results from the two sets of calculations are depicted in Fig. (3.17) and Fig. (3.18) and summarized in Table 3.4.

With the minimal basis set an equilibrium minimum was found at $d_{\mathrm{eq}} = 1.35$ a.u. and with $3-21G$ at $d_{\mathrm{eq}} = 1.39$ a.u. This can be seen in the lower panel of Fig. (3.18), where the $STO-3G$ curve is shifted by a constant value.

Comparing with the experimental value of $d_{\mathrm{eq}} = 1.40$ a.u., is evident that the deviation in the first case is around 3.7 % and in the second case around 0.7 %. The total energies from the both basis sets, corresponding to the two minima, are also comparable with previous ones [91].

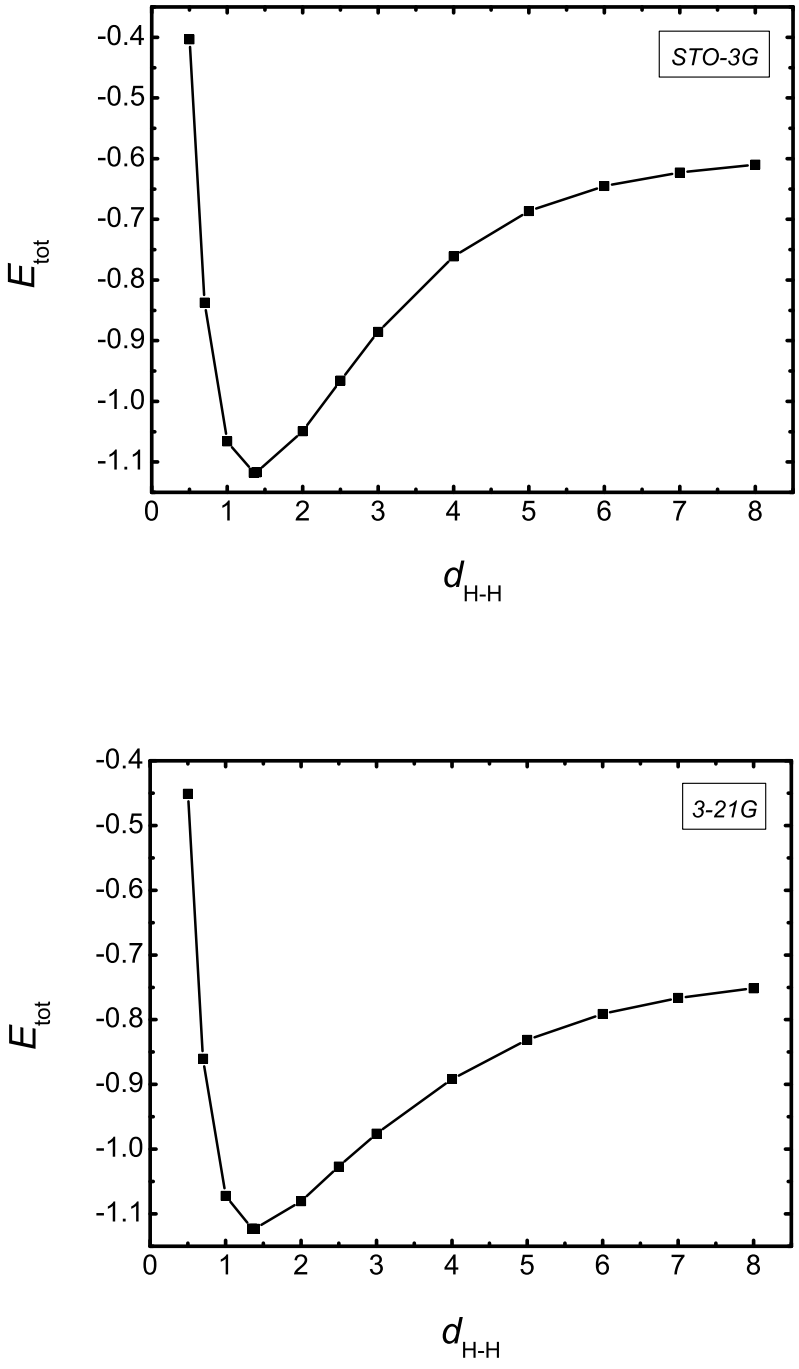

Figure 3.17: The total energy as a function of the bond distance with $STO-3G$ (upper graph) and $3-21G$ (lower graph) basis sets.

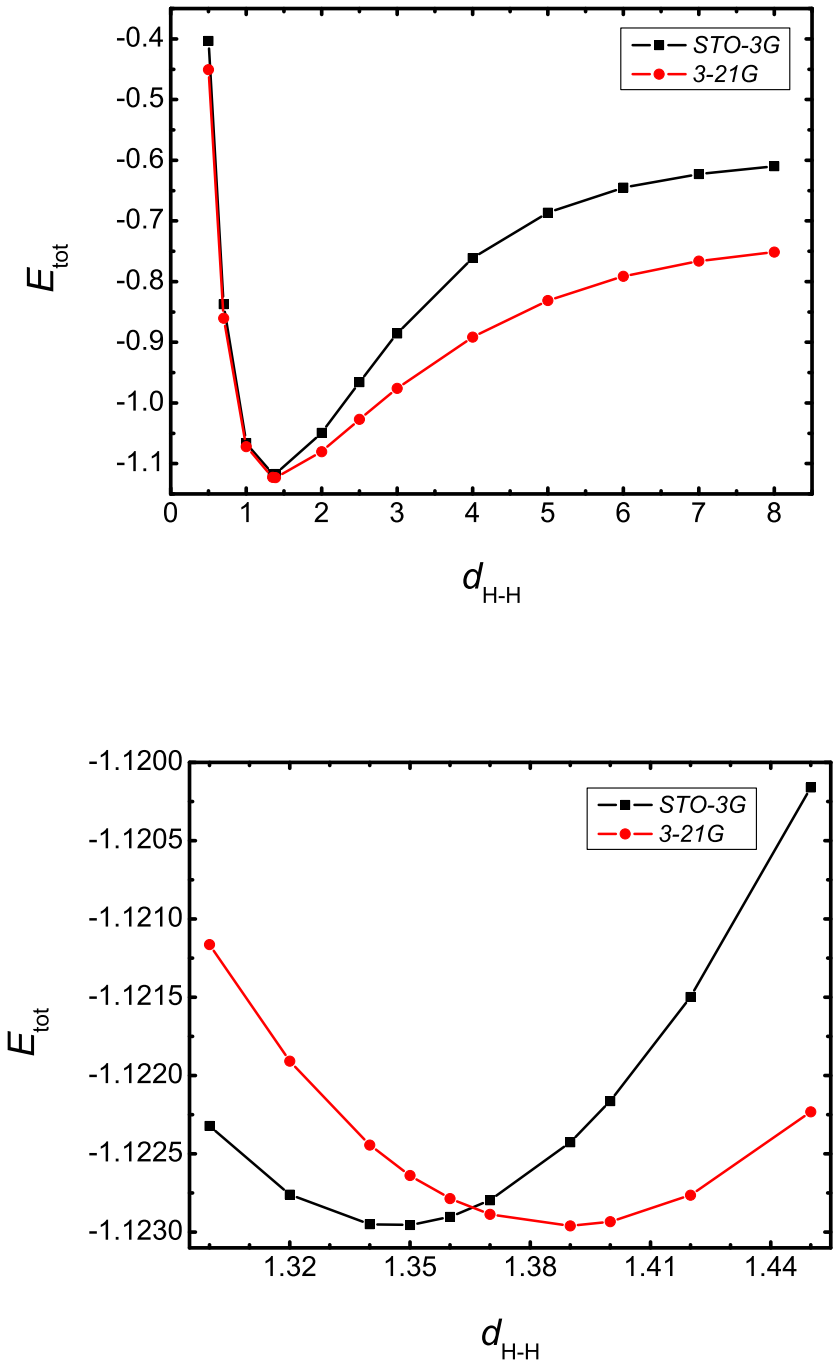

Figure 3.18: The upper panel shows the two curves from Fig. (3.17) in comparison. In the lower graph the $STO-3G$ total energy values around the minimum are shifted by a constant and plotted together with the $3-21G$ values against the intramolecular distance in the range of $1.30 \leq d_{\mathrm{H-H}} \leq 1.45$ a.u.

$d_{\mathrm{H-H}}$	E_{tot} $(STO-3G)$	E_{tot} $(3-21G)$
0.50	-0.40333	-0.45091
0.70	-0.83713	-0.86029
1.00	-1.06000	-1.07195
1.35	**-1.11750**	-1.12264
1.39	-1.11697	**-1.12296**
2.00	-1.04917	-1.08027
2.50	-0.96579	-1.02693
3.00	-0.88527	-0.97585
4.00	-0.76108	-0.89138
5.00	-0.68642	-0.83125
6.00	-0.64508	-0.79114
7.00	-0.62275	-0.76625
8.00	-0.61004	-0.75145

Table 3.4: The total energy in atomic units as a function of the intramolecular distance for both basis sets.

Of the polarization (P)

Again, the total polarization (P_{tot}) was determined via Eq. (3.17). However, here, due to the large unit cell length ($a = 20.0$ a.u.), the charge flow term from Eq. (3.16) is zero

$$P_2 = 2\sum_k \sum_n \sum_{pq} iC^*_{pn}(k)\frac{\partial C_{qn}}{\partial k}S_{pq}(k) = 0 \tag{3.94}$$

since

$$\frac{\partial C_{qn}}{\partial k} = 0. \tag{3.95}$$

Then,

$$P_{\text{tot}} = P_\rho. \tag{3.96}$$

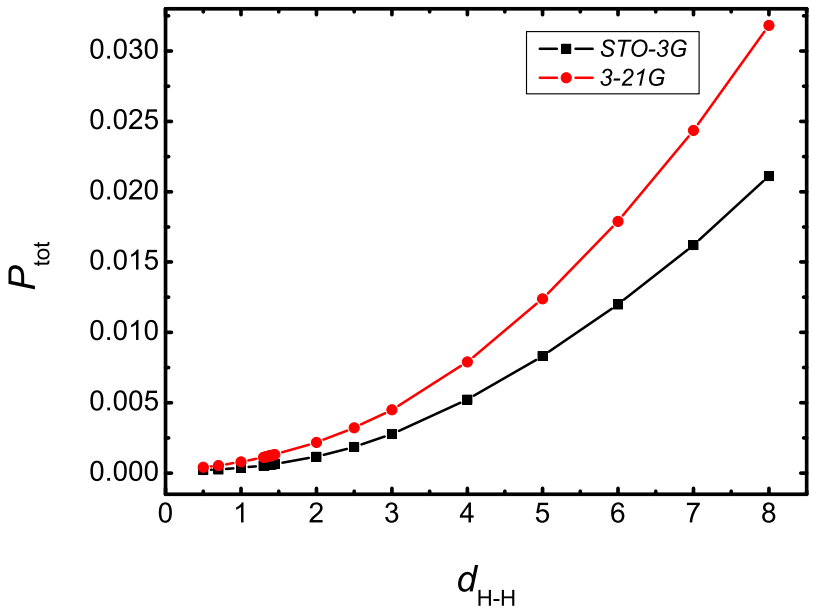

Figure 3.19: The increase of the total polarization with the bond length distance for the both basis sets, $STO-3G$ (black curve) and $3-21G$ (red curve). $P_2 = 0$ and $P_{\text{tot}} = P_1$.

Our results are depicted in Fig. (3.19). The $3-21G$ provides larger polarization, which increases rapidly with the bond distance $d_{\text{H-H}}$.

Of the polarizability (α)

The third quantity determined as a function of the intramolecular distance was the polarizability per unit cell. Eq. (3.92) was used for this purpose, where again the field strength was fixed to $E_{\mathrm{DC}} = 0.0002$ a.u. The results are listed in Table 3.5 and plotted in Fig. (3.20).

$d_{\mathrm{H-H}}$	α $(STO-3G)$	α $(3-21G)$
0.50	1.0850	2.0690
0.70	1.3460	2.7330
1.00	1.9205	4.0085
1.35	2.9060	5.9385
1.39	3.0425	6.1905
2.00	5.8325	10.9240
2.50	9.2815	16.1055
3.00	13.8645	22.5635
4.00	26.0965	39.5545
5.00	41.6260	61.9625
6.00	59.9495	89.4530
7.00	81.0935	121.7310
8.00	105.5180	159.1190

Table 3.5: The change of the polarizability in a.u. with the intramolecular distance.

The two curves have the same tendency and corresponding to the polarization findings the $3-21G$ basis set provides larger polarizability, which increases rapidly with the bond distance $d_{\mathrm{H-H}}$.

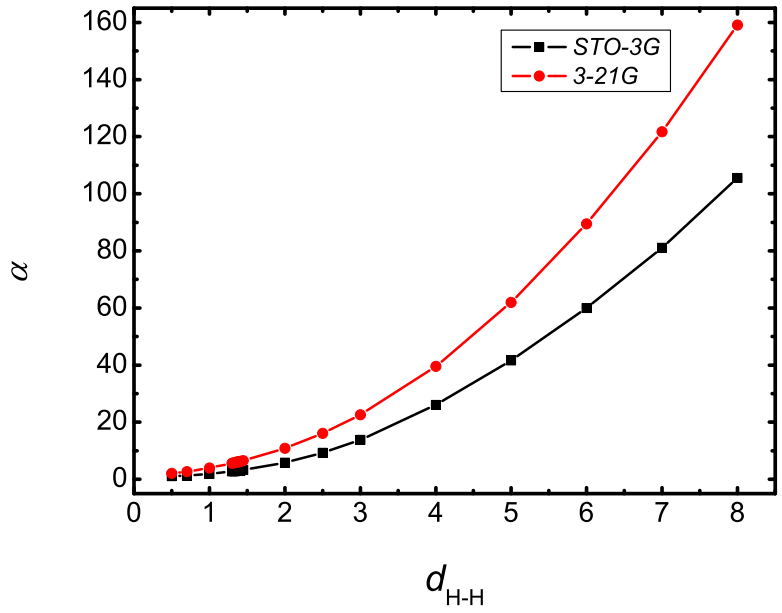

Figure 3.20: The increase of the polarizability with the bond length distance for the both basis sets, $STO-3G$ (black curve) and $3-21G$ (red curve).

3.5.4 The change with the unit cell a

At the end, we investigated the effect of the bond-length alternation on the total energy of the system, on the polarization and on the polarizability in the presence of external electric perturbation. The intramolecular distance and the field amplitude were kept constant, $d_{\mathrm{H-H}} = 2.0$ a.u. and $E_{\mathrm{DC}} = 0.0002$ a.u., respectively, and the intermolecular was changed from 2.5 a.u. to 98.0 a.u. Fig. (3.21) represents three hydrogen chain models with different unit cell length, in type A chain $a = 4.5$ a.u., in type B $a = 5.0$ a.u. and in type C $a = 6.0$ a.u. In addition we explored other 8 models to achieve clear convergence of the investigated quantities.

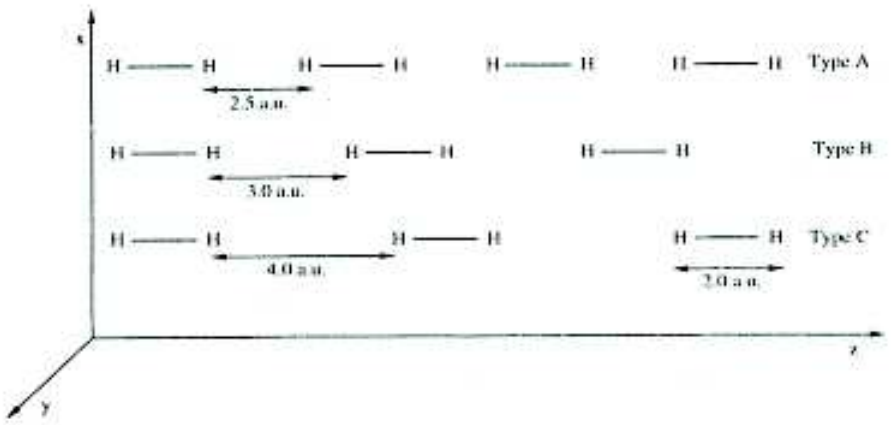

Figure 3.21: Sketch of three molecular hydrogen models with different bond-length alternation, 2.5/2.0 a.u. (type A), 3.0/2.0 a.u. (type B) and 4.0/2.0 a.u. (type C) [4].

How does total energy (E_{tot}) change with the unit cell a?

The answer of the question can be found in Table 3.6 and in Fig. (3.22) and Fig. (3.23). For both atomic basis sets the total energy decreases rapidly at the beginning from $a = 4.5$ a.u. to $a = 12.0$ a.u. and then converges to a value, which corresponds to the total energy of a single hydrogen molecule.

To visualised the $STO - 3G$ and $3 - 21G$ findings in the same diagram (Fig. (3.23)), we shifted the first by a constant value. It is evident that the double-$\zeta 3 - 21G$ basis set curve converges at lower energy.

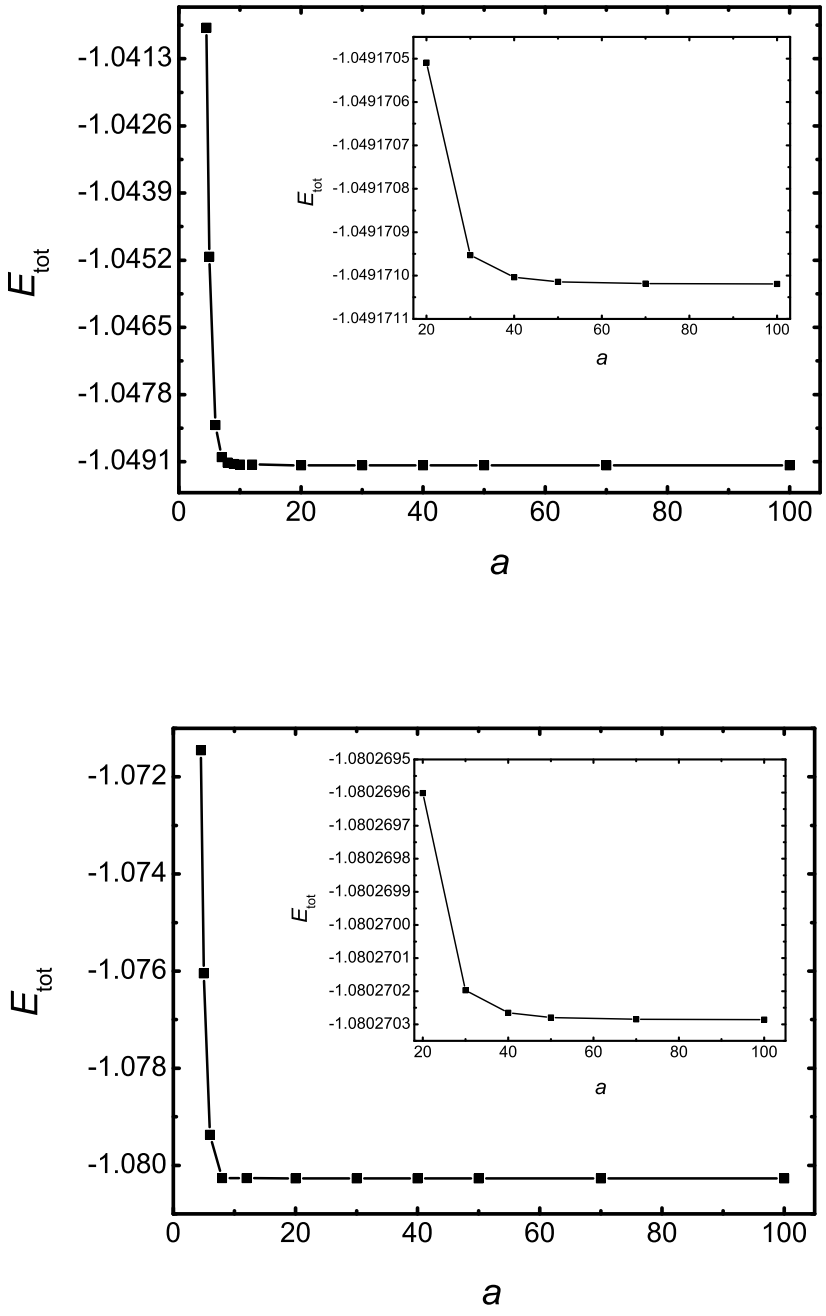

Figure 3.22: The change of the total energy in atomic units as a function of the unit cell length. a changes from 4.5 a.u. to 100.0 a.u. The top graph is for the minimal $STO-3G$ and the bottom one for the $3-21G$ basis set. The both inner graphs show the results in the range of $a = 20.0 - 100.0$ a.u.

a	E_{tot} $(STO-3G)$	E_{tot} $(3-21G)$
4.50	-1.04070	-1.07145
5.00	-1.04513	-1.07605
6.00	-1.04839	-1.07937
8.00	-1.04912	-1.08026
12.00	-1.04915	-1.08026
20.00	-1.04917	-1.08027
30.00	-1.04917	-1.08027
40.00	-1.04917	-1.08027
50.00	-1.04917	-1.08027
70.00	-1.04917	-1.08027
100.00	-1.04917	-1.08027

Table 3.6: The change of the total energy in a.u. with the unit cell length.

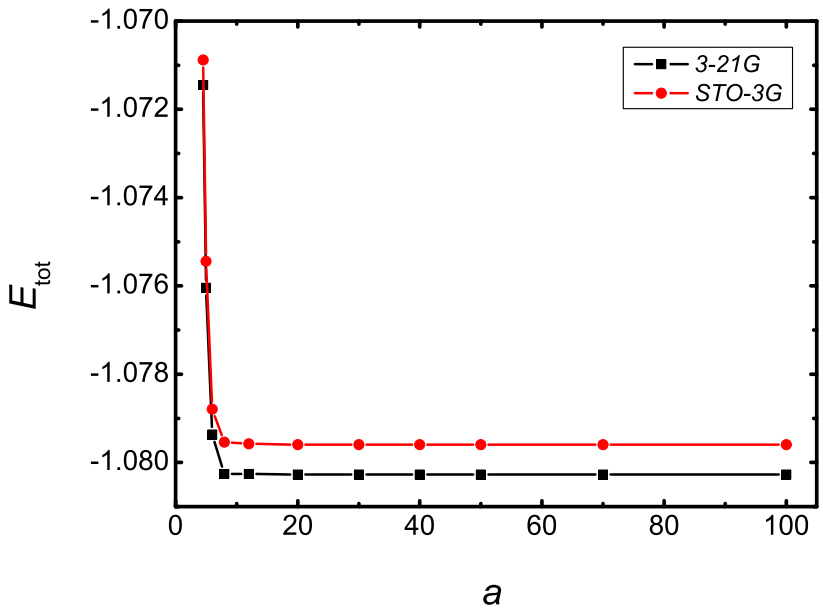

Figure 3.23: The results from the both basis sets in comparison.

How does polarization (P) change with the unit cell a?

The change of the total polarization and its two electronic contributions with increasing unit cell length was also pursued in our work. P_1, P_2 and P_{tot} were computed using Eq. (3.14), Eq. (3.15) and Eq. (3.17), respectively, where $P_n = 0$. The current contribution to the polarization decreases when a increases and becomes zero for long cells, since it contains the term $\partial C/\partial k$ that goes to zero when $a \to \infty$. Our results are summarized in Table 3.7 using $STO-3G$ and in Table 3.8 using $3-21G$ atomic basis sets.

a	P_1	P_2	P_{tot}
4.50	0.00263880	0.00359280	0.00623160
5.00	0.00179510	0.00112710	0.00292220
6.00	0.00139270	0.00020790	0.00160060
8.00	0.00123510	0.00000690	0.00124190
12.00	0.00118200	0	0.00118200
20.00	0.00116650	0	0.00116650
30.00	0.00116360	0	0.00116360
40.00	0.00116290	0	0.00116290
50.00	0.00116270	0	0.00116270
70.00	0.00116250	0	0.00116250
100.00	0.00116250	0	0.00116250

Table 3.7: The values for the charge (P_1) and current (P_2) term and for the total polarization (P_{tot}) from the minimal $STO-3G$ basis set.

It can be seen that the minimal basis set affords larger current term for $a = 4.5$ a.u., i.e., the charge flow in the chain is larger when the intermolecular hydrogen atoms are not far away from each other, i.e., when the bond-length alternation is small (2.0/2.5 a.u. in this case). For the $3-21G$ basis set P_1 and P_2 are almost equal at $a = 4.5$ a.u. In both cases the polarization changes rapidly for the small unit cells and for $a \geq 12.0$ a.u. P_2 becomes zero and $P_{\text{tot}} = P_1$. The values from the two tables are plotted in Fig. (3.24). Fig. (3.25) shows the total polarization for both atomic basis sets in comparison.

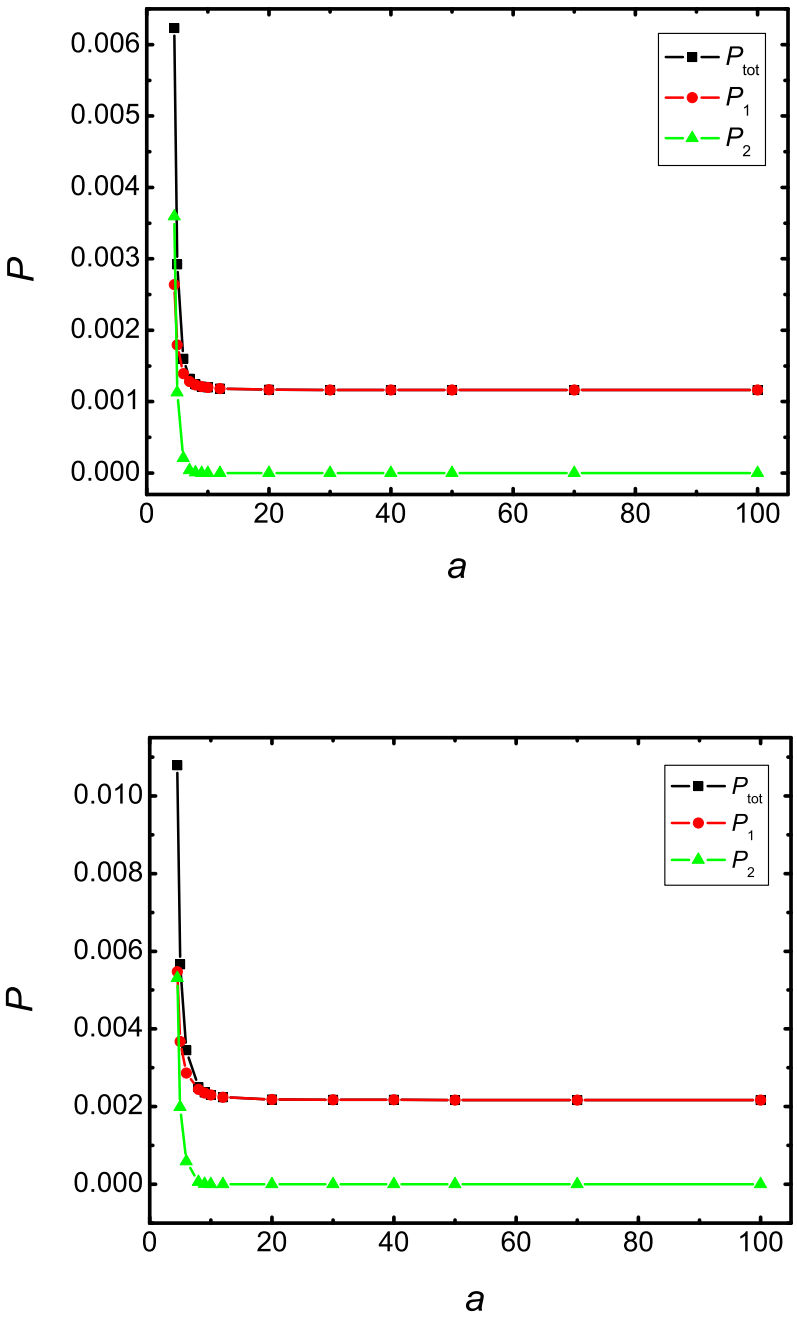

Figure 3.24: The polarization distribution with increasing unit cell length. The upper graph is for the minimal $STO-3G$ and the lower one for the $3-21G$ basis set.

a	P_1	P_2	P_{tot}
4.50	0.00547650	0.00531040	0.01078680
5.00	0.00367950	0.00198630	0.00566580
6.00	0.00286270	0.00058920	0.00345180
8.00	0.00244430	0.00005570	0.00250010
12.00	0.00224010	0	0.00224010
20.00	0.00218480	0	0.00218480
30.00	0.00217470	0	0.00217470
40.00	0.00217220	0	0.00217220
50.00	0.00217130	0	0.00217130
70.00	0.00217080	0	0.00217080
100.00	0.00217050	0	0.00217050

Table 3.8: The values for the charge (P_1) and current (P_2) term and for the total polarization (P_{tot}) from the double-$\zeta 3-21G$ atomic basis set.

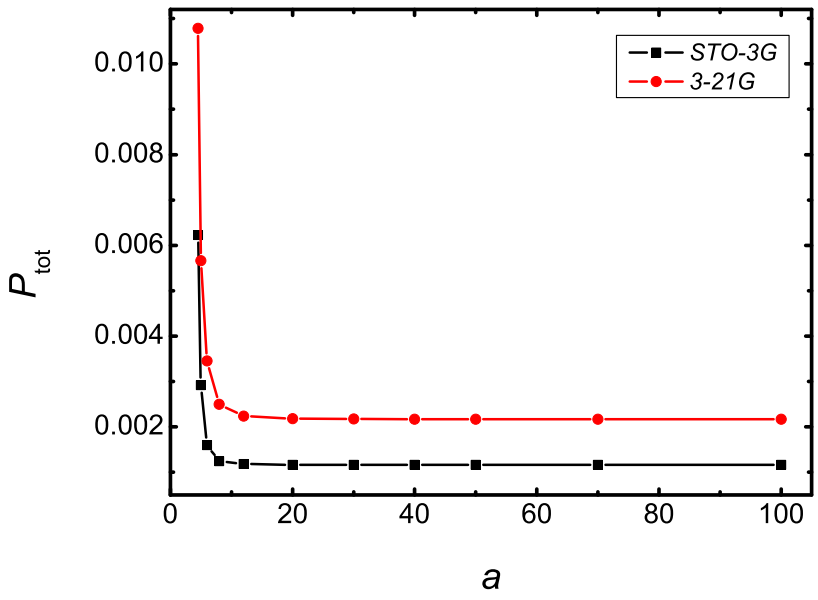

Figure 3.25: The total polarization in atomic units for both basis sets in comparison.

How does polarizability (α) change with the unit cell a?

The polarizability of the model hydrogen chain obeys the same tendency like the total energy and the polarization. The results from Table 3.9 are plotted separately in Fig. (3.26) and for two basis sets in Fig. (3.27). For the small unit cells ($a \leq 12.0$ a.u.) α decreases fast and achieves convergence for $a \geq 20.0$ a.u., where the values correspond to those of a single hydrogen molecule, H_2.

a	α $(STO-3G)$	α $(3-21G)$
4.50	31.1580	53.9340
5.00	14.6110	28.3290
6.00	8.0030	17.2590
8.00	6.2095	12.5005
12.00	5.9100	11.2005
20.00	5.8325	10.9240
30.00	5.8180	10.8735
40.00	5.8145	10.8610
50.00	5.8135	10.8565
70.00	5.8125	10.8540
100.00	5.8125	10.8525

Table 3.9: The polarizability values in a.u. with increasing unit cell length.

In Table 3.10, we compare our polarizability results for a single hydrogen molecule with those of Champagne et al. [3], where the calculations are done at $E_{\mathrm{DC}} = 0.0016$ a.u. and $E_{\mathrm{DC}} = 0.0032$ a.u.

Atomic basis set	here ($a = 100$ a.u.)	CHF [3]
$STO-3G$	5.813	5.812
$3-21G$	10.853	10.852

Table 3.10: Longitudinal polarizabilities of a single hydrogen molecule computed at the CHF level of approximation by means of $STO-3G$ and $3-21G$ atomic basis set.

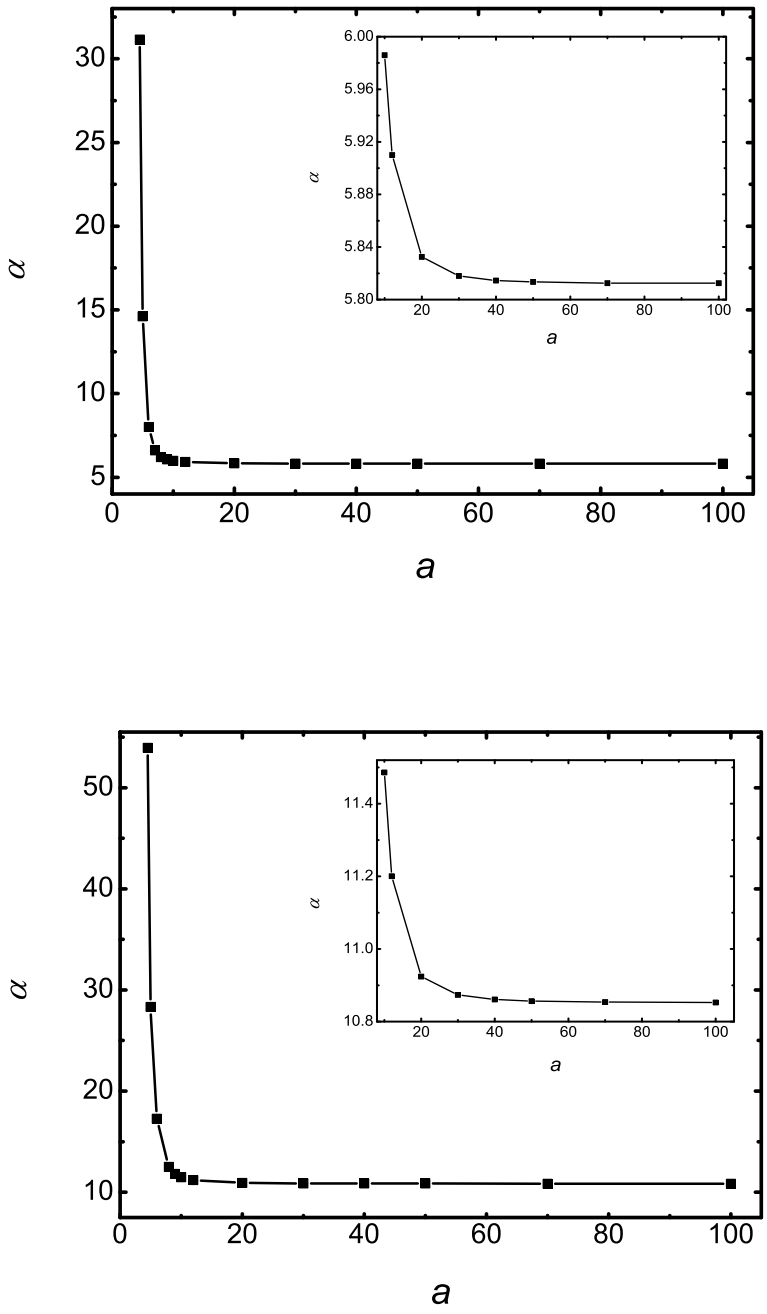

Figure 3.26: The α distribution with increasing unit cell length. The upper graph is for the minimal $STO-3G$ and the lower one for the $3-21G$ basis set.

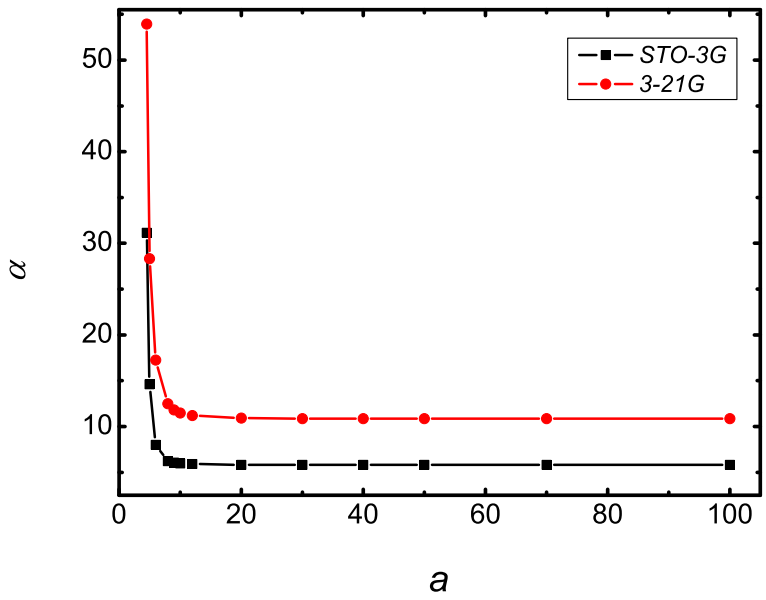

Figure 3.27: The polarizability for the both basis sets in comparison.

3.5.5 Second hyperpolarizability

The longitudinal second hyperpolarizability per unit cell (see Eq. (3.61) and Eq. (3.65)) is important quantity for the nonlinear optics applications of the materials. To prove further the implementation of the vector potential approach (VPA) in the PLH code, we computed γ_l (l for longitudinal) of a model hydrogen chain with bond-length alternation of 2.0 a.u./3.0 a.u., using the Finite Field technique, which required the knowledge of the total energy of the system at different field amplitudes. Then,

$$\gamma_l = -\left(\frac{d^4 E_{\mathrm{tot}}(E_{\mathrm{DC}})}{dE_{\mathrm{DC}}^4}\right)_{E_{\mathrm{DC}}=0} = \lim_{E_{\mathrm{DC}}\to 0} -\frac{8E_{\mathrm{tot}}(E_{\mathrm{DC}}) - 2E_{\mathrm{tot}}(2E_{\mathrm{DC}}) - 6E_{\mathrm{tot}}(0)}{E_{\mathrm{DC}}^4}. \quad (3.97)$$

The adopted field amplitudes are 0.001 a.u., 0.002 a.u., 0.003 a.u. and 0.004 a.u. Larger amplitudes lead to large contaminations that increase as the fourth power of E_{DC}. They could be removed by using the so-called Romberg's procedure [92] that was utilized in [80]. Additionally we determined γ at the amplitudes 0.0016 a.u., 0.0032 a.u. and 0.0064 a.u., as was already done from Champagne et al. Our results for the second hyperpolarizability are presented and compared with those from [80] in Table 3.11.

Atomic basis set	γ_l here	γ_l CHF [80]
$STO-3G$	14 197	13 515
$3-21G$	56 430	55 674

Table 3.11: Longitudinal second hyperpolarizability in a.u. of a infinite hydrogen chain with $STO-3G$ and $3-21G$ atomic basis set.

Here, like in the case of the polarizability per unit, the values of Champagne et al. are asymptotic values, received through γ extrapolation of increasingly large hydrogen model chains containing up to 30 atoms.

3.6 Lithium hydride chain

Our second test system is the lithium hydride quasilinear chain. There are a lot of experimental and theoretical studies [93, 94, 95, 96, 97, 98, 99, 100, 101, 102], however, on the LiH molecule. Most of them are concentrated on ground and excited states properties investigated by means of different methods. For instance, Mo and Zhang [102] explored the bonding features of LiH using 3 and 6 so-called bonded tableaus (BTs) functions in the framework of the valence bond self-consistent field (VBSCF) method and found that the LiH bond is covalent instead of ionic.

Linear and nonlinear properties of LiH chain are presented in [11]. Bishop et al. apply a new theory for the direct and analytical band structure determination of the coupled-perturbed Hartree-Fock dipole moment (μ), polarizability (α), first (β) and second hyperpolarizability (γ) on five quasilinear polymers: $(LiH)_N$, $(FH)_N$, $(H_2O)_N$, trans-polymethineimine $((-CNH-)_N)$ and trans-polyacetylene $((-CH=CH-)_N)$. Comparison with finite oligomer findings confirms the validity of their method.

For our test calculations on lithium hydride we adopt a structure used already in [11]. The input file for the used lithium hydride chain is given in Fig. (3.28). The Clementi's minimum basis set [103] was employed. The intramolecular distance is $d_{\mathrm{Li-H}} = 4.0$ a.u. and the unit cell is $a = 10.0$ a.u., which corresponds to bond-length alternation of 4.0 a.u./6.0 a.u. The single shell (s) of the hydrogen atom is formed by 4 contracted Gaussians with the corresponding exponents, and the two shells (s and p) of the lithium atom by 5 and 2 Gaussians, respectively.

```
$GEOM AU

    LIH


21   10.00    41   0 0
 H       0.00000000   0.00000000  0.00000000
 Li      0.00000000   0.00000000  4.00000000

$BASIS
40529
 1
         1S   S 4  1.00
13.013400,   0.019678,   0.0
 1.962500,   0.137952,   0.0
 0.444569,   0.478313,   0.0
 0.121953,   0.501131,   0.0
****
 2
         1S   S 5  1.00
270.881090,   0.006271,   0.0
 40.760906,   0.046050,   0.0
  9.212495,   0.196771,   0.0
  2.491427,   0.471694,   0.0
  0.732905,   0.433397,   0.0
         2S   S 2  1.00
  0.075307,   0.368683,   0.0
  0.030339,   0.664881,   0.0
****

$END
$SCF  PRINT 3 DEPTHR 4 FILON NKPRT 5
```

Figure 3.28: Input file for a lithium hydride chain using the Clementi's minimum basis set. The distance between the atoms in the unit cell is 4.0 a.u. and the unit cell length is 10.0 a.u.

3.6.1 The change of the phases φ_{pn} with the wavevector k

Using Eq. (3.90) and Eq. (3.91), we calculated the phases φ_{pn} of the LiH chain in the first Brillouin zone and plotted the results against ka/π in order to check the implementation of the smoothing procedure in the PLH program. The distribution of the three phases corresponding to the three molecular orbitals is shown in Fig. (3.29) and Fig. (3.30) with and without field, respectively. The three graphs on the left in each figure show the three original molecular orbitals and the three on the right the corresponding orbitals after smoothing. Comparing the left with the right side, is obvious that the effect of the smoothing is major, and only 2π jumps at $k = 0$ and at the boundaries $k = \pm\pi$ remain after smoothing. However, as already mentioned, they do not affect the differentiation of the orbital coefficients with respect to the wavevector ($\frac{\partial C_{qn}(k)}{\partial k}$).

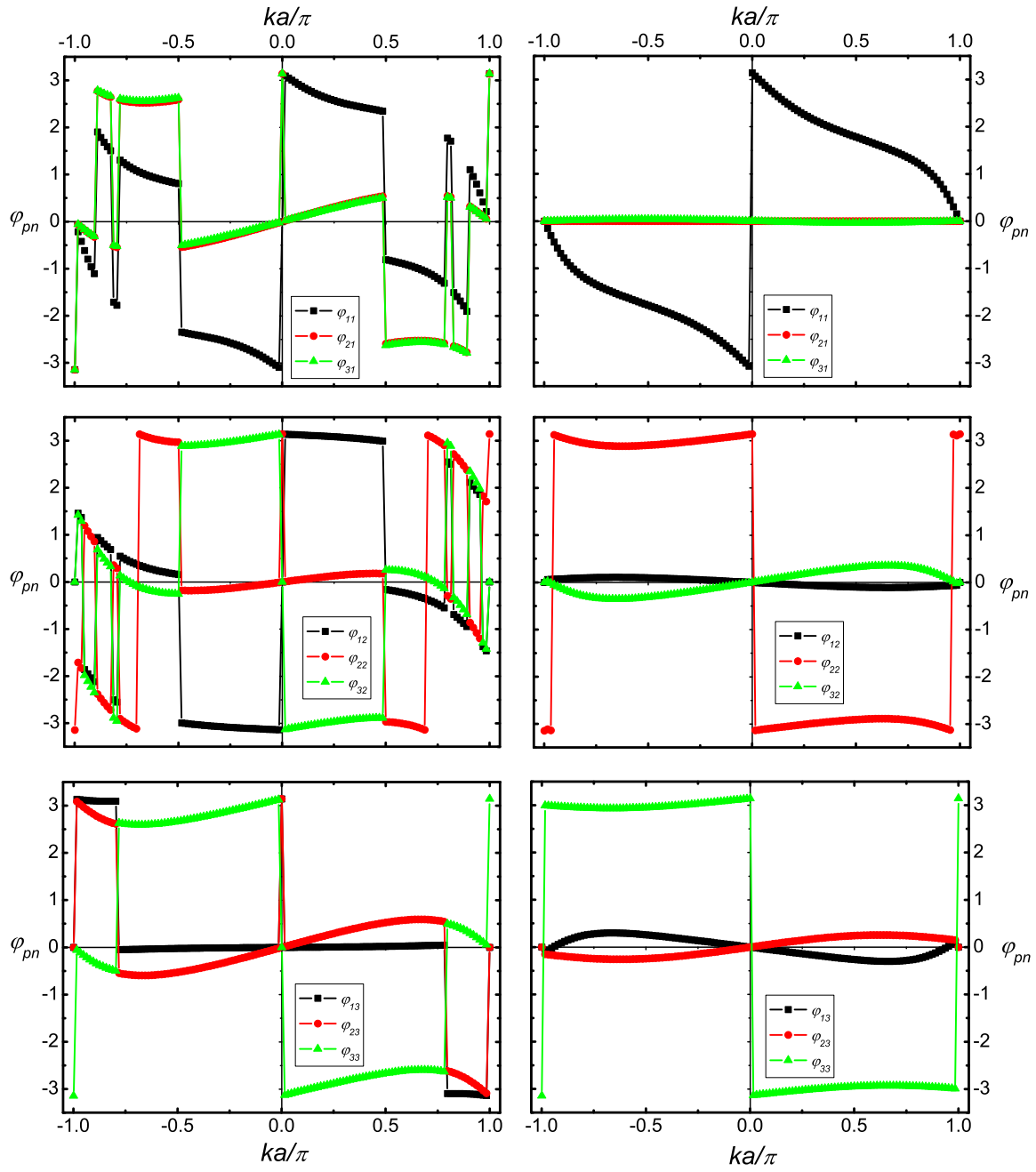

Figure 3.29: The change of the phases for the three orbitals of LiH chain without field. The three graphics on the left show the phases without using the smoothing procedure and the three on the right the phases with the smooth coefficients. $ka/\pi = -1$ and $ka/\pi = 1$ define the first Brillouin zone.

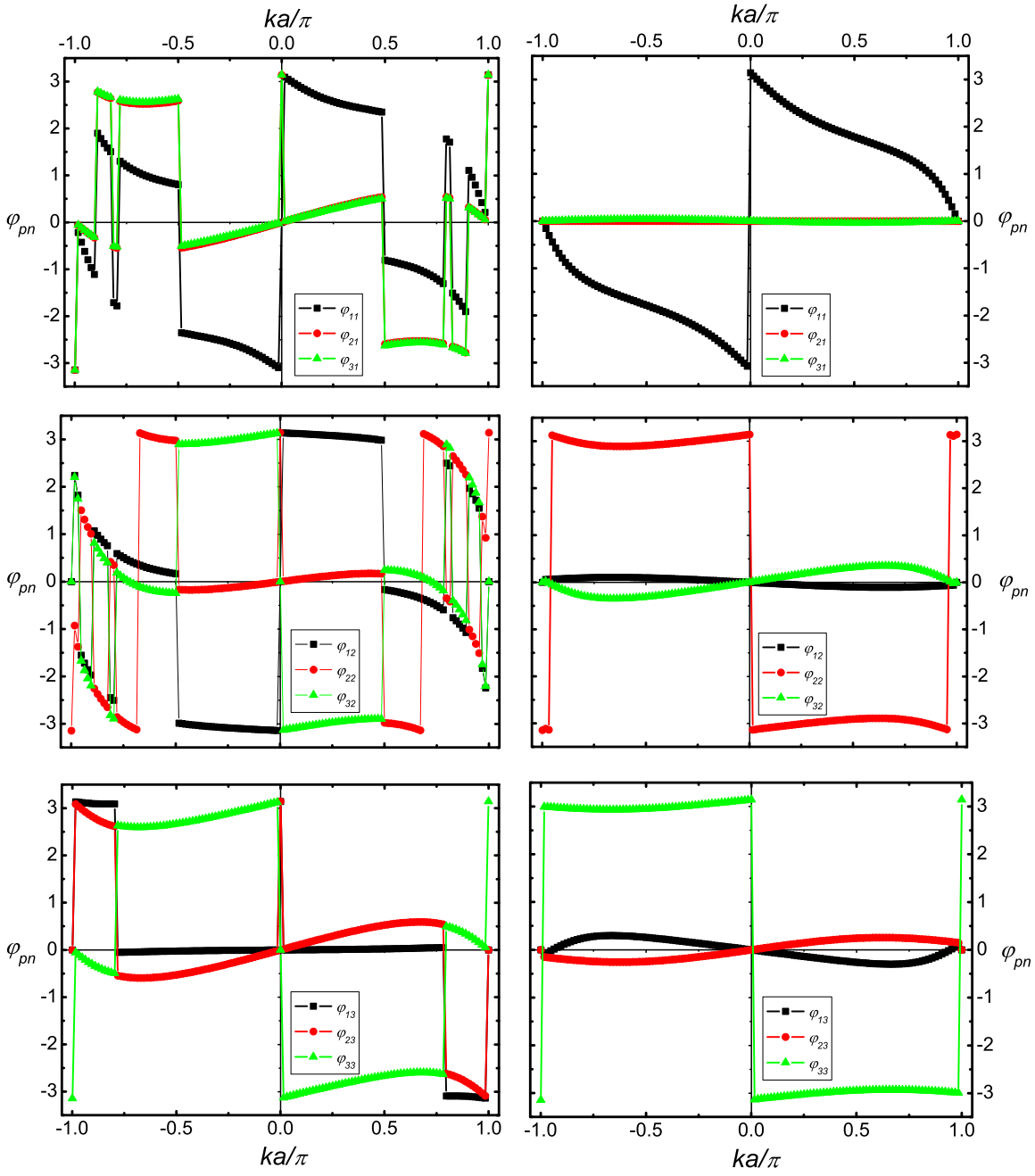

Figure 3.30: The same like in Fig. (3.29) but for $E_{\mathrm{DC}} = 0.0002$ a.u.

3.6.2 The dependence on the electric field (E_{DC})

In the following subsection the external perturbation dependency of the total energy and of the polarization of the investigated system is shown. The electric field changes from $E_{\mathrm{DC}} = -0.0008$ a.u. to $E_{\mathrm{DC}} = 0.0008$ a.u. The polarizability was calculated and compared with previous results.

Of the total energy (E_{tot})

The total energy of the system in the case of $E_{\mathrm{DC}} \neq 0$ was calculated by means of Eq. (3.29). The results are presented in Fig. (3.31). A linear dependency is evident and E_{tot} decreases with the field.

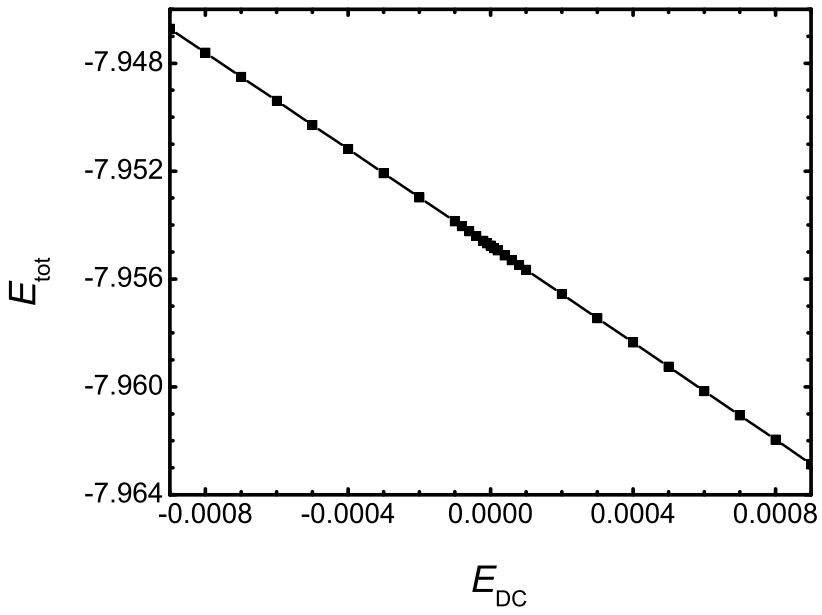

Figure 3.31: The total energy in atomic units as a function of the field amplitude.

Of the polarization (P)

The total polarization (P_{tot}) was determined by means of Eq. (3.17). In Fig. (3.32) the two contributions to the electronic polarization are plotted as a function of the electric field, from which P_2 (the lower graph) has very small values in comparison to P_1 (upper graph). However, they are not negligible, since the nonlinear distribution of the charge term (P_1) becomes linear for the total polarization (Fig. (3.33) upper panel) after addition of the current term.

In the lower panel of Fig. (3.33) the total polarization together with its charge distribution are shown in comparison. It can be seen that P_{tot} increases faster than P_1 due to the existence of a charge flow in the periodic system.

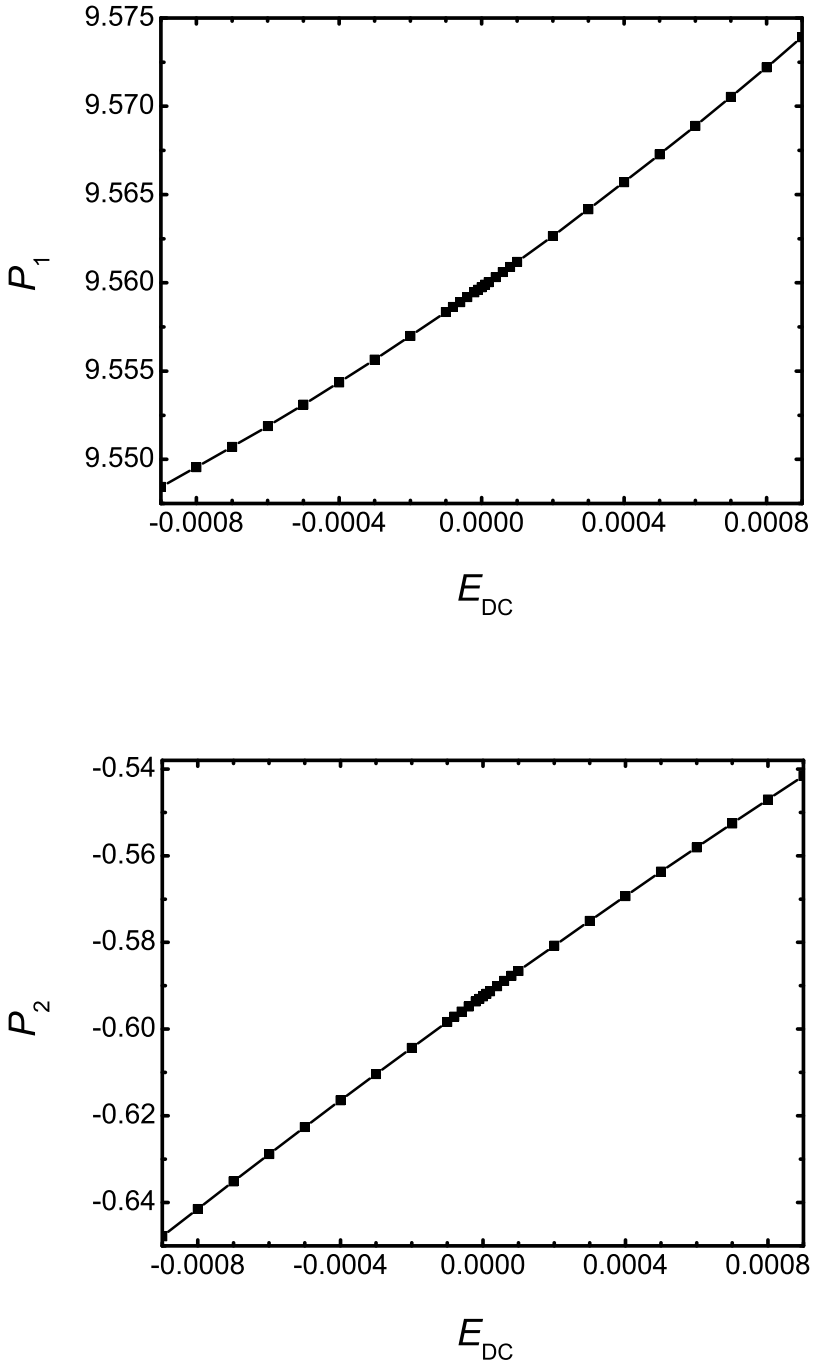

Figure 3.32: The charge (upper panel) and the current (lower panel) contribution to the polarization as a function of E_{DC}.

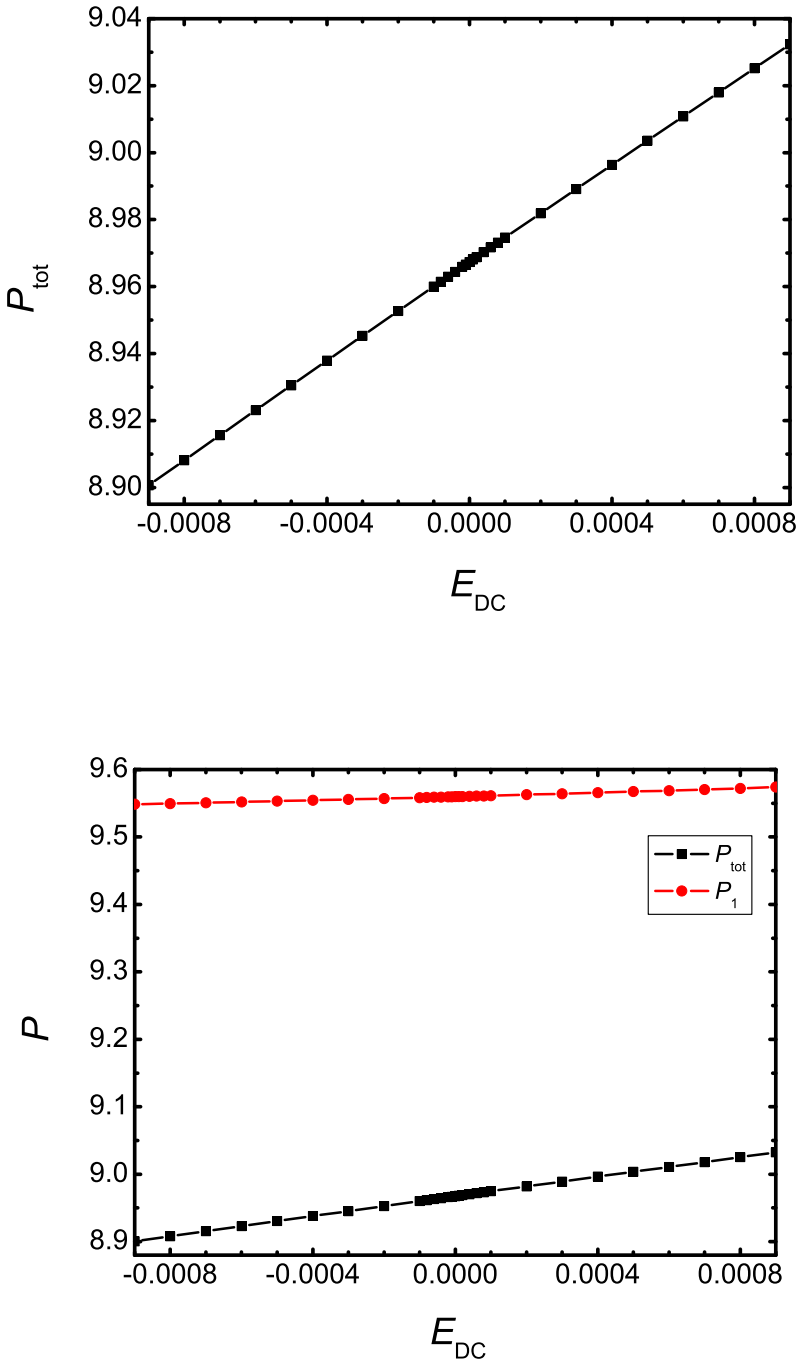

Figure 3.33: The total polarization single (upper graph) and in comparison with its charge contribution (lower graph).

Of the polarizability (α)

To calculate the polarizability along the polymer chain axis, in our case along the z axis, we utilized again the Finite Field (FF) technique and determined α via the already known polarization values at the following field amplitudes: $\pm 0.00006, \pm 0.00008, \pm 0.0001$a.u.

$$\alpha = \left(\frac{dP}{dE_{\mathrm{DC}}}\right)_{E_{\mathrm{DC}}=0} = \lim_{E_{\mathrm{DC}}\to 0} \frac{P(E_{\mathrm{DC}}) - P(-E_{\mathrm{DC}})}{2E_{\mathrm{DC}}}. \tag{3.98}$$

In Table 3.12, our findings are compared with those of Bishop and co-workers [11]. The small difference is because of the fact that in [11] convergence of α was not achieved when using $21k$ points in the first half of the Brilloiun zone and 9 neighboring unit cells on either side of the central unit cell.

α (here)	α ([11])
73.05	73.28

Table 3.12: Longitudinal polarizability in a.u. of a infinite lithium hydride chain compared with the results of Bishop et al.

3.6.3 $Li - H$ bond distance ($d_{\mathrm{Li-H}}$)

To pursue how total energy, polarization and polarizability change with the distance between the Li and H atoms in the LiH molecule, we fixed the unit cell length to be 50.0 a.u. and changed $d_{\mathrm{Li-H}}$ from 0.5 a.u. to 9.0 a.u. at two field amplitudes, $E_{\mathrm{DC}} = \pm 0.0001$ a.u.

The dependence of the total energy (E_{tot})

The dependence of the total energy of the system on the distance between the two atoms in the lithium hydride molecule will give the equilibrium geometry with the equilibrium distance d_{eq} in the case without and with field. The results are summarized in Table 3.13 and depicted in Fig. (3.34). At the three field amplitudes we found an equilibrium geometry at $d_{\mathrm{Li-H}} = 3.051$ a.u.

The accuracy of our finding is confirmed through earlier theoretical and experimental investigation on the equilibrium bond length in LiH. Comparison is shown in Table 3.14.

$d_{\mathrm{Li-H}}$	E_{tot} ($E_{\mathrm{DC}} = -0.0001$)	E_{tot} ($E_{\mathrm{DC}} = 0.0000$)	E_{tot} ($E_{\mathrm{DC}} = 0.0001$)
0.50	-5.40868	-5.40884	-5.40900
1.00	-7.13032	-7.13056	-7.13080
1.50	-7.66382	-7.66413	-7.66444
2.00	-7.87006	-7.87048	-7.87091
2.50	-7.93767	-7.93823	-7.93879
3.05	**-7.95270**	**-7.95342**	**-7.95413**
3.50	-7.94722	-7.94807	-7.94891
4.00	-7.93378	-7.93477	-7.93576
4.50	-7.91739	-7.91852	-7.91965
5.00	-7.90031	-7.90158	-7.90286
6.00	-7.86792	-7.86947	-7.87103
7.00	-7.84027	-7.84210	-7.84394
8.00	-7.81804	-7.82015	-7.82227
9.00	-7.80082	-7.80321	-7.80560

Table 3.13: The total energy values in a.u. with the change of the intramolecular distance at the three field amplitudes.

	d_{eq} (a.u.)
here	3.051
[96]	3.065
[98]	3.021
[99]	3.038
3BTSCF [102]	3.105
6BTSCF [102]	3.063
exp. [95, 97]	3.015

Table 3.14: Comparison of our results with previous theoretical investigation and with the experiment.

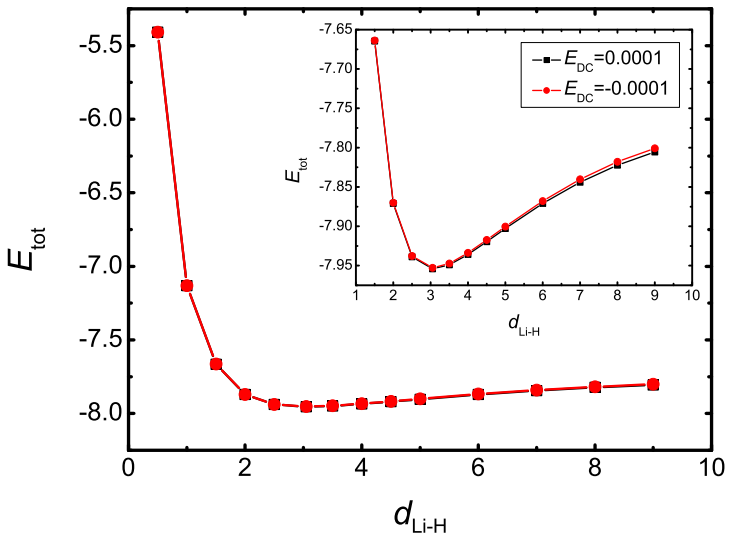

Figure 3.34: The total energy in atomic units as a function of $d_{\mathrm{Li-H}}$. The inner graph shows the distribution from $d_{\mathrm{Li-H}} = 1.5$ a.u. to 9.0 a.u.

The dependence of the polarization (P)

Here also, due to the large unit cell length ($a = 50.0$ a.u.), the charge flow term of the electronic polarization is zero

$$P_2 = 2\sum_k \sum_n \sum_{pq} iC^*_{pn}(k)\frac{\partial C_{qn}}{\partial k}S_{pq}(k) = 0 \tag{3.99}$$

and

$$P_e = P_1 \tag{3.100}$$

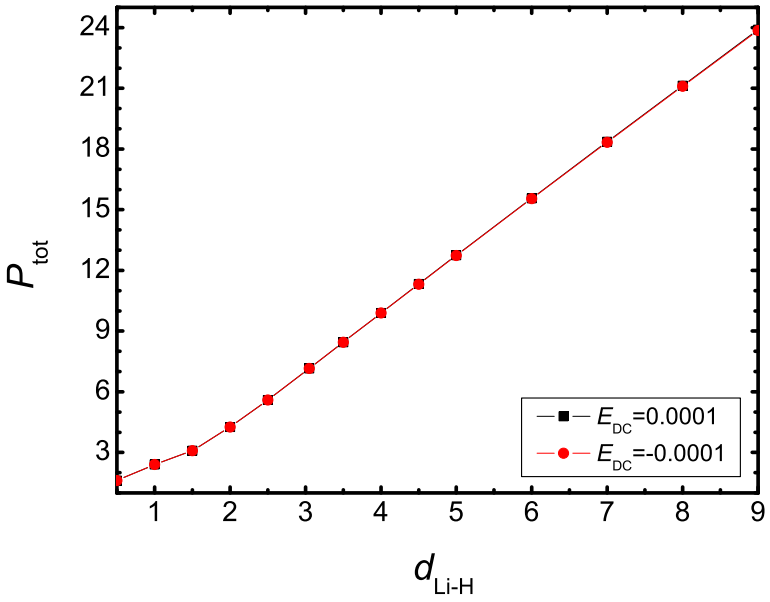

Figure 3.35: The polarization in a.u. as a function of the distance between Li and H at two field amplitudes.

As can be seen in Fig. (3.35), the polarization of a LiH molecule with different bond lengths does not depends significantly on the field amplitude, but depends on the intramolecular distance.

The dependence of the polarizability (α)

The polarizability was computed as before at $E_{\mathrm{DC}} = \pm 0.0001$ a.u. The results are listed in Table 3.15 and plotted in Fig. (3.36) for $d_{\mathrm{H-H}}$ from 0.5 a.u. to 9.0 a.u. At equilibrium $\alpha = 19.6935$ a.u.

$d_{\mathrm{Li-H}}$	α
0.50	1.8000
1.00	2.6590
1.50	4.7625
2.00	6.6300
2.50	11.5825
3.05	**19.6935**
3.50	27.9475
4.00	38.7315
4.50	51.1950
5.00	65.3765
6.00	98.9845
7.00	139.3935
8.00	185.9375
9.00	237.7875

Table 3.15: The polarizability values in a.u. with the change of the intramolecular distance.

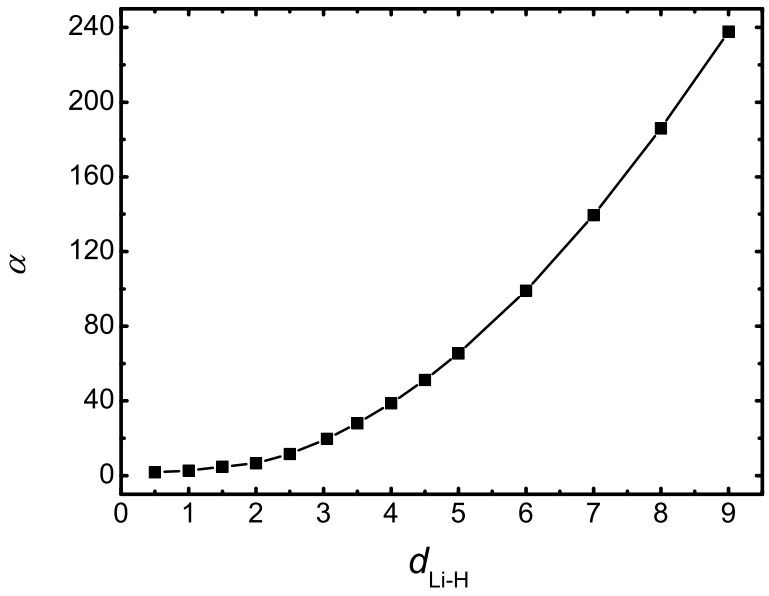

Figure 3.36: Polarizability as a function of the intramolecular distance.

3.6.4 The unit cell (a) length

In order to explore the effect of the unit cell length on the total energy, on the polarization and on the polarizability of a lithium hydride chain, we fixed the intramolecular distance at $d_{\mathrm{Li-H}} = 4.0$ a.u. and changed a from 9.0 a.u. to 100.0 a.u. The quantities were computed at $E_{\mathrm{DC}} = \pm 0.0001$ a.u.

How does total energy (E_{tot}) change?

How the total energy changes with the unit cell is shown in Fig. (3.37). The increase for $a \leq 18.0$ a.u. is very fast, then changes slowly and at the end E_{tot} converges to -7.9337067 Hartree when $E_{\mathrm{DC}} = -0.0001$ a.u. and to -7.9356860 Hartree when $E_{\mathrm{DC}} = 0.0001$ a.u.

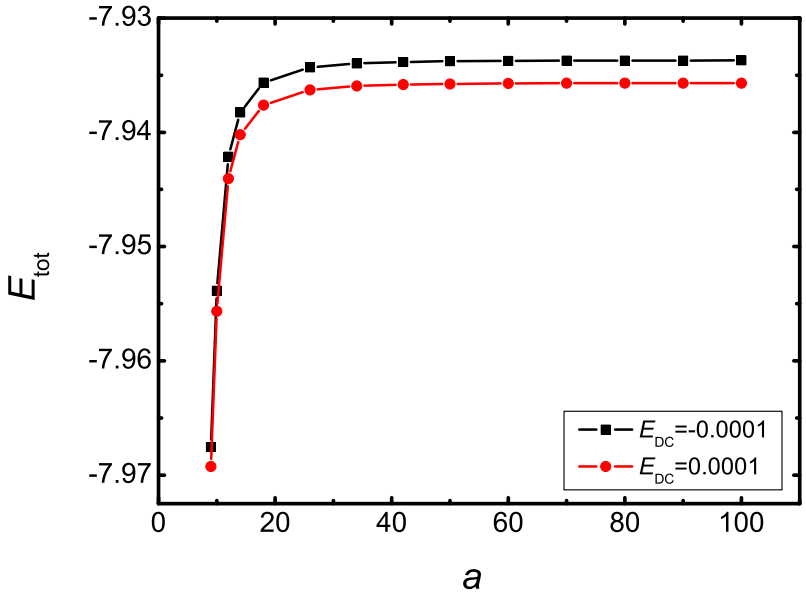

Figure 3.37: The total energy in a.u. as a function of the unit cell length at $E_{\mathrm{DC}} = \pm 0.0001$ a.u.

How does polarization (P_{tot}) change?

The current contribution to the electronic polarization will decrease with increasing a and becomes zero for long cells, then $P_e = P_1$. Here we show (Fig. (3.38)) only the distribution of the total polarization with the unit cell. For $a \leq 14.0$ a.u. P_{tot} increases very fast, then slowly and converges for $a > 34.0$ a.u.

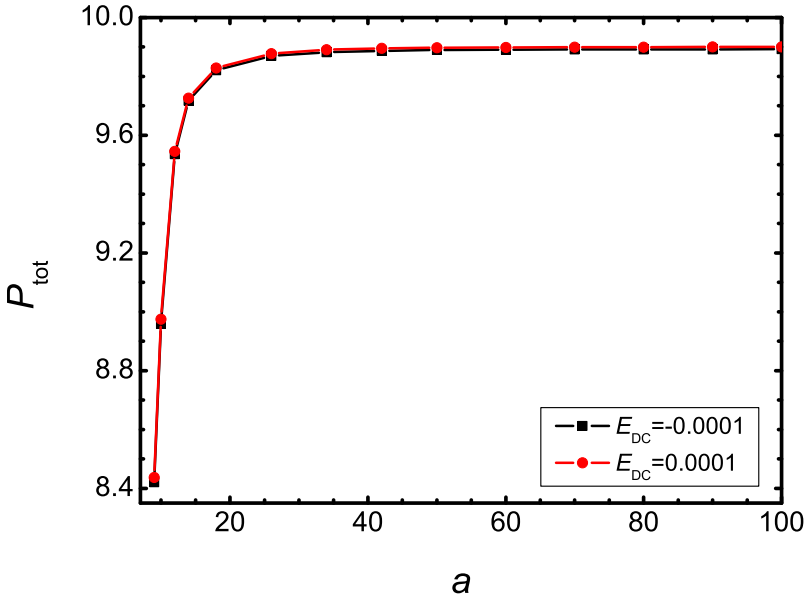

Figure 3.38: The polarization in a.u. as a function of the unit cell length at $E_{\text{DC}} = \pm 0.0001$ a.u.

How does polarizability (α) change?

The behaviour of the polarizability with increasing a, shown in Table 3.16 and in Fig. (3.39), is opposite to the behaviour of the polarization, i.e., α decreases very fast for the smaller a and then slowly till convergence.

a	α
9.0	79.1085
10.0	73.0525
12.0	48.2415
14.0	40.8730
18.0	39.0390
26.0	38.8240
34.0	38.7650
42.0	38.7425
50.0	38.7315
60.0	38.7250
70.0	38.7220
80.0	38.7205
90.0	38.7190
100.0	38.7185

Table 3.16: The polarizability values in atomic units with the change of the unit cell.

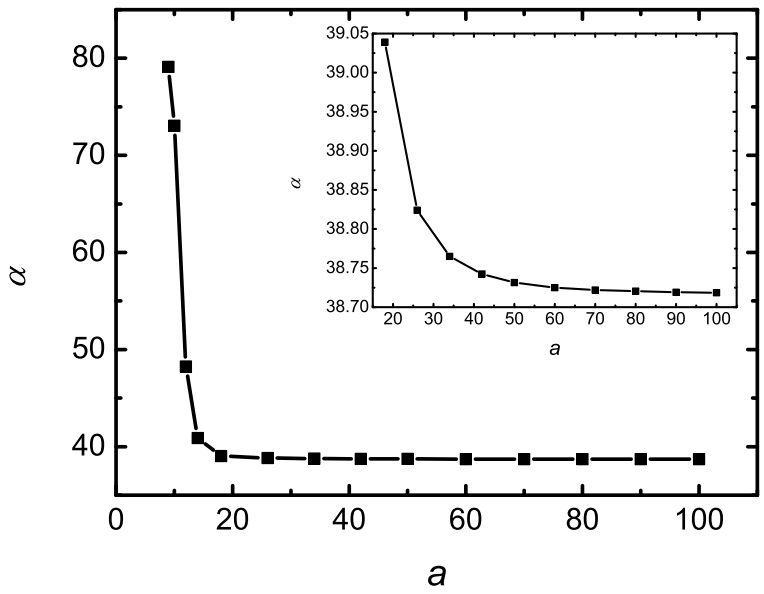

Figure 3.39: The polarizability in atomic units as a function of the unit cell length at $E_{\mathrm{DC}} = \pm 0.0001$ a.u. The inner panel show the distribution for $18.0 \leq a \leq 100.0$ a.u.

3.6.5 Band structures

The band structures of the lithium hydride chain were calculated at the following field strength: $E_{\mathrm{DC}} = 0.0000$ and ± 0.0005 a.u. The results are shown only for the highest occupied (HOMO) and the lowest unoccupied molecular orbital (LUMO). Without external perturbation (Fig. (3.40)) we got a very large energy gap, $E_{\mathrm{gap}} = 0.3010$ a.u., and Fermi level at $E_{\mathrm{F}} = -0.0942$ a.u. Table 3.17 presents the E_{F} and E_{gap} values for the three field amplitudes, and the band structures in the case of field are shown in Fig. (3.41) (for $E_{\mathrm{DC}} = \pm 0.0005$ a.u.). It is obvious that E_{gap} decreases with increasing E_{DC}. This observation was confirmed after we determined the energy gap of the system at different field strength ($-0.0008 \leq E_{\mathrm{DC}} \leq 0.0008$ a.u.). In Fig. (3.42) the almost linear reduction of E_{gap} can be seen.

E_{DC}	E_{F}	E_{gap}
-0.0005	-0.0867	0.3303 (8.99)
0.0000	-0.0942	0.3010 (8.19)
0.0005	-0.1017	0.2718 (7.39)

Table 3.17: Fermi energy (E_{F}) and energy gap (E_{gap}) for three field amplitudes. The values in the parentheses are for E_{gap} in eV. All other values are in a.u.

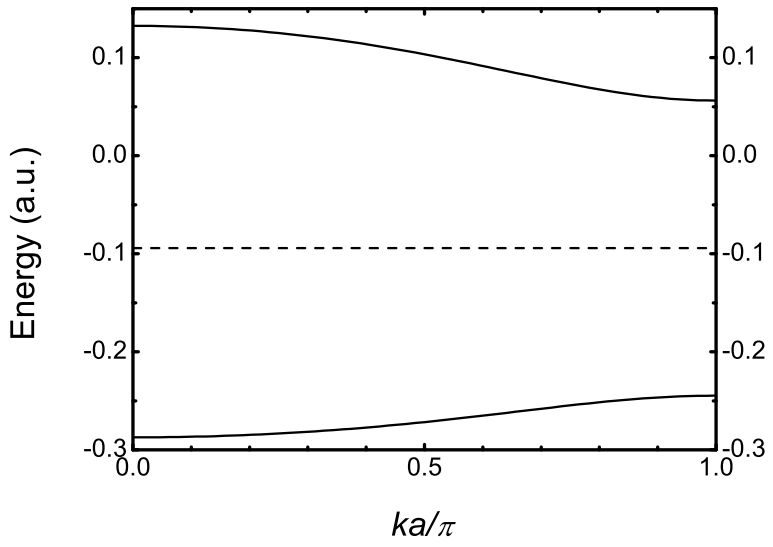

Figure 3.40: The band structure of LiH without field. Only the highest occupied (HOMO) and the lowest unoccupied molecular orbital (LUMO) are shown. $ka/\pi = 0$ and $ka/\pi = 1$ are the center and the edge of the first Brillouin zone, respectively, and the dashed line marks the Fermi level.

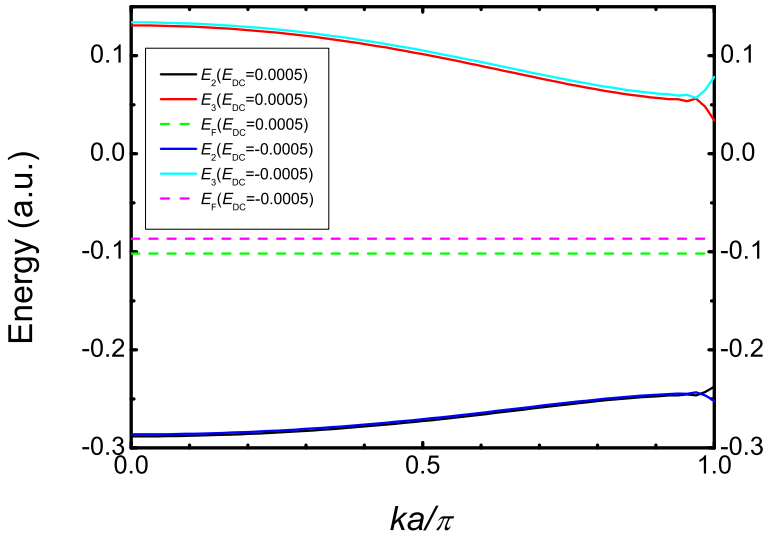

Figure 3.41: The band structures at two different amplitudes, $E_{\mathrm{DC}} = \pm 0.0005$ a.u. Only the highest occupied (HOMO) and the lowest unoccupied molecular orbital (LUMO) are shown. $ka/\pi = 0$ and $ka/\pi = 1$ are the center and the edge of the first Brillouin zone, respectively, and the dashed lines mark the Fermi level.

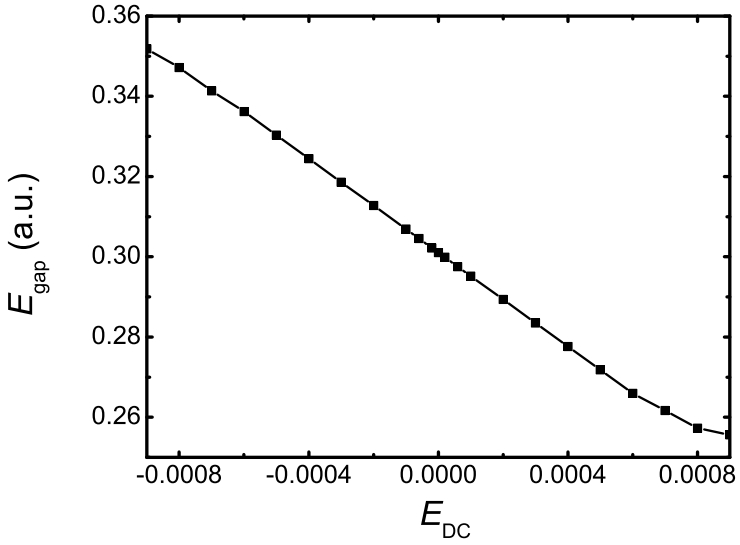

Figure 3.42: The energy gap as a function of the field strength.

Chapter 4

Surface effects in electric field polarization of periodic systems

In this Chapter we will present the second part of our study, which concerns the termination effects in electric field polarization of periodic systems. Only quasi-one-dimensional (quasi-1D) systems are taken into account, but the results may be extended to 2D films and 3D solids. The fundamentals and findings, presented below are taken from [62], where our last results were recently published.

4.1 Introduction

The question of whether terminations or surfaces influence the polarization has been the subject of discussion for several decades [57, 58, 59, 60, 61, 104, 105, 14]. A rigorous formulation establishing that polarization is a bulk property was, finally, presented by Vanderbilt and King-Smith [14]. Nonetheless, there remains a sense in which it is surface-dependent. Thus, as we will demonstrate here, the termination of 1D chains can influence experimental observables determined by the polarization. Specifically, we show that the lattice constant in the inner part of an extended 1D system exposed to a uniform longitudinal electrostatic field may be altered by changing the terminations. The same is true of internal structural parameters as well. Most importantly, we also present a procedure for determining this effect from calculations on the corresponding infinite periodic system.

An experimental realization of the surface-dependent case may be obtained by considering a long chain like that of Fig. 4.1, placed between two electrodes. Applying a potential between the two electrodes, the length of the chain will change. This change is monitored during the experiment and may, in general, be partly due to changes in the

length of the bulk region and partly due to changes in the lengths of the units in the terminations. Often the change in length due to the terminations can be neglected in comparison with the macroscopic effect arising from the change in the bulk lattice constant, a. Sometimes, however, we have found that such will not be the case. In either event the contribution from the terminations can be accounted for by determining the chain length dependence of the structural response. Then, a plot of the change in length per bulk unit versus the fixed field strength, $E_{\rm DC}$, can be used to obtain the zero field limit

$$\frac{da}{dE_{\rm DC}}\Big|_{E_{\rm DC}=0}. \tag{4.1}$$

We shall demonstrate that this change, which can be experimentally obtained [106], depends on the terminations.

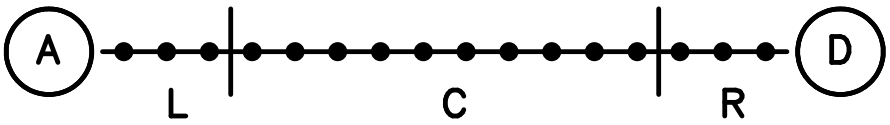

Figure 4.1: Schematic representation of a long, but finite, regular chain. Each filled circle, placed regularly along the chain axis (the z axis), represents a building block containing one or more atoms. Donor and acceptor groups (D and A) may be included at the terminations. The separation into a central (C) and two terminal (L and R) regions is indicated by the vertical lines.

4.2 Theory and Computational Approach

A schematic representation of a long, but finite, 1D chain is shown in Fig. 4.1. It is useful to split this system into three distinct spatial parts, a perfectly regular central region (C) where the electrons do not feel the finite size of the system, and two terminal regions (L and R). The response of the system to an electrostatic field is most conveniently quantized through the dipole moment per unit, which component along the (z) chain axis can be defined as

$$\mu = \lim_{N\to\infty} \left[\mu(N+1) - \mu(N)\right], \tag{4.2}$$

where N is the number of units in the chain and μ is the z component of the total dipole moment. With the spatial separation above we have [107, 108]

$$\begin{aligned}\mu &= \int_L \rho(\vec{r}) z d\vec{r} + \int_C \rho(\vec{r}) z d\vec{r} + \int_R \rho(\vec{r}) z d\vec{r} \\ &= N_C \mu_C + \left[z_R \int_R \rho(\vec{r}) d\vec{r} + z_L \int_L \rho(\vec{r}) d\vec{r} \right] \\ &+ \left[\int_L \rho(\vec{r})(z - z_L) d\vec{r} + \int_R \rho(\vec{r})(z - z_R) d\vec{r} \right],\end{aligned} \tag{4.3}$$

in which $\rho(\vec{r})$ is the total charge density, μ_C is the z component of the dipole moment of a (neutral) central unit and N_C is the number of units in C. Finally, z_R and z_L describe the centers of nuclear charge in the R and L regions, respectively. Assuming that the entire system is neutral, a combination of Eqs. (4.2) and (4.3) gives (see Ref. [107])

$$\mu = \mu_C + Q_R \cdot a, \tag{4.4}$$

where Q_R $(= -Q_L)$ is the total charge in R (L), and a is the unit cell lattice constant of C. According to this expression the dipole moment per unit depends on the charge accumulated in the terminal regions which, at first glance, can vary widely.

There are, however, restrictions on the surface charges as Vanderbilt and King-Smith [14] have shown. They write the electronic part of the dipole moment in terms of localized orbitals w_{lp}

$$\mu_e = \sum_l \sum_p \int |w_{lp}(\vec{r})|^2 z d\vec{r}, \tag{4.5}$$

where w_{lp}, the pth orbital localized to the lth unit, is obtained by a unitary transformation of the occupied canonical orbitals. Then, using the idempotency of the density matrix, it is proved that the number of electrons associated with the terminal regions must be integral. On this basis, the dipole moment per unit (and, consequently, the polarization) is essentially a bulk property, with quantized values that differ from one another only by lattice vectors [107, 109]. It follows that this property is accessible (modulo a lattice vector) through a conventional band-structure calculation on an infinite periodic system, even though there are no terminations (per construction) in the latter case.

For a 1D periodic system the electronic orbitals may be written as

$$\psi_n(k, \vec{r}) = e^{ikz} u_n(k, \vec{r}), \tag{4.6}$$

where n is a band index and $u_n(k,\vec{r})$ is lattice periodic. Usually, a finite set of N equidistant k points in the interval $[-\frac{\pi}{a};\frac{\pi}{a}]$ is employed in a band structure calculation. According to both the MTP and VPA treatments one may write the electronic part of the static dipole moment per unit as [15, 9, 110]

$$\mu_{\mathrm{KSV}} = \frac{i}{N}\sum_{k=1}^{N}\sum_{n=1}^{B}\langle u_n(k)|\frac{\partial}{\partial k}u_n(k)\rangle. \tag{4.7}$$

In Eq. (4.7) B is the number of singly occupied bands (we assume that there is a gap between occupied and empty orbitals and allow for spin-up and spin-down orbitals to be different). The total dipole moment per unit is obtained by adding the contribution from the nuclei in the 0th unit cell.

In Eq. (4.6) the orbitals may be modified by band and k dependent phase factors,

$$\psi_n(k,\vec{r}) \rightarrow e^{i\phi_n(k)}\psi_n(k,\vec{r}), \tag{4.8}$$

in which

$$\phi_n(+\pi/a) - \phi_n(-\pi/a) = \tilde{n}_n \cdot 2\pi \tag{4.9}$$

since

$$e^{i\phi_n(+\pi/a)} = e^{i\phi_n(-\pi/a)}. \tag{4.10}$$

Thus, μ contains an unknown, additive constant, $\tilde{n}\cdot a$, with $\tilde{n} = \sum_n \tilde{n}_n$.

For both the extended, but finite, system and the infinite periodic model for this system the dipole moment per unit may be changed by an integer multiple of the unit cell lattice constant. However, the origin of the integer is quite different in the two cases. For the finite chain it has a physical origin determined by the terminations which govern the charge accumulated at the chain ends. Accordingly, the integer is fixed by the electronic structure. For the infinite periodic model the integer is related to a mathematical ambiguity in the phase of a complex number and is completely arbitrary. Here, we demonstrate that a fixed choice of the integer for the infinite periodic system corresponds to modelling a finite chain with a specific charge in the terminal region. We do this by considering a long finite oligomeric chain with different terminations (see Fig. 4.1) and, as a result, different charge accumulation at the chain ends. When exposed to electrostatic (DC) fields different electronic and structural response properties are obtained. It is, then,

shown that all such properties can be reproduced by maintaining an appropriate fixed value of $\tilde{n}$ in corresponding model infinite periodic chain calculations.

In order to perform extensive calculations, and to avoid truncation and other numerical errors, we use the model Hamiltonian as described in Subsection 3.2.5 and employed in earlier studies [12, 9, 62]. In doing so we emphasize that no attempt is made to reproduce results for any real system, but that the model Hamiltonian contains all important features of a parameter-free electronic structure calculation.

As already introduced, for the finite chain the DC field is included in the electronic Hamiltonian through the term $-\sum_i E_{\rm DC} z_i$, where z_i is the z coordinate of the ith electron, $E_{\rm DC}$ is the amplitude of the DC field, and we have set the magnitude of the elementary charge $|e| = 1$. And for the infinite periodic chains the DC field is included by means of the VPA methodology [10, 11]. If the crystal orbitals are written in the form

$$\psi_n(k,\vec{r}) = \sum_{{\rm X},p} C_{{\rm X},p,n}(k) \frac{1}{\sqrt{N}} \sum_l e^{ikal} \chi_{l{\rm X}p}(\vec{r}) \tag{4.11}$$

then the orbital coefficients are obtained by solving the equations [9, 10, 11, 108, 12]

$$\left\{ \underline{\underline{F}}(k) - E_{\rm DC} \cdot \left[\underline{\underline{M}}(k) + i\underline{\underline{S}}(k) \frac{d}{dk} \right] \right\} \cdot \underline{C}_n(k) = \epsilon_n(k) \cdot \underline{\underline{S}}(k) \cdot \underline{C}_n(k), \tag{4.12}$$

where $S_{pq}(k)$, $M_{pq}(k)$, and $F_{pq}(k)$ are the overlap, unit cell dipole, and Fock (or Kohn-Sham) matrix elements, respectively. In other words, the finite chain dipole moment matrix is replaced by the quantity in square brackets in Eq. (4.12). The dipole moment per unit of the infinite periodic system, which is determined by the operator in square brackets in the last equation, will lie in a certain range of length a. In order to modify this range by an integer times a, the orbitals of one or more bands are given additional phase factors, $e^{iak\tilde{n}_n}$, with $\tilde{n}_n$ being an integer. Then, the phases become discontinuous across the boundary of the Brillouin zone, although the phase factors remain continuous. This leads to an additional term,

$$-E_{\rm DC} \sum_n \tilde{n}_n = -E_{\rm DC} \tilde{n}, \tag{4.13}$$

in the derivative of the total energy with respect to the lattice parameter a.

For the finite chain Eq. (4.2) is used to determine the dipole moment per unit. We found that chains of length $N = 40$ and $N = 41$ were sufficient to achieve convergence. For the infinite periodic chains $N = 80$ k points were used. Finally, in order to obtain

different terminations for the finite chains we modified the on-site energies $\langle\chi_{1\mathrm{A}i}|\hat{h}_0|\chi_{1\mathrm{A}i}\rangle$ and $\langle\chi_{N\mathrm{B}i}|\hat{h}_0|\chi_{N\mathrm{B}i}\rangle$ for $i = 1, 2$. In the calculations below this allowed us to change the charge at the chain ends by ± 2 electrons.

4.3 Results

In the next two figures, Fig. 4.2 and Fig. 4.3, the different symbols in each panel correspond to periodic chain calculations for different values of the integer $\tilde{n}$. The full lines are finite chain values for charge accumulation of either 0 or +2 electrons as compared to the case where the charge in the chain terminations is similar to that of the central region.

Fig. 4.2 shows the results for the optimized lattice constant a (top panel) and the internal structural parameter u (bottom panel) from the model Hamiltonian calculations for finite chains with $N = 40$ units and for periodic chains with 80 k points. Both parameters show a clear dependence on the value of $\tilde{n}$, i.e., on the range inside which the dipole moment per unit is required to lie. This is consistent with the differing chemical nature of the finite chain that is being simulated. The corresponding finite chain results (solid lines) obtained from Eq. (3.32) once more agree with the periodic chain values.

The lower panel in Fig. 4.3 shows the field-dependent dipole moment per unit at the optimized geometry. In the periodic chain calculations the integer was chosen so that the dipole moment coincides with the finite chain value at zero field. For different $\tilde{n}$ (or different charge) there is a large difference in the dipole moment. In order to fit all our results in one panel we have shifted the calculated values by a constant, namely an integer multiple of the field free lattice constant a_0. Evidently, the periodic and representative finite chain results coincide (within numerical accuracy) at all fields. The upper panel of the same figure gives the number of electrons (i.e., the Mulliken gross populations) on one of the central A atoms obtained for the same set of calculations. Again, the infinite periodic chain results and the finite chain values are identical at all fields.

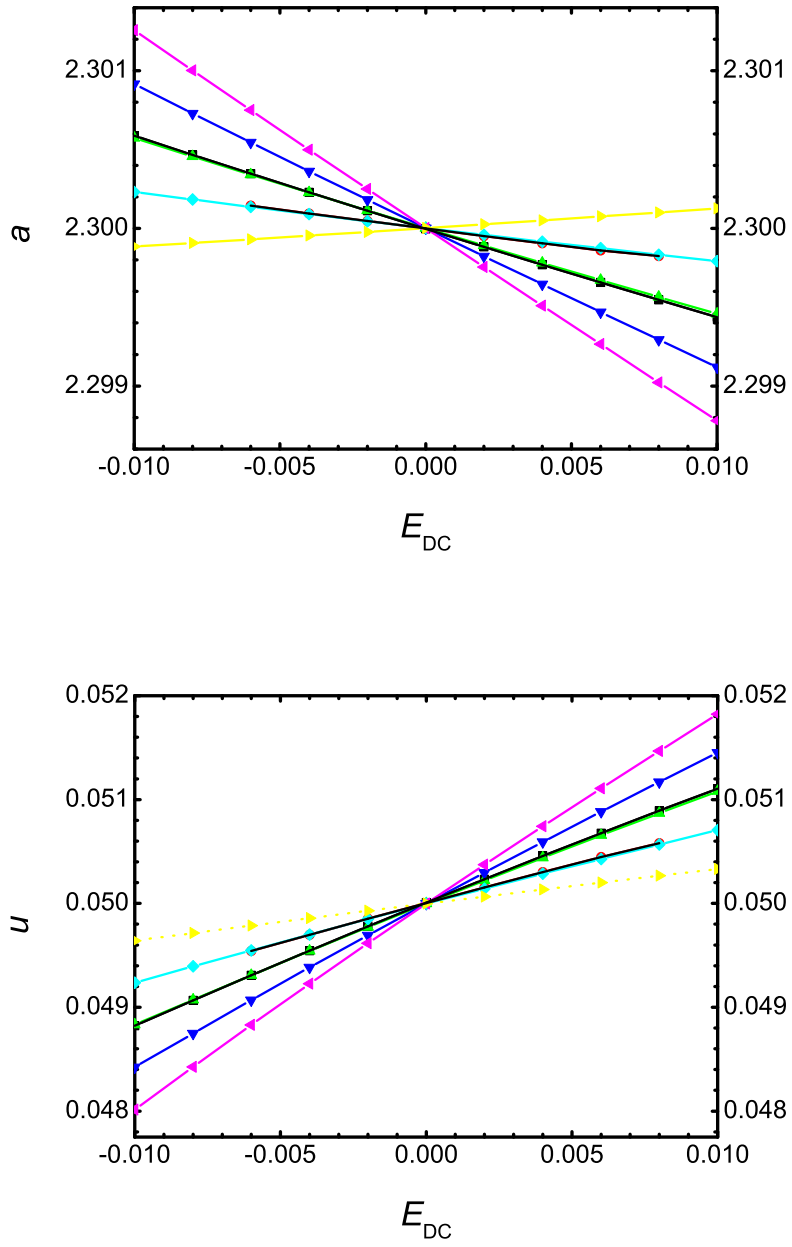

Figure 4.2: Results for the optimized lattice constant a (top panel) and the internal structural parameter u (bottom panel) from the model Hamiltonian calculations for finite chains with $N = 40$ units (full lines) and for periodic chains with 80 k points. For the periodic chains the different symbols represent results for different values of the integer $\tilde{n}$.

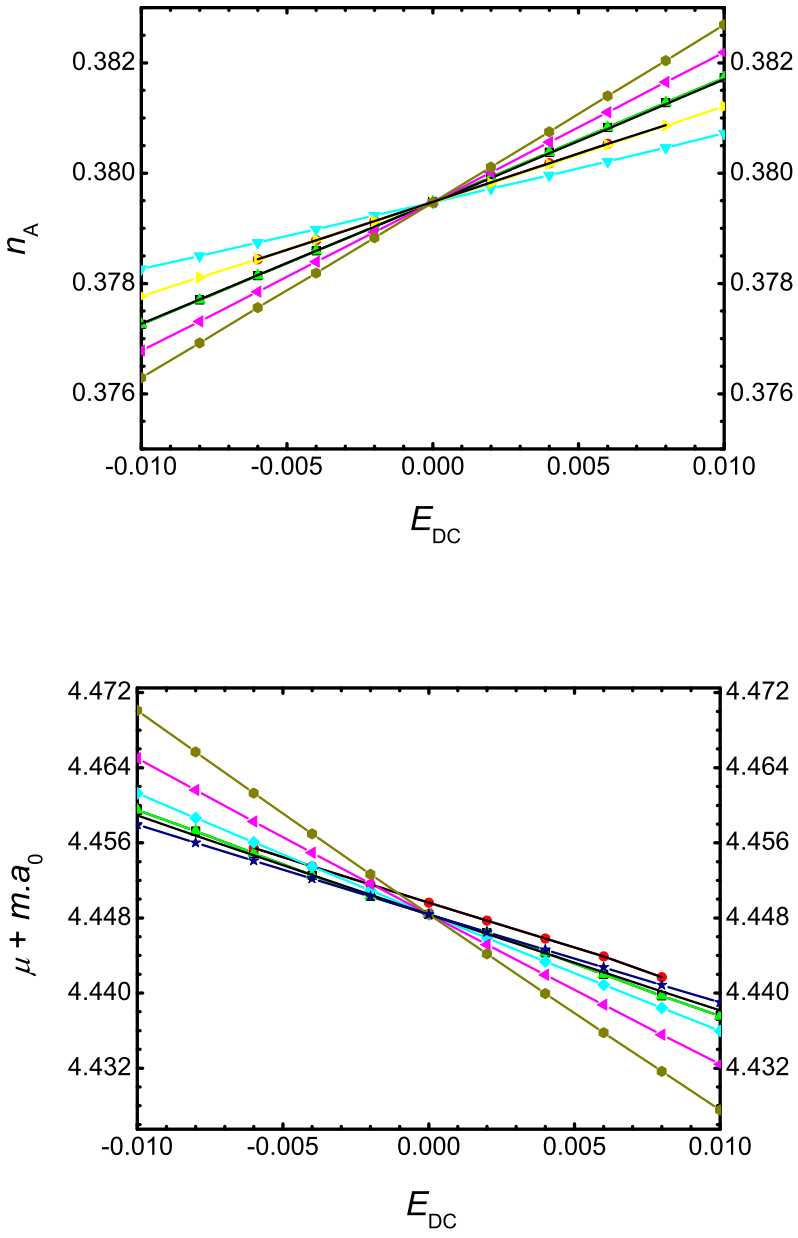

Figure 4.3: Results for the number of electrons n_A on the central A atom relative to the neutral case (upper panel) and the adjusted dipole moment per unit μ (lower panel) from the model Hamiltonian calculations for finite chains with $N = 40$ units (full lines) and for periodic chains with 80 k points. For the periodic chains the different symbols represent results for different values of the integer $\tilde{n}$. In the bottom panel we have added an integer (m) times the field-free lattice constant in order to facilitate a comparison between the different results.

The fact that the structure depends on $\tilde{n}$ can easily be seen by expanding the total energy per unit, $E_{\rm tot}$, about the field-free value through second-order in terms of the lattice constant (a), internal structural parameter (u), and $E_{\rm DC}$

$$\begin{aligned} E_{\rm tot} \equiv E_{\rm tot}(a,u,E_{\rm DC}) \simeq E_{\rm tot,0} &+ E_{\rm DC}\frac{\partial E_{\rm tot}}{\partial E_{\rm DC}} + \frac{1}{2}(a-a_0)^2\frac{\partial^2 E_{\rm tot}}{\partial a^2} \\ &+ \frac{1}{2}(u-u_0)^2\frac{\partial^2 E_{\rm tot}}{\partial u^2} + (u-u_0)(a-a_0)\frac{\partial^2 E_{\rm tot}}{\partial u \partial a} \\ &+ \frac{1}{2}E_{\rm DC}^2\frac{\partial^2 E_{\rm tot}}{\partial E_{\rm DC}^2} + E_{\rm DC}(a-a_0)\frac{\partial^2 E_{\rm tot}}{\partial E_{\rm DC}\partial a} + E_{\rm DC}(u-u_0)\frac{\partial^2 E_{\rm tot}}{\partial E_{\rm DC}\partial u}. \end{aligned} \tag{4.14}$$

Here the field, rather than the voltage (see later), is considered as the independent variable. This corresponds to an experimental setup where different materials that may possess different macroscopic changes in size due to the electrostatic field are experiencing the same field strength.

With the expansion of Eq. (4.14) one may derive an approximate expression for the change in the lattice parameter due to a given electrostatic field by setting the derivative

$$\frac{\partial E_{\rm tot}}{\partial a} = 0 \tag{4.15}$$

at the field value, and the same may be done for the internal structural parameter. The result of solving this pair of coupled simultaneous equations can be expressed in terms of the piezoelectric-like coefficients

$$d_a = \frac{da}{dE_{\rm DC}}\Big|_{E_{\rm DC}=0} \tag{4.16}$$

and

$$d_u = \frac{du}{dE_{\rm DC}}\Big|_{E_{\rm DC}=0} : \tag{4.17}$$

$$\begin{aligned} d_a = &\left[\frac{\partial^2 E_{\rm tot}}{\partial E_{\rm DC}\partial u}\frac{\partial^2 E_{\rm tot}}{\partial u \partial a} - \frac{\partial^2 E_{\rm tot}}{\partial E_{\rm DC}\partial a}\frac{\partial^2 E_{\rm tot}}{\partial u^2}\right] \\ &\times \left[\frac{\partial^2 E_{\rm tot}}{\partial a^2}\frac{\partial^2 E_{\rm tot}}{\partial u^2} - \left(\frac{\partial^2 E_{\rm tot}}{\partial u \partial a}\right)^2\right]^{-1} \end{aligned} \tag{4.18}$$

$$d_u = \left[\frac{\partial^2 E_{\rm tot}}{\partial E_{\rm DC}\partial a}\frac{\partial^2 E_{\rm tot}}{\partial u \partial a} - \frac{\partial^2 E_{\rm tot}}{\partial a^2}\frac{\partial^2 E_{\rm tot}}{\partial E_{\rm DC}\partial u}\right] \times \left[\frac{\partial^2 E_{\rm tot}}{\partial a^2}\frac{\partial^2 E_{\rm tot}}{\partial u^2} - \left(\frac{\partial^2 E_{\rm tot}}{\partial u \partial a}\right)^2\right]^{-1}. \tag{4.19}$$

Since the dipole moment per unit,

$$\mu = -\frac{\partial E_{\rm tot}}{\partial E_{\rm DC}}, \tag{4.20}$$

contains a contribution equal to $\tilde{n}a$, the partial derivative

$$\frac{\partial^2 E_{\rm tot}}{\partial E_{\rm DC}\partial a} \tag{4.21}$$

depends upon $\tilde{n}$. Hence, both piezoelectric-like coefficients will depend upon this integer.

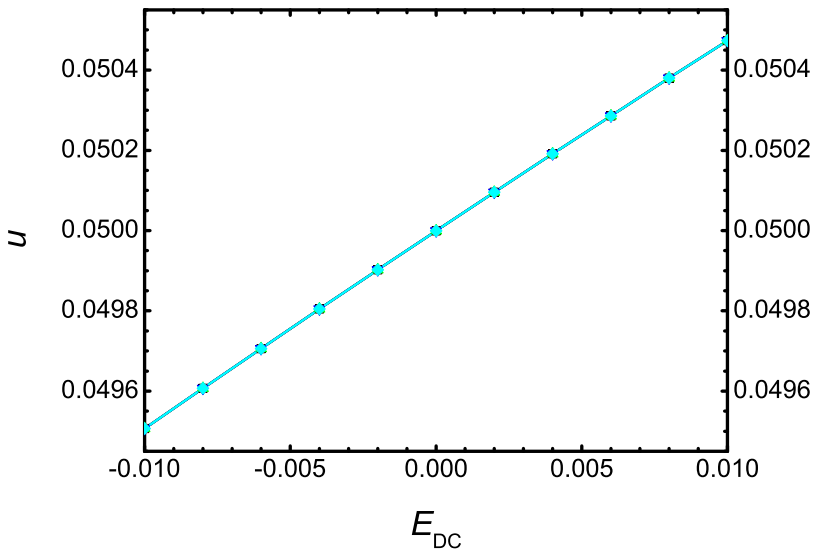

Figure 4.4: Results for the internal structural parameter u from model Hamiltonian calculations with fixed lattice parameter.

The dependence of the bulk quantities on the surfaces is solely due to the fact that the lattice parameter depends on $\tilde{n}$. This can be seen by repeating the periodic chain calculations of Fig. 4.2 and Fig. 4.3 but with this parameter fixed at the field-free value,

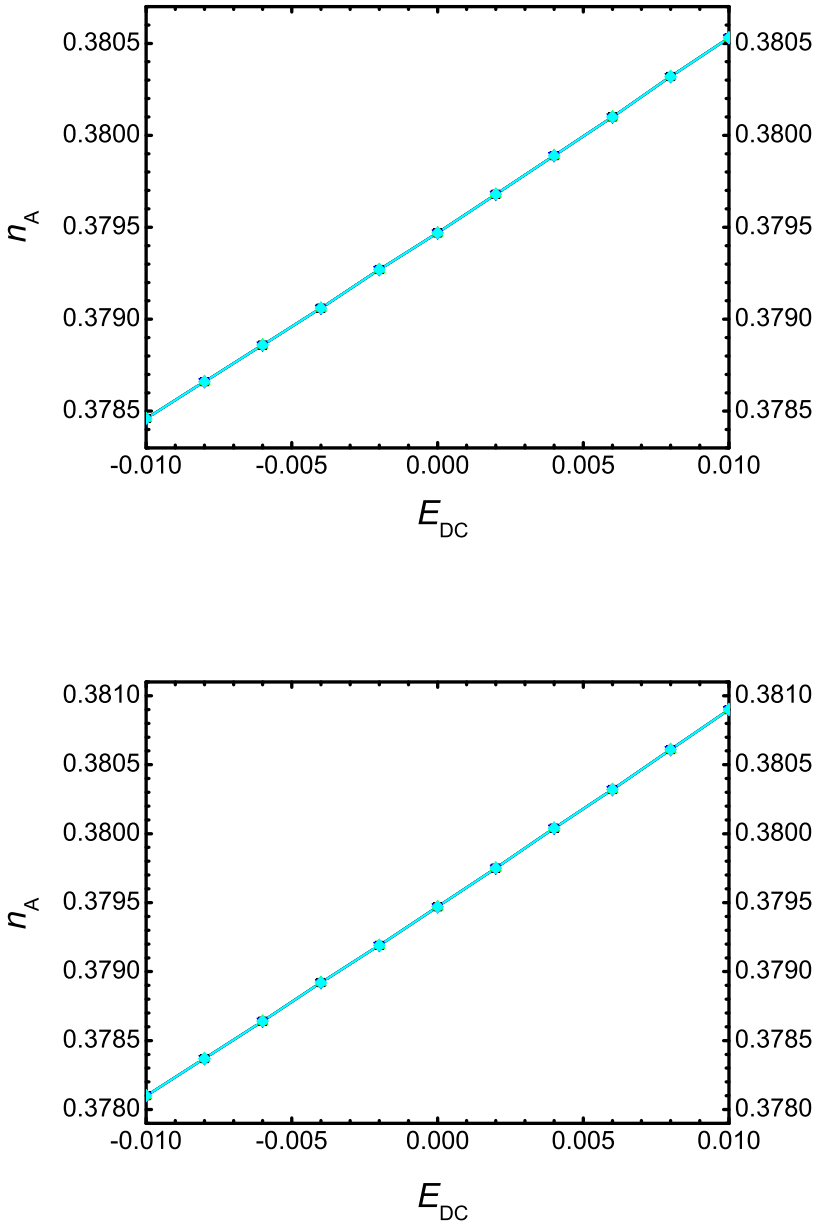

Figure 4.5: Results for the number of electrons n_A on the central A atom relative to the neutral case from model Hamiltonian calculations with fixed lattice parameter. The upper panel is for the initial structure, and the bottom one after relaxing u.

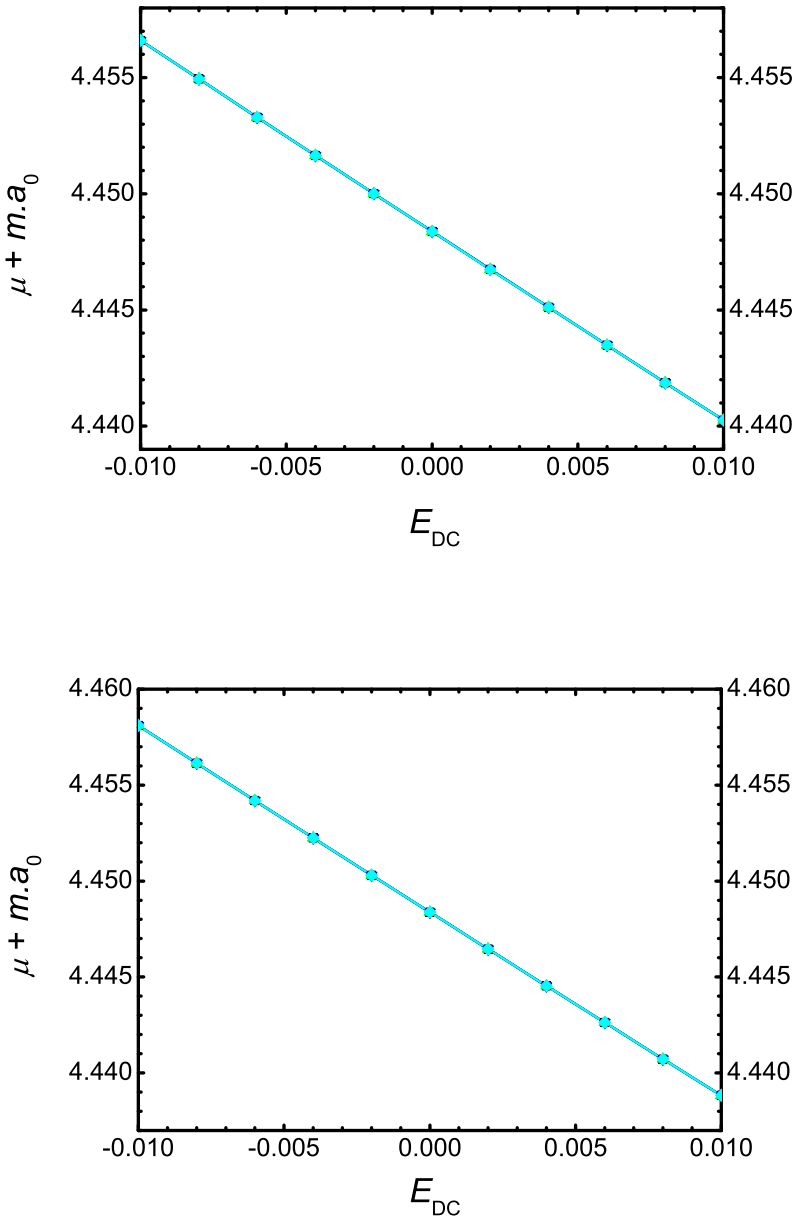

Figure 4.6: Results for the adjusted dipole moment per unit μ from model Hamiltonian calculations with fixed lattice parameter. The upper panel is for the initial structure, and the bottom one after relaxing u.

a_0. In Fig. 4.4, Fig. 4.5 and Fig. 4.6 are shown the results for the internal structural parameter u, for the number of electrons n_{A} on the central A atom relative to the neutral case and for the adjusted dipole moment per unit μ, respectively. It is evident that all symbols fall on the same curve. Thus, all values of $\tilde{n}$ lead to the same results. Moreover, by comparing with Fig. 4.2 and Fig. 4.3 it is seen that relaxing a leads, in general, to considerably stronger property variations, as a function of field strength, than just relaxing u.

So far we have considered how the structural parameters change as a function of the field strength. In particular, the analogue of da/dE_{DC} for thin films can be determined by phase modulation measurements [106]. Alternatively, one may determine the variation of the structural parameters as a function of the voltage. Assuming that the length of the macroscopic chain in the absence of the field equals L ($L \gg a_0$), the total potential across the sample, V_{ext} is given by

$$V_{\mathrm{ext}} = \frac{L}{a_0} V_{\mathrm{DC}} = \frac{La}{a_0} E_{\mathrm{DC}}. \tag{4.22}$$

Here, V_{DC} is the potential drop over one unit cell, i.e., $a \cdot E_{\mathrm{DC}}$. In an experiment where different samples are exposed to the same external voltage, V_{ext} or V_{DC}, the field strength will generally be different. For that case, we express E_{tot} in terms of the independent variables V_{DC}, a, and u. This leads to the piezoelectric-like coefficients defined as

$$d_{a,\mathrm{V}} = a_0 \frac{da}{dV_{\mathrm{DC}}}\Big|_{V_{\mathrm{DC}}=0} \tag{4.23}$$

and

$$d_{u,\mathrm{V}} = a_0 \frac{du}{dV_{\mathrm{DC}}}\Big|_{V_{\mathrm{DC}}=0}. \tag{4.24}$$

These coefficients have the same dimension as those of Eq. (4.18) and Eq. (4.19). After transforming the analogue of Eq. (4.14) to the same set of partial derivatives that appear in the latter, it turns out that $d_{a,\mathrm{V}}$ and $d_{u,\mathrm{V}}$ are given by the same expressions as in Eq. (4.18) and Eq. (4.19) except for the replacement

$$\frac{\partial^2 E_{\mathrm{tot}}}{\partial E_{\mathrm{DC}} \partial a} \rightarrow \frac{\partial^2 E_{\mathrm{tot}}}{\partial E_{\mathrm{DC}} \partial a} - \frac{1}{a_0} \frac{\partial E_{\mathrm{tot}}}{\partial E_{\mathrm{DC}}} = - \left(\frac{\partial \mu}{\partial a} - \frac{\mu}{a} \right) \Bigg|_{a=a_0}. \tag{4.25}$$

This term is independent of $\tilde{n}$ and, consequently, the dependence of the responses

$$d_{a,\mathrm{V}} = a_0 \frac{da}{dV_{\mathrm{DC}}}\Big|_{V_{\mathrm{DC}}=0} \tag{4.26}$$

and

$$d_{u,\mathrm{V}} = a_0 \frac{du}{dV_{\mathrm{DC}}}\Big|_{V_{\mathrm{DC}}=0} \tag{4.27}$$

on the surfaces is removed.

Chapter 5

Summary and Conclusions

In the present work we have investigated the electronic and structural responses of materials to external electrostatic field.

The first part of our study introduced a new way for *ab initio* calculations of the dipole moment per unit, i.e., of the polarization of quasi-one-dimensional infinite and periodic systems. In order to achieve this, two different methods were used - a Vector Potential Approach (VPA) and an *ab initio* Linear Combination of Atomic Orbitals-Self Consistent Field (LCAO-SCF) method. The first one is a very efficient for determining the electronic and nuclear responses of infinite periodic systems to finite electric field, and the second enables the computation of band structures of regular and helical polymers, taking into account the one-dimensional translational symmetry. This part of the present research deals only with the electronic responses. The model Hamiltonian constructed within the VPA contains an additional polarization energy term ($E_{\mathrm{DC}} \cdot P$) when the system is exposed to external field, and all essential elements of an *ab initio* Hartree-Fock (or Kohn Sham) Hamiltonian including band orbitals with phases that may vary randomly from one k point to the next. Thus, it was possible to take the polarization energy expression from the VPA Hamiltonian and to implement it in the *ab initio* Hartree-Fock Hamiltonian, which was the first step towards a full *ab initio* treatment of periodic system in external electrostatic fields.

To show the accuracy of our results we used two test systems - infinite hydrogen and infinite lithium hydride chains. In the first case minimal $STO-3G$ and double-zeta $3-21G$ basis sets were used, and in the second case the Clementi's minimum basis set. In both cases we investigated: 1). The change of the band orbital phases with the wavevector k; 2). The dependence of the total energy (E_{tot}) and of the polarization (P) on the electric field strength (E_{DC}), on the intramolecular distance ($d_{\mathrm{H-H}}$ and $d_{\mathrm{Li-H}}$) and on the unit cell

length (a). The polarizabilities (α) of the two chains were calculated and compared with previous values. Furthermore, the change of α with the distance between the hydrogen atoms in H_2 and between the lithium and hydrogen atom in LiH, and with the unit cell of the both chains was investigated. The second hyperpolarizability (γ) in the case of H_2 chain was calculated, and band structures for the LiH chain at $E_{\rm DC} = 0$ and $E_{\rm DC} \neq 0$ were introduced.

To check the implementation of the smoothing procedure, which is used for the numerical differentiation of the orbital coefficients, in order to calculate self-consistently the charge flow contribution to the polarization, the change of the band orbital phases with the wavevector k before and after smoothing was investigated. For both test systems, the correct implementation of the smoothing in the PLH code was shown through comparison of the non smooth and smooth phases. The effect of the field on the band orbital phases is only for the LiH chain evident and discontinuities at the boundaries $k = 0, \pm\pi$ after smoothing exist in both cases. Since these jumps in the curve distributions are equal to $\tilde{n}2\pi$, they are irrelevant and do not affect the derivatives of the coefficients.

The $3-21G$ basis set results afford more stable H_2 chain than the minimal $STO-3G$ ones in absence and presence of electric field. The change of the total energy with the field follows the same tendency using both basis sets and for $E_{\rm DC} > 0.001$ a.u. $E_{\rm tot}$ decreases rapidly. The total electronic polarization was calculated as a sum of charge (P_ρ or P_1) and current ($P_{\rm I}$ or P_2) contributions and changes linearly with the electric field strength for both test systems. Furthermore, it is evident that the contribution from the current term, which is equivalent to the charge flow in the chain, is important and neglecting it is not a good approximation. The polarizability along the polymer chain axis (the longitudinal polarizability per unit cell) was evaluated by means of the Finite Field (FF) technique via the polarization and via the total energy for the H_2 chain and for the LiH one only using the calculated polarization values. The average value of α for the hydrogen chain is in very good agreement with previous results of Champagne et al. [3], and this for the lithium hydride chain with the theoretical results of Bishop et al. [11].

To investigate the dependence of $E_{\rm tot}$, P and α on the intramolecular distance ($d_{\rm H-H}$ and $d_{\rm Li-H}$), single molecules were considered. For this purpose, the unit cell was chosen to be 20.0 a.u. for H_2 and 50.0 a.u. for LiH. The distance between the two atoms was changed in the range from 0.5 a.u. to 8.0 a.u. at field strength $E_{\rm DC} = 0.0002$ a.u. in the first case and from 0.5 a.u. to 9.0 a.u at $E_{\rm DC} \pm 0.0001$ a.u. in the second case. For the H_2 molecule an equilibrium structure was found at $d_{\rm eq} = 1.35$ a.u. ($STO-3G$) and $d_{\rm eq} = 1.39$ a.u. ($3-21G$). Compared with the experimental value of $d_{\rm eq} = 1.40$

a.u. a deviation of 3.7% and 0.7%, respectively, was found. For the LiH molecule an equilibrium geometry was found at $d_{\mathrm{eq}} = 3.051$ a.u. at the three field amplitudes, which is in good agreement with experimental and previous theoretical results. Due to the large unit cell lengths ($a = 20.0$ a.u. and $a = 50.0$ a.u.) the current contribution to the polarization (P_2) becomes zero and only the charge term contributes to the total electronic polarization ($P_{\mathrm{tot}} = P_1$). The results show that P_{tot} increases rapidly for larger intramolecular distances and that the $3-21G$ basis set provides larger polarization than the minimal one in the case of H_2. The change of the polarizability with the distance between the two atoms in the H_2 molecule follows the same tendency like the polarization for $STO-3G$ and $3-21G$ basis sets. A perfect agreement with the results of Champagne et al. confirms the accuracy of our results. The tendency of α of the lithium hydride single molecule is different from the polarization tendency and at equilibrium $\alpha = 19.69$ a.u.

In order to explore the effect of the bond-length alternation on the total energy of the system, on the polarization and on the polarizability in the presence of external electric perturbation, the intramolecular distances were fixed at $d_{\mathrm{H-H}} = 2.0$ a.u. and $d_{\mathrm{Li-H}} = 4.0$ a.u. The intermolecular distances were changed from 2.5 a.u. to 98.0 a.u. at $E_{\mathrm{DC}} = 0.0002$ a.u. for the H_2 chain and from 5.0 a.u. to 96.0 a.u. at $E_{\mathrm{DC}} = \pm 0.0001$ a.u. for the LiH chain. The total energies of the two systems converged to values that correspond to these of a single molecule. However, before convergence E_{tot} of the H_2 chain decreased (at the beginning rapidly) and of LiH chain increased (also rapidly at the beginning), i.e., a single hydrogen molecule is more stable than the hydrogen chain and a single lithium hydride molecule is less stable than the chain. According to this the total polarization of the first test system decreased with the unit cell length and of the second test system increased till convergence. The polarizability of both systems showed the same behaviour with the change of the unit cell length, namely it decreased rapidly for the smaller a and converged for $a \geq 40.0$ a.u.

Important for the nonlinear optics applications of materials is their second hyperpolarizability γ. Using the FF technique we determined the longitudinal second hyperpolarizability per unit cell, γ_l, of the hydrogen chain at different field amplitudes and got values that are in good agreement with previous results.

Band structures of the LiH chain were calculated at three different field strength and the change of the energy gap (E_{gap}) in the range $-0.0008 \leq E_{\mathrm{DC}} \leq 0.0008$ a.u. was investigated. With increasing field E_{gap} decreased almost linearly.

Our results confirm the successful implementation of the VPA in the *ab initio* PLH code. The next step will be the *ab initio* treatment of larger periodic systems in exter-

nal electrostatic fields, where not only the electronic but also the nuclear responses are investigated.

The second issue in the present work was to investigate the effect of the surface in electric field polarization of periodic systems. We have demonstrated that, for a long finite chain with repeated units, the structural responses to an external applied field of fixed strength depends upon the charge at the chain ends which, in turn, is governed by the terminations. Different terminations of an otherwise identical chain can lead to different responses. In passing we note that different responses will be observed only if the field is held constant rather than the potential drop over a unit cell. Although an infinite periodic chain does not have terminations, the effect of introducing such terminations is indirectly included in the MTP/VPA crystal orbital treatment through an (undefined) integer, $\tilde{n}$, that appears in the boundary conditions for the crystal orbitals. Thus, this arbitrary integer has now been linked to a physical observable.

The dependence of the structural responses to an electrostatic field described above arises because the general expression for the electronic dipole moment per unit contains a term given by the integer, $\tilde{n}$, multiplied by the lattice constant, and the latter couples mechanically with the internal structural parameters of the unit cell. If the lattice parameter is fixed, then the internal structural responses are suppressed. By chemically modifying the terminations (for example, by attaching specifically designed ligands) one can modify the integer and thereby observe an effect on the piezoelectric properties.

Theoretical arguments show that the dipole moment per unit cannot be changed arbitrarily, but only by an integer multiple of a lattice vector (times the elementary charge). This is borne out here by calculations on a model system, i.e., long, but finite, chains. In simulating the same system through an infinite periodic treatment we have shown that all physical effects can be reproduced 'exactly' by making a specific choice for an integer related to a mathematical phase ambiguity that occurs in determining the crystal orbitals. Thus, an integer quantity, previously considered to be unphysical, has been related to an observable physical surface effect.

It has been shown elsewhere [11] that (hyper)polarizabilities of infinite periodic systems do not depend upon surface charge if the structure is fixed. They will do so, however, due to structural changes induced by an electrostatic field. Moreover, the effects of the latter on experimental properties can be quite large (see, for example, [111] and references cited therein). Finally, even the charge distribution in the central region (also experimentally accessible and here quantified through the net number of electrons on atom A) depends on $\tilde{n}$ for $E_{\mathrm{DC}} \neq 0$. Our numerical model studies have shown that piezoelectric surface

effects can be quite significant.

In the present study only 1D systems were considered. A future purpose is to translate our 1D results to a 2D films and 3D solids.

Bibliography

[1] J. M. André, D. H. Mosley, B. Champagne, J. Delhalle, J. G. Fripiat, J. L. Brédas, D. J. Vanderveken, and D. P. Vercauteren, *Methods and techniques in computational chemistry*, METECC-94 B, STEF, 1993.

[2] B. Champagne, *Molecular simulation methods for predicting polymer properties*, chapter Ab initio Polymer Quantum Theory, p. 1, Wiley & Sons, New York, 2005.

[3] B. Champagne, D. H. Mosley, M. Vračko, and J.-M. André, *Phys. Rev. A* **52**, 178 (1995).

[4] B. Champagne, D. H. Mosley, M. Vračko, and J.-M. André, *Phys. Rev. A* **52**, 1039 (1995).

[5] B. Meyer and D. Vanderbilt, *Phys. Rev. B* **63**, 205426 (2001).

[6] I. Souza, J. Íñiguez, and D. Vanderbilt, *Phys. Rev. Lett.* **89**, 117602 (2002).

[7] P. Umari and A. Pasquarello, *Phys. Rev. Lett.* **89**, 157602 (2002).

[8] O. Diéguez and D. Vanderbilt, *Phys. Rev. Lett.* **96**, 056401 (2006).

[9] M. Springborg and B. Kirtman, *Phys. Rev. B* **77**, 045102 (2008).

[10] B. Kirtman, F. L. Gu, and D. M. Bishop, *J. Chem. Phys.* **113**, 1294 (2000).

[11] D. M. Bishop, F. L. Gu, and B. Kirtman, *J. Chem. Phys.* **114**, 7633 (2001).

[12] M. Springborg and B. Kirtman, *J. Chem. Phys.* **126**, 104107 (2007).

[13] R. D. King-Smith and D. Vanderbilt, *Phys. Rev. B* **47**, 1651 (1993).

[14] D. Vanderbilt and R. D. King-Smith, *Phys. Rev. B* **48**, 4442 (1993).

[15] R. Resta, *Rev. Mod. Phys.* **66**, 899 (1994).

[16] R. Resta, *J. Phys. Cond. Matt.* **12**, R107 (2000).

[17] E. I. Blount, *Formalisms of Band Theory*, volume 13 of *Solid State Physics*, Academic Press, 1962.

[18] M. Springborg, B. Kirtman, and Y. Dong, *Chemical Physics Letters* **396**, 404 (2004).

[19] M. Springborg, B. Kirtman, Y. Dong, and V. Tevekeliyska, *Lecture Series on Computer and Computational Sciences* **7**, 1234 (2006).

[20] M. Springborg, *Methods of Electronic-Structure Calculations: from Molecules to Solids*, Wiley series in theoretical chemistry, John Wiley and Sons, Ltd., Chichester, 2000.

[21] J. Ladik, *Acta Phys. Hung.* **18**, 173 (1965).

[22] J. Ladik, *Acta Phys. Hung.* **18**, 185 (1965).

[23] J. M. André, L. Gouverneur, and G. Leroy, *Int. J. Quantum Chem.* **1**, 427 (1967).

[24] J. M. André, L. Gouverneur, and G. Leroy, *Int. J. Quantum Chem.* **1**, 451 (1967).

[25] S. Suhai and J. Ladik, *Int. Solid State Commun.* **22**, 227 (1977).

[26] A. Karpfen, *Int. J. Quantum Chem.* **19**, 1297 (1981).

[27] M. Kertesz, *Acta Phys. Acad. Sci. Hung.* **41**, 127 (1976).

[28] C. Pisani, R. Dovesi, and C. Roetti, *Hartree-Fock ab initio treatment of crystalline systems*, Lecture Notes in Chemistry, Springer-Verlag, Berlin, 1988.

[29] P. Otto, E. Clementi, and J. Ladik, *IBM Technical Report* **POK-13** (1982).

[30] J. M. André, D. P. Vercauteren, V. P. Bodart, J. L. Brédas, J. Delhalle, and J. G. Fripiat, *Documentation for an ab initio polymer program (PLH)*, volume POK-28, IBM IS&TG, 1983.

[31] J. M. André, *Comput. Phys. Comm.* **1**, 391 (1970).

[32] J. M. André, V. P. Bodart, J. L. Brédas, J. Delhalle, and J. G. Fripiat, *Quantum Theory of Polymers: Solid State Aspects*, NATO-ASI Series C123, Riedel Publishing Co., 1984.

[33] D. R. Hartree, *Proc. Cambr. Phil. Soc.* **21**, 625 (1923).

[34] D. R. Hartree, *Proc. Cambr. Phil. Soc.* **24**, 89, 111, 246 (1923).

[35] V. Fock, *Zeitschrift für Physik A Hadrons and Nuclei* **61**, 126 (1930), 10.1007/BF01340294.

[36] J. André, J. Delhalle, and J. L. Brédas, *Quantum chemistry aided design of organic polymers: an introduction to the quantum chemistry of polymers and its applications*, World scientific lecture and course notes in chemistry, World Scientific Publishing Company, London, 1991.

[37] T. K. Rebane, *Methods of Quantum Chemistry*, chapter Methods of Quantum Chemistry, p. 147, Academic Press, New York, 1965.

[38] W. L. McCubbin and R. Manne, *Chem. Phys. Lett.* **2**, 230 (1968).

[39] M. H. Wangbo, R. Hoffmann, and R. B. Woodward, *Proc. R. Soc. Ser. A* **366**, 23 (1979).

[40] K. Morokuma, *Chem. Phys. Lett.* **6**, 186 (1970).

[41] D. L. Beveridge, I. Jano, and J. Ladik, *J. Chem. Phys.* **56**, 4744 (1972).

[42] M. J. Dewar, Y. Yamaguchi, and S. H. Suck, *Chemical Physics Letters* **51**, 175 (1977).

[43] J. M. André, L. A. Burke, J. Delhalle, G. Nicolas, and P. Durand, *Int. J. Quantum Chem.* **16**, 283 (1979).

[44] M. Kertész, *Chem. Phys.* **44**, 349 (1979).

[45] P. Hohenberg and W. Kohn, *Phys. Rev.* **136**, B864 (1964).

[46] W. Kohn and L. J. Sham, *Phys. Rev.* **140**, A1133 (1965).

[47] J. W. Mintmire and C. T. White, *Phys. Rev. Lett.* **50**, 101 (1983).

[48] J. W. Mintmire and C. T. White, *Phys. Rev. B* **28**, 3283 (1983).

[49] J. W. Mintmire, *Phys. Rev. B* **39**, 13350 (1989).

[50] J. W. Mintmire, J. R. Sabin, and S. B. Trickey, *Phys. Rev. B* **26**, 1743 (1982).

[51] M. Springborg and O. K. Andersen, **87**, 7125 (1987).

[52] M. Springborg, J.-L. Calais, O. Goscinski, and L. A. Eriksson, *Phys. Rev. B* **44**, 12713 (1991).

[53] M. Springborg, *International Reviews in Physical Chemistry* **12**, 241 (1993).

[54] H. Meider and M. Springborg, *The Journal of Physical Chemistry B* **101**, 6949 (1997).

[55] M. Springborg, *Journal of the American Chemical Society* **121**, 11211 (1999).

[56] M. Springborg, *International Journal of Quantum Chemistry* **77**, 843 (2000).

[57] J. W. F. Woo, *Phys. Rev. B* **4**, 1218 (1971).

[58] R. M. Martin, *Phys. Rev. B* **5**, 1607 (1972).

[59] R. M. Martin, *Phys. Rev. B* **6**, 4874 (1972).

[60] J. W. F. Woo and R. Landauer, *Phys. Rev. B* **6**, 4876 (1972).

[61] C. Kallin and B. I. Halperin, *Phys. Rev. B* **29**, 2175 (1984).

[62] M. Springborg, V. Tevekeliyska, and B. Kirtman, *Phys. Rev. B* **82**, 165442 (2010).

[63] V. N. Genkin and P. M. Mednis, *Sov. Phys. JETP* **27**, 609 (1968).

[64] B. Kirtman, B. Champagne, F. L. Gu, and D. M. Bishop, *Int. J. Quantum Chem.* **90**, 709 (2002).

[65] B. champagne, D. Jacquemin, F. L. Gu, Y. Aoki, B. Kirtman, and D. M. Bishop, *Chem. Phys. Lett.* **373**, 539 (2003).

[66] F. L. Gu, D. M. Bishop, and B. Kirtman, *J. Chem. Phys.* **115**, 10548 (2001).

[67] F. L. Gu, Y. Aoki, and D. M. Bishop, *J. Chem. Phys.* **117**, 385 (2002).

[68] M. Dvornikov, *arXiv:math/0306092v4 and JCAAM* **5**, 77 (2007).

[69] M. Springborg, V. Tevekeliyska, B. Kirtman, B. Champagne, and Y. Dong, *Z. Phys. Chem.* **224**, 617 (2010).

[70] M. Abramowitz and I. Stegun, *Handbook of Mathematical Functions*, Dover, New York, 1968.

[71] L. N. G. Filon, *Proc. Roy. Soc. Edinburgh Sect. A* **49**, 38 (1928-1929).

[72] W. J. Schneider and J. Ladik, *J. Comput. Chem.* **2**, 376 (1981).

[73] D. Jacquemin, B. Champagne, J. M. André, E. Deumens, and Y. Öhrn, *J. Comput. Chem.* **23**, 1430 (2002).

[74] P. O. Löwdin, *Rev. Mod. Phys.* **39**, 259 (1967).

[75] P. de Montgolfier and A. Hoareau, *J. Chem. Phys.* **65**, 2477 (1976).

[76] R. P. Feynmann, *Phys. Rev.* **36**, 340 (1939).

[77] H. D. Cohen and C. C. J. Roothaan, *J. Chem. Phys.* **43**, S34 (1965).

[78] C. Møller and M. S. Plesset, *Phys. Rev.* **46**, 618 (1934).

[79] R. J. Bartlett, *J. Phys. Chem.* **93**, 1697 (1989).

[80] B. Champagne and D. H. Mosley, *J. Chem. Phys.* **105**, 3592 (1996).

[81] J. A. Pople, R. Krishnan, H. B. Schlegel, and J. S. Binkley, *Int. J. Quantum Chem. S13* **16**, 225 (1979).

[82] L. Piela, J. M. Andre, J. L. Bredas, and J. Delhalle, *Int. J. Quantum Chem.* **18**, 405 (1980).

[83] J. M. André, D. P. Vercauteren, and J. G. Fripiat, *J. Comput. Chem.* **5**, 349 (1984).

[84] J. M. André, D. P. Vercauteren, V. P. Bodart, and J. G. Fripiat, *J. Comput. Chem.* **5**, 535 (1984).

[85] J. M. André, J. Delhalle, C. Demanet, and M. E. Lambert-Gerard, *Int. J. Quantum Chem.* **S10**, 99 (1976).

[86] J. M. André, J. Delhalle, G. S. Kapsomenos, and G. Leroy, *Chem. Phys. Lett.* **14**, 485 (1972).

[87] J. Delhalle and S. Delhalle, *Int. J. Quantum Chem.* **11**, 349 (1977).

[88] B. Champagne and J. M. André, *Int. J. Quantum Chem.* **42**, 1009 (1992).

[89] J. A. Pople and W. J. Hehre, *J. Comput. Phys.* **27**, 161 (1978).

[90] L. E. McMurchie and E. R. Davidson, *J. Comput. Phys.* **26**, 218 (1978).

[91] A. Szabó and N. S. Ostlund, *Modern quantum chemistry: introduction to advanced electronic structure theory*, Dover Publications, New York, 1996.

[92] H. Rutishauser, *Numerische Mathematik* **5**, 48 (1963), 10.1007/BF01385877.

[93] E. F. Pearson and W. Gordy, *Phys. Rev.* **177**, 59 (1969).

[94] P. E. Cade and W. M. Huo, *J. Chem. Phys.* **47**, 614 (1967).

[95] K. R. Way and W. C. Stwalley, *J. Chem. Phys.* **59**, 5298 (1973).

[96] J. E. Gready, G. B. Bacskay, and N. S. Hush, *Chemical Physics* **24**, 333 (1977).

[97] K. P. Huber and G. Herzberg, *Molecular Spectra and Molecular Structure*, volume 4, Van Nostrand, Princeton, NJ, 1978.

[98] H. Partridge and S. R. Langhoff, *J. Chem. Phys.* **74**, 2361 (1981).

[99] P. Lazzeretti, E. Rossi, and R. Zanasi, *Journal of Physics B: Atomic and Molecular Physics* **15**, 521 (1982).

[100] W. Klopper and W. Kutzelnigg, *J. Chem. Phys.* **94**, 2020 (1991).

[101] Y. Mo, W. Wu, and Q. Zhang, *Journal of Molecular Structure: THEOCHEM* **283**, 237 (1993).

[102] Y. Mo and Q. Zhang, *The Journal of Physical Chemistry* **99**, 8535 (1995).

[103] I. Gianolio and E. Clementi, *Gazz. Chim. Ital.* **110**, 179 (1980).

[104] Q. Niu, *Phys. Rev. B* **33**, 5368 (1986).

[105] D. Vanderbilt, *Journal of Physics and Chemistry of Solids* **61**, 147 (2000).

[106] V. V. Spirin, I. A. Sokolov, and K. No, *Opt. Laser Technol.* **36**, 337 (2004).

[107] M. Springborg and B. Kirtman, *Chemical Physics Letters* **454**, 105 (2008).

[108] M. Springborg and B. Kirtman, *Canadian Journal of Chemistry* **87**, 984 (2009).

[109] K. N. Kudin, R. Car, and R. Resta, *J. Chem. Phys.* **127**, 194902 (2007).

[110] R. Resta, *Phys. Rev. Lett.* **80**, 1800 (1998).

[111] J. M. Luis, M. Duran, B. Champagne, and B. Kirtman, *J. Chem. Phys.* **113**, 5203 (2000).

List of publications

1. *Structural and Electronic Properties of Metal Clusters*
M. Springborg, V.G. Grigoryan, Y. Dong, D. Alamanova, H. ur Rehman and V. Tevekeliyska,
Advances in Computational Methods in Science and Engineering 2005 **4A**, 1026 (2005).

2. *Infinite, periodic systems in external fields*
M. Springborg, B. Kirtman, Y. Dong and V. Tevekeliyska,
Lecture Series on Computer and Computational Sciences **7**, 1234 (2006).

3. *Structural and Energetic Properties of Sodium clusters*
V. Tevekeliyska, Y. Dong, M. Springborg, and V. G. Grigoryan,
Eur. Phys. J. D **43**, 19 (2007).

4. *Theoretical studies of structural, energetic, and electronic properties of clusters*
M. Springborg, Y. Dong, V. G. Grigoryan, V. Tevekeliyska, D. Alamanova, E. Kasabova,
S. Roy, J.-O. Joswig, and A. M. Asaduzzaman,
Z. Phys. Chem. **222**, 387 (2008).

5. *Structural responses of infinite periodic systems to electrostatic fields*
M. Springborg, B. Kirtman, and V. Tevekeliyska,
Am. Inst. Phys. Conf. Proc. **1148**, 305 (2009).

6. *Extended systems in elektrostatic fields*
M. Springborg, V. Tevekeliyska, B. Kirtman, B. Champagne, and Y. Dong,
Z. Phys. Chem. **224**, 617 (2010).

7. *Termination effects in electric field polarization of periodic quasi-one-dimensional sys-*

tems
M. Springborg, V. Tevekeliyska, and B. Kirtman,
Phys. Rev. B **82**, 165442 (2010).

8. *Using theory in determining the properties of metal clusters: sodium as a case study in Aromaticity and Metal Clusters.*
V. Tevekeliyska, Y. Dong, M. Springborg, and V. G. Grigoryan,
Ed. P. K. Chattaraj, Taylor & Francis , 161 (2011).

9. *Ab initio treatment of periodic systems in external electrostatic fields*
V. Spurk, M. Springborg, and B. Champagne,
in preparation.